

Dêivid Rodrigo da Silva

# **Employing dark matter and phantom-like fluids to alleviate the Hubble tension**

Brazil

June - 2023



Dêivid Rodrigo da Silva

# **Employing dark matter and phantom-like fluids to alleviate the Hubble tension**

Thesis presented to the Graduate Program in Physics of the Center for Exact and Natural Sciences at the Universidade Federal da Paraíba (Federal University of Paraíba) as a requirement for obtaining the title of Doctor in Physics.

Universidade Federal da Paraíba – UFPB

Graduate Program in Physics

Supervisor: Farinaldo da Silva Queiroz

Brazil

June - 2023

**Catálogo na publicação**  
**Seção de Catalogação e Classificação**

S586e Silva, Deivid Rodrigo da.

Employing dark matter and phantom-like fluids to  
alleviate the Hubble tension / Deivid Rodrigo da Silva.

- João Pessoa, 2023.

120 f. : il.

Orientação: Farinaldo da Silva Queiroz.

Tese (Doutorado) - UFPB/CCEN.


1. Cosmologia. 2. Matéria escura. 3. Tensão de  
Hubble. 4. Teoria de campo efetiva. I. Queiroz,  
Farinaldo da Silva. II. Título.

UFPB/BC


CDU 524.8(043)

Ata da Sessão Pública da Defesa de tese de Doutorado do aluno  
Deivid Rodrigo Da Silva, candidato ao Título de Doutor em  
Física na Área de Concentração Gravitação e Cosmologia.


Aos vinte e três dias do mês de junho do ano de dois mil e vinte e três, às 14:00, nas dependências do Centro de Ciências Exatas e da Natureza da Universidade Federal da Paraíba, reuniram-se os membros da Banca Examinadora constituída para avaliar a tese de Doutorado, na área de Gravitação e Cosmologia, de **Deivid Rodrigo Da Silva**. A banca foi composta pelos(as) professores(as) doutores(as): Farinaldo da Silva Queiroz (PPGF/UFPB), orientador e presidente da banca examinadora, Bertúlio de Lima Bernardo (PPGF/UFPB), Valdir Barbosa Bezerra (PPGF/UFPB), Júlio César Fabris (UFES) e Davi Cabral Rodrigues (UFES). Dando início aos trabalhos, o Prof. Farinaldo da Silva Queiroz comunicou aos presentes a finalidade da reunião. A seguir, passou a palavra para o candidato para que o mesmo fizesse, oralmente, a exposição da pesquisa de tese intitulada "*Employing dark matter and phantom-like fluids to alleviate the Hubble tension*". Concluída a exposição, o candidato foi arguido pela Banca Examinadora, que emitiu o parecer "**aprovado**". Assim sendo, deve a Universidade Federal da Paraíba expedir o respectivo diploma de Doutor em Física na forma da lei. E para constar, Danilo Wilson Lemos Menezes, Técnico em Assuntos Educacionais, redigiu a presente ata que vai assinada pelos membros da Banca Examinadora. João Pessoa, Paraíba, **23 de junho de 2023**.

Documento assinado digitalmente  
 FARINALDO DA SILVA QUEIROZ  
Data: 27/06/2023 17:18:26-0300  
Verifique em <https://validar.iti.gov.br>

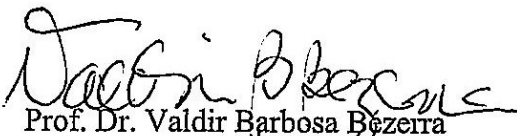
Prof. Dr. Farinaldo da Silva Queiroz  
Orientador

Documento assinado digitalmente  
 BERTULIO DE LIMA BERNARDO  
Data: 26/06/2023 15:01:13-0300  
Verifique em <https://validar.iti.gov.br>

Prof. Dr. Bertúlio de Lima Bernardo  
PPGF/UFPB

Documento assinado digitalmente  
 DAVI CABRAL RODRIGUES  
Data: 26/06/2023 14:11:31-0300  
Verifique em <https://validar.iti.gov.br>

Prof. Dr. Davi Cabral Rodrigues  
UFES

  
Prof. Dr. Valdir Barbosa Bezerra  
PPGF/UFPB

Prof. Dr. Júlio César Fabris  
UFES



UNIVERSIDADE FEDERAL DO ESPÍRITO SANTO

**PROTOCOLO DE ASSINATURA**



O documento acima foi assinado digitalmente com senha eletrônica através do Protocolo Web, conforme Portaria UFES nº 1.269 de 30/08/2018, por  
JULIO CESAR FABRIS - SIAPE 297051  
Departamento de Física - DF/CCE  
Em 26/06/2023 às 14:24

Para verificar as assinaturas e visualizar o documento original acesse o link:  
<https://api.lepisma.ufes.br/arquivos-assinados/736844?tipoArquivo=O>

# Acknowledgements

I begin by thanking all the taxpayers of Brazil, who, by paying their taxes, make it possible to offer undergraduate, master's, and doctoral scholarships to students and researchers. Throughout these four years, I was supported by CAPES (Coordenação de Aperfeiçoamento de Pessoal de Nível Superior), a public agency that promotes research and science. Finishing this work would be impossible without this support. I highlight that valuing science and us researchers is of fundamental importance to our country, as researchers are workers who foster the construction of knowledge and help a nation become sovereign.

The accomplishment of this work was only possible thanks to the support of family members, friends, teachers, and the giants of Physics who paved the roads that we, students and researchers, explored. A special thanks to my wife, Alyra dos Santos Oliveira, for encouraging me, for being by my side during these difficult years, and for being my refuge in the darkest hours. I am immensely grateful for the supervision of Prof. Farinaldo da Silva Queiroz, who performed his role as an advisor very well, being accessible to discuss the research we developed, helping me with his academic experience, and providing a lot of support in some difficult moments. You accepted me into your research group and respected my research and scientific vision to the fullest. I am also grateful to some of my colleagues from the Astroparticles group at UFRN, of which I am a part. In particular, I thank Yoxara Sánchez Villamizar, the queen of LaTeX and a wizard of Python, for her tips and assistance. I was also very happy to be a colleague of Yohan Mauricio Oviedo Torres, the terror of capybaras, and Álvaro Santos de Jesus, the encyclopedia of memes and chaotic videos, during these years of doctoral studies. You made the workdays very enjoyable. I also thank all the other members of the Astroparticles group, who have always been very fun and welcoming, which is not very common in physics. I also want to thank all the other teachers who, in the past, recognized my interest in Physics and Mathematics and encouraged me. Among these countless educators, I emphasize the importance of Prof. Paulo Peixoto in my undergraduate studies, as he was one of my greatest inspirations as a human being.

I worked very hard to finish this cycle, but I was not alone. I had a lot of support from friends, family, teachers, and institutions. Nothing would have been possible alone. I thank everyone who, even though not mentioned here, in some way contributed to my academic formation.





*“The realization that the majority of the matter in the Universe might be non-baryonic is the ultimate Copernican viewpoint; not only are we in no special place in the Universe, but we aren’t even made out of the same stuff as dominates the matter density of the Universe.”*  
(Andrew Liddle, *An Introduction to Modern Cosmology*, 3rd ed)



# Abstract

In this doctoral thesis, I investigate how the decay of a very heavy particle into dark matter and photons (or neutrinos) can alleviate the Hubble tension, that is, it can reconcile the value of the Hubble constant ( $H_0$ ) measured through the analysis of the cosmic microwave background (CMB) radiation with the measurements obtained in regions of the universe with low redshift. I show that by adopting the standard cosmological model,  $\Lambda$ CDM, this mechanism is unable to completely remove the tension, resulting in only a small reduction between the measurements of  $H_0$ . However, in a universe with a phantom-like fluid, the decay adds enough radiation to the point where CMB measurements allow for  $H_0$  within the range of  $70-74 \text{ km s}^{-1} \text{ Mpc}^{-1}$ , which would completely eliminate the tension. I also use constraints from BBN to show that many of the important results of the standard cosmology are preserved, which prevents the model from being phenomenologically excluded.

**Keywords:** Cosmology. Dark Matter. Hubble Tension. Effective Field Theory.



# Resumo

Nesta tese de doutorado, eu investigo como um decaimento de uma partícula muito pesada em matéria escura e photons (ou neutrinos) podem aliviar a tensão de Hubble, ou seja, pode fazer o valor da constante de Hubble ( $H_0$ ) medido através da análise da radiação cósmica de fundo (CMB) ser compatível com as medidas obtidas em regiões do universo com pequeno redshift. Mostro que adotando o modelo cosmológico padrão,  $\Lambda$ CDM, esse mecanismo não é capaz de remover totalmente a tensão, produzindo apenas uma pequena redução entre as medições de  $H_0$ . Contudo, em um universo com um fluido do tipo fantasmagórico, o decaimento adiciona radiação suficiente ao ponto de medidas da CMB permitirem  $H_0$  no intervalo  $70 - 74 \text{ km s}^{-1} \text{ Mpc}^{-1}$ , o que eliminaria totalmente a tensão. Também utilizo restrições oriundas da BBN para mostrar que muitos dos importantes resultados da cosmologia padrão são mantidos, o que faz o modelo não ser fenomenologicamente excluído.

**Palavras-chave:** Cosmologia. Matéria Escura. Tensão de Hubble. Teoria de Campo Efetiva.



# List of Figures

- Figure 1 – Ratio between the energy density and the ultrarelativistic energy density for a generic bosonic and a fermionic fluid. For  $m \ll T$  both densities are equivalent. . . . . 48
- Figure 2 – Ratio between the energy density of a generic fluid and the dust energy density. When  $m \gg T$  the ratio is 1, which shows that in this regime the fluid is cold. This behavior is valid for a generic bosonic and fermionic gas. 49
- Figure 3 – Energy density evolution for radiation, matter, and dark energy. The energy density ( $\rho$ ) is normalized by the present-day critical density ( $\rho_{\text{crit},0}$ ). The horizontal axis is the scale factor, and the orange region represents the radiation phase, the blue region represents the matter phase, and the gray region represents the dark energy phase. . . . . 61
- Figure 4 – Allowed regions of parameters that connect the non-thermal dark matter mechanism presented here and the value of Hubble constant in the  $\Lambda$ CDM and phantom-like cases [1]. The first row corresponds to the  $\Lambda$ CDM model, and in the second and third rows, a phantom-like quintessence is introduced, first in a spatially flat model, then with non-null spatial curvature. The data set that connects  $\Delta N_{\text{eff}}$  and  $H_0$  showed in (a), (c), and (e) is taken from [2]. In all figures, the lighter regions correspond to 99% of CL, while the darkest regions correspond to 68% of CL. In (b), (d), and (f) the orange, blue and gray regions correspond to the cases where  $\chi'$  lifetime is  $10^2 s$ ,  $10^3 s$  and  $10^4 s$  respectively. The bounds use Planck 2018 CMB data, BAO, and type Ia data from the Pantheon sample. . . . . 80
- Figure 5 – Allowed parameter space for dark matter lifetime  $\tau$  and Hubble constant  $H_0$  for phantom-like cases. The data used to create this figure is the same as in Fig. 4. The lighter regions in both figures represent 99% of the confidence level, while the darkest regions represent 68% of the confidence level. The orange region represents the null curvature case, while the gray region represents the curved case. In both cases, it is assumed that only 1% of the present-day dark matter abundance is generated by the  $\chi'$  decay, i.e.,  $f = 0.01$ . The left figure considers a mass ratio of  $m_{\chi'}/m_{\chi} = 10^3$ , while the right figure represents the case where  $m_{\chi'}/m_{\chi} = 10^4$ . . . . . 82

Figure 6 – Time evolution of dark matter energy [1]. Dark matter mother lifetime is  $\tau = \{10^2 \text{ s}, 10^3 \text{ s}, 10^4 \text{ s}\}$  and the ratio between dark matter mother and dark matter mass is  $m_{\chi'}/m_{\chi} = \{10^3, 10^4, 10^5, 10^6\}$ . In all situations of **(a)** and **(b)**, dark matter is cold at matter-radiation equality ( $t_{\text{eq}}$ ), while in **(c)** and **(d)** dark matter is hot in all lifetime scenarios. . . . . 83

Figure 7 – BBN bounds based on light element abundances [3]. The shaded regions are excluded because they represent a situation where the electromagnetic energy released by  $\chi'$  decay alters the well-understood light element abundance. The nearly vertical dotted line is the constraint stemming from the spectral distortion of the CMB is also present. All region to its left is excluded. The diagonal lines are the superior limit for theoretical prediction for  $H_0$  using the non-thermal dark matter production mechanism. In Fig.7(a) I display the results for  $E_{\gamma} = E_{\nu}$  and  $k \neq 0$ , where  $E_{\gamma}$  is the energy of the gamma-rays produced after the  $\chi' \rightarrow \chi + \nu$  or  $\chi' \rightarrow \chi + \gamma$  decay. In Fig.7(b) I show the results for  $E_{\gamma} = E_{\nu}$ , but with  $k = 0$ . The detail of these geometrical considerations is in the text. . . 87

Figure 8 – Relative entropy variation as a function of  $\Delta N_{\text{eff}}$ . The blue solid line is obtained by Eq. 4.38, while the orange dotted line is a linear approximation. 89

Figure 9 – Diagrammatic representation of a heavy particle ( $\chi'$ ) that decay in hot dark matter ( $\chi$ ) and photon ( $\gamma$ ). Three cases are considered: **(a)**  $\chi'$  is spin-1 and  $\chi$  is a spin-0 particle; **(b)**  $\chi'$  and  $\chi$  are spin-1/2 particles; **(c)**  $\chi'$  is spin-0 and  $\chi$  is a spin-1 particle. . . . . 91

Figure 10 – The figure presents the plots of  $\Lambda$  as a function of  $m_{\chi'}$  and  $m_{\chi}$  for the scenario where  $\chi'$  is a spin-1 particle and  $\chi$  is a spin-0 particle [1]. In panel **(a)**, the curves for  $m_{\chi'} \times \Lambda$  are shown, calculated using Eq. (4.46) for different lifetimes  $\tau = 10^2, 10^3$  and  $10^4$  s. In panel **(b)**, the curves for  $m_{\chi} \times \Lambda$  are displayed, obtained from Eqs. (4.14) and (4.46). The parameter space is explored for cases where  $\Delta N_{\text{eff}} = 0.1 - 0.6$ , with a fixed ratio  $f = 0.01$  and  $m_{\chi'}/m_{\chi} = 10^4$ . . . . . 92

Figure 11 – Plot of  $\Lambda$  as a function of the masses of  $\chi$  and  $\chi'$  for the case where  $\chi'$  and  $\chi$  are spin-1/2 particles [1]. In panel **(a)**, the curves of  $m_{\chi'} \times \Lambda$  are generated using Eq. 4.49 with  $\tau = 10^2, 10^3$ , and,  $10^4$  s. Panel **(b)** displays the curves of  $m_{\chi} \times \Lambda$  constructed from Eqs. 4.14 and 4.49. The cases where  $\Delta N_{\text{eff}} = 0.1 - 0.6$  are considered, with  $f = 0.01$  and  $m_{\chi'}/m_{\chi} = 10^4$ . 94



|  |     |
|--|-----|
| Figure 12 – Plot of $\Lambda$ as a function of the $\chi$ and $\chi'$ masses for the case where $\chi'$ is a spin-0 particle and $\chi$ is a spin-1 particle [1]. <b>(a)</b> Curves of $m_{\chi'} \times \Lambda$ are constructed using Eq. 4.52 with $\tau = 10^2, 10^3$ , and $10^4$ s. <b>(b)</b> Curves of $m_\chi \times \Lambda$ are constructed using Eqs. 4.14 and 4.52 for different values of $\Delta N_{\text{eff}}$ ranging from 0.1 to 0.6. The parameters $f = 0.01$ and $m_{\chi'}/m_\chi = 10^4$ are considered. . . . . | 96  |
| Figure 13 – Diagrammatic representation of a heavy particle ( $\chi'$ ) that decay in hot dark matter ( $\chi$ ) and neutrino ( $\nu$ ). Three cases are considered: <b>(a)</b> $\chi'$ is spin-1/2 and $\chi$ is a spin-0 particle; <b>(b)</b> $\chi'$ has spin-1 and $\chi$ has spin-1/2 particles; <b>(c)</b> $\chi'$ is spin-1/2 and $\chi$ is a spin-1 particle. . . . .  | 97  |
| Figure 14 – Plot of $\Lambda$ as a function of the $\chi$ and $\chi'$ masses for the case where $\chi'$ is a spin-1/2 particle and $\chi$ is a spin-0 particle. <b>(a)</b> $m_{\chi'} \times \Lambda$ curves built from Eq. 4.55, using $\tau = 10^2, 10^3$ , and, $10^4$ s and $\Lambda_1 = \Lambda_2 = \Lambda$ . <b>(b)</b> $m_\chi \times \Lambda$ curves constructed from Eqs. 4.14 and 4.55. I consider the cases where $\Delta N_{\text{eff}} = 0.1 - 0.6$ , with $f = 0.01$ and $m_{\chi'}/m_\chi = 10^3$ . . . . .              | 99  |
| Figure 15 – Plot of $\Lambda$ as a function of the masses $m_{\chi'}$ and $m_\chi$ for the case where $\chi'$ is a spin-1/2 particle and $\chi$ is a spin-0 particle. <b>(a)</b> Curves of $m_{\chi'}$ as a function of $\Lambda$ built from Eq. 4.58, using $\tau = 10^2, 10^3$ , and $10^4$ s. <b>(b)</b> Curves of $\Lambda$ as a function of $m_\chi$ constructed from Eqs. 4.14 and 4.58. I consider the cases where $\Delta N_{\text{eff}} = 0.1 - 0.6$ , with $f = 0.01$ and $m_{\chi'}/m_\chi = 10^3$ . . . . .                  | 100 |
| Figure 16 – Plot of $\Lambda$ as a function of the $\chi$ and $\chi'$ masses for the case where $\chi'$ is a spin-1/2 and $\chi$ is a spin-0 particle. <b>(a)</b> $m_{\chi'} \times \Lambda$ curves built from Eq. (4.61), using $\tau = 10^2, 10^3$ and $10^4$ s. <b>(b)</b> $m_\chi \times \Lambda$ curves constructed from Eqs. (4.14) and (4.61). I consider the cases where $\Delta N_{\text{eff}} = 0.1 - 0.6$ , with $f = 0.01$ and $m_{\chi'}/m_\chi = 10^3$ . . . . .   | 103 |



# List of Tables

|   |     |
|---|-----|
| Table 1 – Present-day density parameter for photons, baryonic matter, matter, cold dark matter, neutrinos, curvature, and dark energy. The table also has the CMB inferred value for the Hubble constant and the present-day CMB temperature. . . . . | 60  |
| Table 2 – Early and late universe measurements of the Hubble constant and their respective data sets. . . . .   | 71  |
| Table 3 – Numerical value of Planck units in SI. . . . .  | 118 |
| Table 4 – Conversion factors from SI to natural units. . . . .  | 119 |



# List of abbreviations and acronyms

|     |                              |
|-----|------------------------------|
| BAO | Baryon Acoustic Oscillations |
| BBN | Big Bang Nucleosynthesis     |
| CMB | Cosmic Microwave Background  |
| FRW | Friedmann–Robertson–Walker   |



# Contents

|            |   |           |
|------------|---|-----------|
| <b>1</b>   | <b>INTRODUCTION</b>   | <b>25</b> |
| <b>2</b>   | <b>COSMOLOGY</b>  | <b>29</b> |
| <b>2.1</b> | <b>Special Relativity</b>   | <b>29</b> |
| <b>2.2</b> | <b>General Relativity</b>   | <b>31</b> |
| 2.2.1      | Tensors   | 31        |
| 2.2.2      | Metric and Connection   | 32        |
| 2.2.3      | The covariant derivative and the Riemann tensor                   | 33        |
| 2.2.4      | The Einstein equation   | 35        |
| <b>2.3</b> | <b>Friedmann-Robertson-Walker Geometry</b>                        | <b>35</b> |
| 2.3.1      | Friedmann's and acceleration equation                             | 35        |
| 2.3.2      | Four-momentum in null curvature case                              | 38        |
| 2.3.3      | Geodesic on flat FRW geometry using spatial spherical coordinates | 41        |
| <b>2.4</b> | <b>Number density, energy density, and pressure</b>               | <b>42</b> |
| 2.4.1      | Equation of state   | 42        |
| 2.4.2      | Equilibrium thermodynamics  | 43        |
| 2.4.3      | Equation of state for dust  | 43        |
| 2.4.4      | Equation of state for radiation                                   | 44        |
| 2.4.4.1    | Ultrarelativistic bosonic gas                                     | 44        |
| 2.4.4.2    | Ultrarelativistic fermionic gas                                   | 45        |
| 2.4.4.3    | Effective energy density and pressure for radiation               | 45        |
| 2.4.4.4    | Radiation   | 46        |
| 2.4.5      | Mass and temperature comparison                                   | 47        |
| 2.4.6      | Equation of state for dark energy                                 | 49        |
| <b>2.5</b> | <b>Entropy</b>  | <b>49</b> |
| <b>2.6</b> | <b>Density parameter</b>  | <b>51</b> |
| <b>2.7</b> | <b>Cosmic catalogue</b>   | <b>52</b> |
| 2.7.1      | Photons   | 52        |
| 2.7.2      | Baryons   | 54        |
| 2.7.3      | Dark matter   | 55        |
| 2.7.4      | Neutrinos   | 57        |
| 2.7.5      | Dark energy   | 59        |
| <b>2.8</b> | <b><math>\Lambda</math>CDM: the benchmark model</b>               | <b>60</b> |
| <b>2.9</b> | <b>Cosmological eras</b>  | <b>60</b> |
| 2.9.1      | Radiation era   | 62        |

|            |   |            |
|------------|---|------------|
| 2.9.2      | Matter era . . . . .  | 62         |
| 2.9.3      | Dark energy era . . . . .   | 63         |
| <b>3</b>   | <b>THE HUBBLE TENSION . . . . .</b>   | <b>65</b>  |
| <b>3.1</b> | <b>The many definitions of distance in cosmology . . . . .</b>  | <b>65</b>  |
| 3.1.1      | Proper distance and Hubble's law . . . . .  | 65         |
| 3.1.2      | Luminous distance . . . . .   | 67         |
| <b>3.2</b> | <b>Standard candles for local measurements . . . . .</b>  | <b>68</b>  |
| 3.2.1      | Cepheids . . . . .  | 68         |
| 3.2.2      | Type Ia Supernovae . . . . .  | 68         |
| <b>3.3</b> | <b>Standard sirens . . . . .</b>  | <b>69</b>  |
| <b>3.4</b> | <b>Measurement from the Early Universe: Cosmic Microwave Background . . . . .</b>   | <b>69</b>  |
| <b>3.5</b> | <b>The Hubble tension . . . . .</b>   | <b>70</b>  |
| <b>3.6</b> | <b>Possible solutions for the Hubble tension . . . . .</b>  | <b>72</b>  |
| <b>4</b>   | <b>ALLEVIATING THE HUBBLE TENSION WITH DARK MATTER<br/>AND NON-STANDARD COSMOLOGIES . . . . .</b>                         | <b>75</b>  |
| <b>4.1</b> | <b>Dark matter particles as the source of dark radiation: a particle<br/>physics model-independent approach . . . . .</b> | <b>76</b>  |
| 4.1.1      | Energy evolution of dark matter . . . . .   | 82         |
| <b>4.2</b> | <b>BBN constraints . . . . .</b>  | <b>84</b>  |
| <b>4.3</b> | <b>Entropy injection bounds . . . . .</b>   | <b>88</b>  |
| <b>4.4</b> | <b>Effective theory for the case where decay yields dark matter and<br/>photons . . . . .</b>                             | <b>90</b>  |
| 4.4.1      | Decay in spin-0 dark matter and photon . . . . .  | 91         |
| 4.4.2      | Decay in spin-1/2 dark matter and photon . . . . .  | 93         |
| 4.4.3      | Decay in spin-1 dark matter and photon . . . . .  | 95         |
| 4.4.4      | Considerations about lifetime, energy scale and truncation of effective La-<br>grangians . . . . .                        | 96         |
| <b>4.5</b> | <b>Effective theory for the case where decay yields dark matter and<br/>standard model neutrinos . . . . .</b>            | <b>98</b>  |
| 4.5.1      | Decay in spin-0 dark matter and neutrino . . . . .  | 98         |
| 4.5.2      | Decay in spin-1/2 dark matter and neutrino . . . . .  | 100        |
| 4.5.3      | Decay in spin-1 dark matter and neutrino . . . . .  | 101        |
| <b>4.6</b> | <b>Considerations about the decay dynamics . . . . .</b>  | <b>102</b> |
| <b>5</b>   | <b>CONCLUSIONS . . . . .</b>  | <b>105</b> |
|            | <b>BIBLIOGRAPHY . . . . .</b>   | <b>107</b> |



|            |  |            |
|------------|--|------------|
|            | <b>APPENDIX</b>  | <b>115</b> |
|            | <b>APPENDIX A – PLANCK SCALE AND NATURAL UNITS . . . .</b> | <b>117</b> |
| <b>A.1</b> | <b>Planck units . . . . .</b>                              | <b>117</b> |
| <b>A.2</b> | <b>Natural units . . . . .</b>                             | <b>118</b> |
| <b>A.3</b> | <b>Rewriting expressions in NU into SI . . . . .</b>       | <b>118</b> |



# 1 Introduction

The  $\Lambda$ CDM model is the standard cosmological framework and is highly consistent with observational data. It successfully explains various phenomena such as the formation of light elements in the cosmos, the existence of the homogeneous and isotropic cosmic microwave background (CMB), and the ongoing accelerated expansion of the universe. Nonetheless, there are certain challenges that remain the subject of extensive research. One of these challenges is known as the Hubble tension, which arises from the discrepancy between the value of the Hubble constant ( $H_0$ ) obtained from early universe analysis and the value derived from late universe observations.

To elaborate further, the Planck Collaboration analyzed the slight anisotropies in the CMB and determined  $H_0 = 67.27 \pm 0.6 \text{ km s}^{-1} \text{ Mpc}^{-1}$  [4]. On the other hand, local measurements of the Hubble constant typically rely on standard candles, which are stars with known intrinsic luminosity, allowing for accurate distance measurements. By determining the distance and redshift caused by the expanding universe, astronomers can estimate  $H_0$ . Using this technique, values of  $H_0$  above  $70 \text{ km s}^{-1} \text{ Mpc}^{-1}$  are often obtained [5].

The essence of the Hubble tension lies not only in the discrepancy between the central values of the Hubble constant obtained from early and late universe measurements but also in the fact that these measurements are highly precise with small error bars. Additionally, the error bars of the early and late universe measurements do not overlap, further emphasizing the tension.

There exist several potential solutions to alleviate the Hubble tension, and in this discussion, I will highlight two of them. The first approach involves introducing additional radiation before the formation of the cosmic microwave background (CMB). This extra radiation contributes to an effective number of neutrinos, resulting in a range of  $3 < N_{\text{eff}} < 3.7$  [5, 6, 7]. Although this additional radiation can slightly reduce the aforementioned discrepancy, it is insufficient to completely eliminate it [7].

The second solution involves considering an alternative dark energy model with an equation of state described by a linear relation between its pressure  $P$  and energy density  $\rho$ , where  $P = w\rho$  and  $w < -1$ . This type of fluid is referred to as phantom-like dark energy.

The core of this thesis is to unify these two solutions and provide an explanation for the extra source of radiation. The proposed model suggests the existence of a heavy particle, denoted as  $\chi'$ , which decoupled from the fundamental plasma. This particle can undergo decay processes producing photons ( $\gamma$ ) and dark matter ( $\chi$ ), or it can decay into

dark matter and standard model neutrinos ( $\nu$ ). The particles generated by the decay of  $\chi'$  contribute to the relativistic energy of the fundamental plasma, providing a reason for the requirement of  $N_{\text{eff}} > 3$ . However, to ensure consistency with observations, the dark matter produced through this mechanism should be cold at the time of matter-radiation equivalence. This ensures compatibility with cosmic microwave background data and structure formation, while only constituting a small fraction of the overall dark matter budget. The primary advantage of this solution is its ability to alleviate the Hubble tension while satisfying the constraints imposed by primordial nucleosynthesis (BBN). Furthermore, it establishes a connection between the Hubble tension and the nature of dark matter.

This thesis is structured as follows:

Chapter 2 provides a comprehensive review of standard cosmology. It begins with an exploration of the general relativity approach, deriving the fundamental equations for cosmology. The chapter then employs statistical mechanics to describe the state equations governing the universe's budget. Finally, I categorize the different phases of the universe and present the corresponding scale factor solutions.

Chapter 3 is dedicated to a detailed presentation of the Hubble tension. Within this chapter, I review the methods employed by cosmologists to estimate the Hubble constant using distance and redshift measurements. Furthermore, I delve into the intricacies of the Hubble tension, analyzing the discrepancies and possible solutions proposed by the scientific community.

In Chapter 4, I conduct an extensive investigation on how the decays  $\chi' \rightarrow \chi + \gamma$  or  $\chi' \rightarrow \chi + \gamma$  can alleviate the Hubble tension within both a  $\Lambda$ CDM universe and a universe featuring a phantom-like fluid. This chapter serves as an expansion of two articles where I was the main author. One of these articles, titled "The Hubble constant troubled by dark matter in non-standard cosmologies," was published in Nature - Scientific Reports [3]. The second article, titled "The Hubble rate trouble: an effective field theory of dark matter," was published in The European Physical Journal C [1].

Chapter 5 concludes the thesis by providing my final considerations and outlining potential avenues for future research and analysis.

Overall, this thesis is structured to provide a comprehensive examination of standard cosmology, an in-depth exploration of the Hubble tension, and a detailed investigation of possible solutions to address this discrepancy.

Throughout this text, I employ natural units in which fundamental constants, namely the speed of light in vacuum  $c$ , the reduced Planck constant  $\hbar$ , the Boltzmann constant  $k_B$ , and the gravitational constant  $G$ , are set to unity, i.e.,  $c = \hbar = k_B = G = 1$ . This choice greatly simplifies calculations in general relativity, cosmology, and quantum

field theory. Appendix [A](#) provides a comprehensive review of these units and outlines the procedure for recovering the fundamental constants when necessary.



## 2 Cosmology

The first two sections are a review of special and general relativity. The goal of these sections is to introduce the conventions of general relativity that I use throughout the entire text. This is important because there are various conventions for the Minkowski metric, Riemann tensor, Ricci tensor, Einstein's equation, and the energy-momentum tensor. Therefore, I explain the specific convention I am using and provide a brief review of some useful concepts for the development of cosmology. To avoid citing the same reference multiple times in these two sections, I would like to emphasize that they are primarily based on reference [8].

The remaining sections of this chapter are dedicated to a non-perturbative review of cosmology. These concepts are crucial for the development of the subsequent chapters; therefore, I will take the necessary time to review them thoroughly. It is important to note that the cosmology review will only cover topics that are relevant to the upcoming chapters. Subjects such as inflation, perturbative theory of cosmology, and primordial gravitational waves will not be explored in this review as they are beyond the scope of this thesis. However, there will be instances in the subsequent chapters where I will briefly incorporate perturbative information, such as the CMB power spectrum, in a superficial manner without delving deeply into the topic. Hence, it is not necessary to extensively review this aspect.

### 2.1 Special Relativity

The theory of special relativity is grounded on two principles [9]: **(i)** the speed of light has the same value for any inertial frame; **(ii)** the physics laws are the same for all inertial frame. These both postulates have profound consequences for our space and time knowledge. In classical mechanics, both space and time are two independent concepts, while in relativity they are aspects of the same thing, the space-time. Time should be considered as a geometric coordinate [8].

Using Cartesian coordinates, the infinitesimal distance between two points in Euclidean space is calculated using the line element

$$ds^2 = dx^2 + dy^2 + dz^2 = \delta_{ij} dx^i dx^j. \quad (2.1)$$

This object is invariant under rotations and translations. It is also always positive.

Special relativity requires that the line element in Minkowski coordinates takes the

following form

$$ds^2 = dt^2 - dx^2 - dy^2 - dz^2 = \eta_{\mu\nu} dx^\mu dx^\nu. \quad (2.2)$$

This object is invariant under Lorentz transformation (or Lorentz boost). It is a global transformation that connects the measurement between two inertial frames. The matrix  $\eta_{\mu\nu}$  is the Minkowski metric and the above line element describe the so-called Minkowski space-time.

The matrix that represents the Lorentz transformation is denoted by  $[\Lambda^\mu{}_\nu]$ . Therefore, the components of a event  $\{\bar{x}^\mu\}$  in a inertial frame are connected with the components  $\{x^\mu\}$  from the other inertial frame trough the relation

$$\bar{x}^\mu = \Lambda^\mu{}_\nu x^\nu. \quad (2.3)$$

Four-vectors (or Lorentz vectors) are objects whose modules are invariant under Lorentz transformations, and their components transform in the same way that the above relation.

A particle with mass  $m$  has a four-position  $x^\mu = (t, \mathbf{x})$  and its four-velocity is  $U^\mu \equiv dx^\mu/d\tau$ , where  $\tau$  is the proper time. The four-velocity is a useful concept because it is a Lorentz vector. The four-momentum is  $p^\mu \equiv mU^\mu = (E, \mathbf{p})$ , where  $E$  is the energy and  $\mathbf{p}$  is the momentum of the particle. The four-momentum is also a Lorentz vector and its modulus provides the particle mass, i.e.,  $p_\mu p^\mu \equiv p^2 = m^2$ . The immediate consequence of this equation is the famous equation

$$E^2 = \mathbf{p}^2 + m^2, \quad (2.4)$$

which tells us that the mass is the particle rest energy ( $E_0 = m$ ). That also informs that massless energy particles is  $E = |\mathbf{p}|$ .

The Minkowski metric has the matrix representation

$$[\eta_{\mu\nu}] = \text{diag}(+1, -1, -1, -1), \quad (2.5)$$

and its inverse matrix is

$$[\eta^{\mu\nu}] = \text{diag}(+1, -1, -1, -1). \quad (2.6)$$

Thus, we can write

$$\eta^{\mu\alpha} \eta_{\alpha\nu} = \delta^\mu_\nu. \quad (2.7)$$

A Lorentz four-vector has its components in a covariant representation  $V_\mu$ , and it also has the components in a contravariant representation  $V^\mu$ . The relation between these two components is  $V^\mu = \eta^{\mu\nu} V_\nu$  or  $V_\mu = \eta_{\mu\nu} V^\nu$ .



We can define the Lorentz tensor as an object with many indices that upon undergoing a Lorentz transformation (LT) its contravariant components change in the following way:

$$T^{\alpha_1 \dots \alpha_n} \xrightarrow{LT} \bar{T}^{\alpha_1 \dots \alpha_n} = \Lambda^{\alpha_1}_{\beta_1} \dots \Lambda^{\alpha_n}_{\beta_n} T^{\beta_1 \dots \beta_n}. \quad (2.8)$$

The connection between covariant and contravariant Lorentz tensors is provided by the Minkowski metric, i.e.,

$$T_{\alpha_1 \dots \alpha_n} \equiv \eta_{\alpha_1 \beta_1} \dots \eta_{\alpha_n \beta_n} T^{\beta_1 \dots \beta_n}. \quad (2.9)$$

It is important to emphasize that any identity with Lorentz tensors is true for all the inertial frames. This section began with the requirement that the physics laws are the same for all inertial frames, thus writing the physical equation in tensor form is enough for the special relativity second postulate to be obeyed.

The energy-momentum tensor  $T^{\mu\nu}$  is one of the most important objects of special relativity. It is symmetric and obeys the conservation equation

$$\partial_\mu T^{\mu\nu} = 0. \quad (2.10)$$

In many applications, we deal with perfect fluids, with a four-velocity field  $U^\mu$ , a scalar pressure  $P$ , and a scalar energy density  $\rho$ . Such fluids are described by the energy-momentum tensor

$$T^{\mu\nu} = (\rho + P)U^\mu U^\nu - P\eta^{\mu\nu}. \quad (2.11)$$

This tensor when inserted in the conservation law Eq. 2.10 provides the relativistic version of the continuity equation and Euler equation for fluids, which are the necessary relation to describe a perfect fluid.

## 2.2 General Relativity

### 2.2.1 Tensors

General Relativity extends the second postulate of Special Relativity replacing inertial frame to all frames, i.e., the laws of physics must be the same for all frames. Therefore, the Lorentz tensor should be replaced by a more general class of tensors, where tensor identities hold in all reference frames.

To construct this idea of tensor, let's suppose that exists a scalar field  $\phi$  defined over all spacetime. We calculate the value of  $\phi$  in each point of a region using the set of coordinates  $x^\mu$ . But, there is nothing special in this coordinate system, therefore we can calculate  $\phi$  using other coordinates  $\bar{x}^\mu$ .

Lets calculate,

$$\frac{\partial \phi}{\partial \bar{x}^\mu} = \frac{\partial \phi}{\partial x^\nu} \frac{\partial x^\nu}{\partial \bar{x}^\mu} \Rightarrow \bar{\partial}_\mu = \frac{\partial x^\nu}{\partial \bar{x}^\mu} \partial_\nu. \quad (2.12)$$

The above equation is the prototype of a covariant tensor, i.e., an n-rank covariant tensor  $T$  is defined as an object whose components transform in the following way

$$\bar{T}_{\mu_1 \dots \mu_n} = \frac{\partial x^{\nu_1}}{\partial \bar{x}^{\mu_1}} \dots \frac{\partial x^{\nu_n}}{\partial \bar{x}^{\mu_n}} T_{\nu_1 \dots \nu_n}, \quad (2.13)$$

when a coordinate transformation  $x^\mu \rightarrow \bar{x}^\mu$  is made.

The prototype for the contravariant tensor is the transformation law of the differential  $dx^\mu$  under the coordinate transformation  $x^\mu \rightarrow \bar{x}^\mu$ ,

$$d\bar{x}^\mu = \frac{\partial \bar{x}^\mu}{\partial x^\nu} dx^\nu. \quad (2.14)$$

Therefore, a contravariant n-rank tensor  $T$  is defined as an object whose components transform as

$$T^{\mu_1 \dots \mu_n} = \frac{\partial \bar{x}^{\mu_1}}{\partial x^{\nu_1}} \dots \frac{\partial \bar{x}^{\mu_n}}{\partial x^{\nu_n}} T^{\nu_1 \dots \nu_n}, \quad (2.15)$$

when a coordinate transformation  $x^\mu \rightarrow \bar{x}^\mu$  is made.<sup>1</sup>

To show the straightforward way to define a mixed tensor, consider the tensor

$$\bar{T}^\alpha_{\beta} = \frac{\partial \bar{x}^\alpha}{\partial x^\mu} \frac{\partial x^\nu}{\partial \bar{x}^\beta} T^\mu_{\nu}. \quad (2.16)$$

Supposing that in a reference frame the identity  $T^\mu_{\nu} = 0$ , the above equation implies that in any other frame, this equality holds true, i.e.,  $\bar{T}^\alpha_{\beta} = 0$ . As anticipated at the beginning of this subsection, the main important consequence of the definition of tensors is that a tensor equation holds for all coordinates. General Relativity is constructed on the demand that physical laws should hold for all frames. Therefore, all fundamental equations should be written in the tensor form.

## 2.2.2 Metric and Connection

General relativity is the best description of gravity that we have until now. In this theory, gravity is the manifestation of the curvature of spacetime. The presence of matter and energy generates curvature. Unlike the Newtonian formulation, gravity is no longer treated as a force. A remarkable point that makes this paradigm very clear is the idea that particles that interact only gravitationally are considered free particles, i.e., they move in geodesics. Therefore, the role of the other interactions is to make the particles deviate from the geodesic path.

<sup>1</sup> The Lorentz tensor is only a special class of tensors where  $\frac{\partial x^\mu}{\partial \bar{x}^\nu} = \Lambda^\mu_{\nu}$ .

The first important object of the theory is the metric  $g_{\mu\nu}$ , a second-rank tensor that is a unique function of the coordinates  $\{x^\mu\}$  used to describe spacetime. It informs us how to calculate distance, proper time, proper length, area, volume, and any other geometric information needed.

The line element

$$ds^2 = g_{\mu\nu}(x)dx^\mu dx^\nu \quad (2.17)$$

is an object with a pseudo-Riemannian structure, invariant under coordinates transformations. It is pseudo-Riemannian because  $ds^2$  can be positive, null, or negative. Free massive particles move in geodesics with a positive line element, while free massless particles move in geodesics with a null line element. No particle moves on trajectories with  $ds^2 < 0$ , otherwise, there would be a causality break.

To find the geodesic equations it is necessary to extremize the functional

$$\int d\lambda \sqrt{g_{\mu\nu} \frac{dx^\mu}{d\lambda} \frac{dx^\nu}{d\lambda}}, \quad (2.18)$$

where  $\lambda$  is an affine parameter defined over the entire geodesic. This is done using the Euler-Lagrange equation,

$$\left[ \frac{\partial}{\partial x^\alpha} - \frac{d}{d\lambda} \frac{\partial}{\partial (dx^\alpha/d\lambda)} \right] \sqrt{g_{\mu\nu} \frac{dx^\mu}{d\lambda} \frac{dx^\nu}{d\lambda}} = 0. \quad (2.19)$$

Thus, the geodesic  $x = x(\lambda)$  is the solution of the equation

$$\frac{d^2 x^\mu}{d\lambda^2} + \Gamma_{\alpha\beta}^\mu \frac{dx^\alpha}{d\lambda} \frac{dx^\beta}{d\lambda} = 0. \quad (2.20)$$

Where the connection  $\Gamma_{\alpha\beta}^\mu$  is a symmetric object ( $\Gamma_{\alpha\beta}^\mu = \Gamma_{\beta\alpha}^\mu$ ) and it is related to the metric through the identity

$$\Gamma_{\alpha\beta}^\mu = \frac{1}{2} g^{\mu\nu} (\partial_\alpha g_{\nu\beta} + \partial_\beta g_{\alpha\nu} - \partial_\nu g_{\alpha\beta}). \quad (2.21)$$

It is interesting to note extremize the functional

$$\int d\lambda g_{\mu\nu} \frac{dx^\mu}{d\lambda} \frac{dx^\nu}{d\lambda} \quad (2.22)$$

also provides the geodesic equation (Eq. 2.20). This greatly facilitates the work of finding the geodesic of a specific geometry. Another important point is that extremize the above functional is a direct way to determine the connections without using Eq. 2.21.

### 2.2.3 The covariant derivative and the Riemann tensor

Unfortunately, the partial derivative of a vector does not transform as a tensor. To address this issue, the concept of a covariant derivative is introduced. The covariant derivative of a contravariant vector component is defined as:

$$\nabla_\mu V^\nu = \partial_\mu V^\nu + \Gamma_{\alpha\mu}^\nu V^\alpha. \quad (2.23)$$

Similarly, the covariant derivative of a covariant vector component is defined as:

$$\nabla_\mu V_\nu = \partial_\mu V_\nu - \Gamma_{\nu\mu}^\alpha V_\alpha. \quad (2.24)$$

The generalization of the covariant derivative to higher-ranked tensors is straightforward. As an example, the covariant derivative of a generic contravariant tensor of rank 2, denoted as  $T^{\alpha\beta}$ , is given by:

$$\nabla_\mu T^{\alpha\beta} = \partial_\mu T^{\alpha\beta} + \Gamma_{\nu\mu}^\alpha T^{\nu\beta} + \Gamma_{\nu\mu}^\beta T^{\alpha\nu}. \quad (2.25)$$

The covariant derivative of the metric tensor and its inverse satisfies the following relations:

$$\nabla_\mu g_{\alpha\beta} = 0 \quad \text{and} \quad \nabla_\mu g^{\alpha\beta} = 0. \quad (2.26)$$

Partial derivatives commutes, however, this is not true for the covariant derivative. The commutator of covariant derivatives is defined as:

$$[\nabla_\beta, \nabla_\alpha]V_\nu \equiv R^\mu_{\nu\alpha\beta}V_\mu, \quad (2.27)$$

where  $R^\mu_{\nu\alpha\beta}$  represents the components of the Riemann tensor. It is given by:

$$R^\mu_{\nu\alpha\beta} = \nabla_\alpha \Gamma_{\nu\beta}^\mu - \nabla_\beta \Gamma_{\nu\alpha}^\mu + \Gamma_{\nu\beta}^\lambda \Gamma_{\lambda\alpha}^\mu - \Gamma_{\nu\alpha}^\lambda \Gamma_{\lambda\beta}^\mu. \quad (2.28)$$

The Riemann tensor characterizes the curvature of spacetime. If all components of the Riemann tensor are null, the spacetime is Minkowskian [8].

The Riemann tensor components obey the following properties:

$$R^\mu_{\nu\alpha\beta} + R^\mu_{\alpha\beta\nu} + R^\mu_{\beta\nu\alpha} = 0 \quad (2.29a)$$

$$R^\mu_{\nu\alpha\beta} = -R^\mu_{\nu\beta\alpha} \quad (2.29b)$$

$$R_{\mu\nu\alpha\beta} = -R_{\nu\mu\alpha\beta} \quad (2.29c)$$

$$R_{\mu\nu\alpha\beta} = R_{\alpha\beta\mu\nu} \quad (2.29d)$$

$$R^\mu_{\mu\alpha\beta} = 0 \quad (2.29e)$$

$$\nabla_\lambda R^\mu_{\nu\alpha\beta} + \nabla_\alpha R^\mu_{\nu\beta\lambda} + \nabla_\beta R^\mu_{\nu\lambda\alpha} = 0. \quad (2.29f)$$

These properties reduce the number of independent components of the Riemann tensor to 20.

## 2.2.4 The Einstein equation

The Ricci tensor is one of the terms of the equation that describes the space-time dynamics. It is a symmetric 2-rank tensor defined by

$$R_{\mu\nu} \equiv R^\alpha_{\mu\nu\alpha} = \partial_\nu \Gamma^\alpha_{\mu\alpha} - \partial_\alpha \Gamma^\alpha_{\mu\nu} + \Gamma^\alpha_{\mu\beta} \Gamma^\beta_{\alpha\nu} - \Gamma^\alpha_{\mu\nu} \Gamma^\beta_{\alpha\beta}. \quad (2.30)$$

The contraction between the Ricci tensor and the metric is called the Ricci scalar:

$$R = g^{\alpha\beta} R_{\alpha\beta} \quad (2.31)$$

The combination

$$G_{\mu\nu} = R_{\mu\nu} - \frac{1}{2} R g_{\mu\nu} \quad (2.32)$$

is called Einstein tensor and has a vanishing covariant divergence, i.e.,

$$\nabla_\mu G^{\mu\nu} = 0. \quad (2.33)$$

Einstein's equation,

$$R_{\mu\nu} - \frac{1}{2} R g_{\mu\nu} + \Lambda g_{\mu\nu} = -8\pi T_{\mu\nu}, \quad (2.34)$$

describes the dynamics of spacetime. The left-hand side involves metric derivatives in a highly nonlinear manner. The right-hand side is a multiple of the energy-momentum tensor  $T_{\mu\nu}$ , which serves as the source of curvature. In summary, Einstein's equation is a nonlinear equation for the metric tensor. Solving it is equivalent to obtaining all the geometric information of a given spacetime.

It is fundamental to note that the energy-momentum tensor is divergenceless, i.e.,

$$\nabla_\mu T^{\mu\nu} = 0, \quad (2.35)$$

which represents the general conservation equation.

## 2.3 Friedmann-Robertson-Walker Geometry

### 2.3.1 Friedmann's and acceleration equation

Cosmological observations show that on large scales the universe is homogeneous and isotropic [8, 10, 11].<sup>2</sup> Homogeneity is understood as a translation symmetry, while isotropy is a rotation symmetry. In a philosophic way, the cosmological principle means that there is no privileged place in the Universe.

<sup>2</sup> In the Cosmology development there was an understanding that structure formation like galaxies and galaxy clusters requires some fluctuations in the matter density. The microwave background also has anisotropy in photons' temperature. Hence, a more accurate study of the Universe requires small inhomogeneities.

A homogeneous and isotropic universe is a maximal symmetric spacetime that is described by a Friedmann-Robertson-Walker (FRW) metric [12, 10, 8]:

$$ds^2 = dt^2 - R^2(t) \left[ \frac{dr^2}{1 - kr^2} + r^2(d\theta^2 + \sin^2 \theta d\phi^2) \right]. \quad (2.36)$$

The constant  $k$  is related to the spatial geometry. For  $k = -1$ , the space is open and has a flat hyperbolic geometry. When  $k = 0$  the geometry is flat. If  $k = 1$ , the space is closed and has a spherical geometry.<sup>3</sup>

It is important to understand that homogeneity and isotropy do not mean that the universe has no dynamic. The presence of matter and energy induces a certain geometry that describes space-time on large scales. This curvature source can be modeled as a perfect fluid, the cosmological fluid, in which the energy-momentum tensor is

$$T^{\mu\nu} = (\rho + P)U^\mu U^\nu - Pg^{\mu\nu}, \quad (2.37)$$

where  $P$  is the pressure,  $\rho$  is the energy density, and  $U^\mu$  is the fluid four-velocity.

The comoving coordinate system is the one adopted in Cosmology comoving frame the four-velocity is  $U^\mu = (1, \mathbf{0})$

All the mathematics of cosmology is developed in the comoving coordinate system, where the cosmological fluid has fixed spatial coordinates, i.e., the fluid four-velocity is  $U^\mu = \delta^\mu_\nu$  [8]. Consequently, the approximation or distancing of comoving observers is due to the malleability of spacetime itself, generating a recession velocity.

The FRW metric allows us to define the functional

$$L = \dot{t}^2 - R^2(t) \left[ \frac{\dot{r}^2}{1 - kr^2} + r^2(\dot{\theta}^2 + \sin^2 \theta \dot{\phi}^2) \right], \quad (2.38)$$

where  $\dot{x}^\mu \equiv dx^\mu/d\lambda$ ,  $\lambda$  being an affine parameter.<sup>4</sup>

Extremizing this functional provides the geodesic equations for FRW geometries, which gives the connections below.

$$\Gamma_{rr}^t = \frac{R\dot{R}}{1 - kr^2} \quad \Gamma_{\theta\theta}^t = r^2 R\dot{R} \quad \Gamma_{\phi\phi}^t = (r \sin \theta)^2 R\dot{R} \quad (2.39a)$$

$$\Gamma_{tr}^r = \frac{\dot{R}}{R} \quad \Gamma_{rr}^r = \frac{kr}{1 - kr^2} \quad \Gamma_{\theta\theta}^r = -r(1 - kr^2) \quad \Gamma_{\phi\phi}^r = -r(1 - kr^2) \sin^2 \theta \quad (2.39b)$$

<sup>3</sup> Here, I will sketch how to deduce that  $k = \pm 1$  are hyperbolic and spherical geometries. First, it is necessary to take the hypersurface that delimits the desired geometric shape, after that, the metric should be induced. The hyperbolic hypersurface  $w^2 - (x^2 + y^2 + z^2) = R^2$  in the Minkowski spacetime has  $d\sigma^2 = dw^2 - (dx^2 + dy^2 + dz^2) = -R^2 \left[ \frac{dr^2}{1 - r^2} + r^2(d\theta^2 + \sin^2 \theta d\phi^2) \right]$  as the induced metric. A spherical hypersurface  $x^2 + y^2 + z^2 + w^2 = R^2$  in the 4D Euclidean space has  $d\sigma^2 = dw^2 + dx^2 + dy^2 + dz^2 = \frac{dr^2}{1 - r^2} + r^2(d\theta^2 + \sin^2 \theta d\phi^2)$  as the induced metric.

<sup>4</sup> Here there is a notation that can be misleading. In almost all moments I use the dot notation to express a time derivative, but in the context of extremizing the  $L$  functional to obtain the geodesic equation, the dot notation means a derivative with respect to the affine parameter  $\lambda$ .

$$\Gamma_{t\theta}^\theta = \frac{\dot{R}}{R} \quad \Gamma_{r\theta}^\theta = \frac{1}{r} \quad \Gamma_{\phi\phi}^\theta = -\sin\theta \cos\theta \quad (2.39c)$$

$$\Gamma_{t\phi}^\phi = \frac{\dot{R}}{R} \quad \Gamma_{t\phi}^\phi = \frac{1}{r} \quad \Gamma_{\theta\phi}^\phi = \cot\phi \quad (2.39d)$$

Applying these connections in Eq. 2.30 gives the Ricci tensor components:

$$R_{tt} = \frac{3\ddot{R}}{R}, \quad (2.40a)$$

$$R_{rr} = -\frac{R\ddot{R} + 2\dot{R}^2 + 2k}{1 - kr^2}, \quad (2.40b)$$

$$R_{\theta\theta} = -r^2(R\ddot{R} + 2\dot{R}^2 + 2k), \quad (2.40c)$$

$$R_{\phi\phi} = R_{\theta\theta} \sin^2\theta. \quad (2.40d)$$

To describe the universe it is needed to solve Einstein's equation (Eq. 2.34).

$$R_{00} = -8\pi T_{00} \Rightarrow \ddot{R} = -\frac{4\pi}{3}(\rho + 3P)R + \frac{\Lambda}{3}R. \quad (2.41)$$

Which is the so-called acceleration-equation. It is important to note that this equation does not depend explicitly on the curvature  $k$ .

$$R_{11} = -8\pi T_{11} \Rightarrow \dot{R}^2 = \frac{8\pi}{3}\rho R^2 + \frac{\Lambda}{3}R^2 - k. \quad (2.42)$$

It is usual to work with the normalized scale factor,

$$a(t) \equiv \frac{R(t)}{R(t_0)} = \frac{R}{R_0}. \quad (2.43)$$

Where  $t_0$  is the “current” moment of the Universe. Note that  $a(t_0) = a_0 = 1$ .

Therefore, Eq. 2.41 becomes

$$\boxed{\ddot{a} = -\frac{4\pi}{3}(\rho + 3P)a + \frac{\Lambda}{3}a.} \quad (2.44)$$

Diving Eq. 2.42 by  $R^2$  and setting the Hubble parameter to

$$H(t) \equiv \frac{\dot{R}}{R} = \frac{\dot{a}}{a}, \quad (2.45)$$

one of the standard forms of Friedmann equations is obtained.

$$\boxed{H^2 = \frac{8\pi}{3}\rho + \frac{\Lambda}{3} - \frac{k}{R^2}.} \quad (2.46)$$

The above equation provides a clue that the cosmological constant should be considered a non-trivial fluid with constant energy density

$$\boxed{\rho_\Lambda = \frac{\Lambda}{8\pi}.} \quad (2.47)$$

This is the so-called dark energy density. With this definition, Eq. 2.46 can be rewrite in the following way:

$$H^2 = \frac{8\pi}{3} \left[ \rho + \rho_\Lambda - \left( \frac{3}{8\pi} \right) \frac{k}{R^2} \right] = H_0^2 \left( \frac{8\pi}{3H_0^2} \right) \left[ \rho + \rho_\Lambda - \left( \frac{3}{8\pi} \right) \frac{k}{R^2} \right], \quad (2.48)$$

where  $H_0 \equiv H(t_0)$ .

It is usual to define the critical density as

$$\rho_{\text{crit}} = \frac{3H^2}{8\pi}. \quad (2.49)$$

Therefore, the Friedmann equation becomes

$$H^2 = \frac{H_0^2}{\rho_{\text{crit},0}} \left[ \rho + \rho_\Lambda - \left( \frac{3}{8\pi} \right) \frac{k}{R^2} \right]. \quad (2.50)$$

Where,  $\rho_{\text{crit},0} \equiv \rho_{\text{crit}}(t_0)$ .

Einstein's equation also provides the condition  $\nabla_\mu T^{\mu\nu} = 0$ , which does not generate any new independent equation, but  $\nabla_\mu T^{\mu 0} = 0$  gives a very physical identity:

$$\boxed{\dot{\rho} + 3H(\rho + P) = 0}. \quad (2.51)$$

That is the cosmological manifestation of the first law of Thermodynamics! <sup>5</sup>

### 2.3.2 Four-momentum in null curvature case

The most important FRW geometry case is the null curvature, in which the line element is

$$ds^2 = dt^2 - a^2 (dx^2 + dy^2 + dz^2). \quad (2.52)$$

Note that here I am using the Minkowskian coordinates,  $t, x, y, z$ , while in Eq. 2.36 it was used the spherical coordinates for the spatial part.

In this case, the proper time is given by

$$d\tau^2 = dt^2(1 - a^2\mathbf{v}^2), \quad (2.53)$$

where I am using the traditional definition of velocity  $\mathbf{v} = d\mathbf{x}/dt$ . Hence the relation between the proper time and the coordinate times is

$$dt = \frac{d\tau}{\sqrt{1 - a^2\mathbf{v}^2}}. \quad (2.54)$$

<sup>5</sup> To see this, imagine a perfect fluid with no heat exchange and no chemical potential. The variation of the internal energy of this system is  $dU = -PdV$ . The internal energy is proportional to the energy density and the volume, thus

$$d(\rho R^3) = -PdR^3 \Rightarrow \dot{\rho} + 3H(\rho + P) = 0.$$

This gives us a clue that the Universe entropy is constant, something that I will explore more in Sect. 2.5.



In special relativity, the Lorentz factor ( $\gamma$ ) is defined by the relation  $dt = \gamma d\tau$  [9]. Using this same definition and the above equation, the Lorentz factor to FRW geometry with null curvature is

$$\gamma \equiv \frac{1}{\sqrt{1 - a^2 \mathbf{v}^2}}. \quad (2.55)$$

In special relativity, the four-momentum of a massive particle is defined as  $p^\mu \equiv m dx^\mu / d\tau$ . For general relativity, the definition is the same, because of the equivalence principle [8]. The difference is that in special relativity the space-time is Minkowskian, while in general relativity the space-time is curved. The famous energy-momentum relation,  $E^2 = \mathbf{p}^2 + m^2$ , comes from the identity  $g_{\mu\nu} p^\mu p^\nu = m^2$ . Using the equivalence principle this must also hold for general relativity, but this generates a non-usual expression for the energy and momentum.

In special relativity, the four-momentum of a massive particle is defined as  $p^\mu \equiv m dx^\mu / d\tau$ . This definition remains the same in general relativity due to the equivalence principle [8]. The key difference is that in special relativity, the space-time is Minkowskian, whereas, in general relativity, the space-time is curved. The well-known energy-momentum relation  $E^2 = \mathbf{p}^2 + m^2$  arises from the identity  $g_{\mu\nu} p^\mu p^\nu = m^2$ . Utilizing the equivalence principle, this relation must also hold in general relativity, but it yields new expressions for energy and momentum.

Adopting the line element given by Eq. 2.52, the  $p^2$  expression gives

$$m^2 \left( \frac{dt}{d\tau} \right)^2 - m^2 a^2 \left( \frac{d\mathbf{x}}{d\tau} \right)^2 = m^2. \quad (2.56)$$

It is straighter to interpret the term

$$E \equiv m \frac{dt}{d\tau} = m\gamma, \quad (2.57)$$

as the massive particle energy, and

$$\mathbf{p} \equiv ma \frac{d\mathbf{x}}{d\tau} = ma\gamma \mathbf{v} \quad (2.58)$$

is the massive particle momentum.

At this moment is interesting to obtain the geodesic equation for this geometry. This is done by extremizing the functional

$$L = \dot{t}^2 - a^2 (\dot{x}^2 + \dot{y}^2 + \dot{z}^2). \quad (2.59)$$

Again I warn you that just in this case dot notation represents a derivative in the affine parameter, not in time.

The Euler-Lagrange equation

$$\frac{\partial L}{\partial t} - \frac{d}{d\lambda} \left( \frac{\partial L}{\partial \dot{t}} \right) = 0, \quad (2.60)$$

provides that time geodesic equation is given by

$$\frac{d^2 t}{d\lambda^2} + a \frac{da}{d\lambda} \left[ \left( \frac{dx}{d\lambda} \right)^2 + \left( \frac{dy}{d\lambda} \right)^2 + \left( \frac{dz}{d\lambda} \right)^2 \right] = 0. \quad (2.61)$$

The spatial Euler-Lagrange equation,

$$\frac{\partial L}{\partial \mathbf{x}} - \frac{d}{dt} \left( \frac{\partial L}{\partial \mathbf{v}} \right) = 0, \quad (2.62)$$

results that the vector  $a^2 d\mathbf{x}/d\lambda$  is constant over the geodesic path. Since  $ad\mathbf{x}/d\lambda$  is the momentum of a free particle, it follows that the vector  $a\mathbf{p}$  is constant along the geodesic path. Therefore, momentum is inversely proportional to the scale factor:

$$\boxed{\mathbf{p} \propto \frac{1}{a}.} \quad (2.63)$$

This result has significant implications. In an expanding universe, the scale factor increases over time, leading to a decrease in the momentum of free particles. This observation highlights a key aspect introduced by general relativity: there is no momentum conservation in an expanding universe. As a consequence, massive particles eventually become non-relativistic at a certain stage. Due to the energy-momentum relation, the energy of a free massive particle is not conserved in the same manner.

Photons move along null geodesics, which means that the proper time cannot be used as an affine parameter. However, any affine parameter can be used to define the photon four-momentum, denoted as  $p_\gamma^\mu = dx^\mu/d\lambda$ . In this case,  $E_\gamma \equiv dt/d\lambda$  and  $\mathbf{p}_\gamma \equiv ad\mathbf{x}/d\lambda$ . These definitions preserve the well-known energy-momentum relation for photons:  $E_\gamma = |\mathbf{p}_\gamma|$ . There is an interesting consequence in this case: just like massive particles, the momentum of photons also decreases with time. As a result, the energy of free photons decreases with the passage of time:

$$\boxed{E_\gamma \propto \frac{1}{a}.} \quad (2.64)$$

This implies that cosmological photons experience a redshift due to the expansion of the universe [8, 12, 11, 10].

If a source of photons emits photons at a frequency  $\nu$  at time  $t$ , and these photons are detected today at a frequency  $\nu_0$ , the redshift parameter  $z$  is defined as [8, 13]:

$$z = \frac{\nu - \nu_0}{\nu_0} \Rightarrow 1 + z = \frac{\nu}{\nu_0}. \quad (2.65)$$

It is important to note that a positive value of  $z$  corresponds to a redshift, indicating that the observed frequency  $\nu$  is lower than the emitted frequency  $\nu_0$ . Conversely, a negative value of  $z$  represents a blueshift, indicating that the observed frequency is higher than the

emitted frequency. The case where  $z = 0$  corresponds to no shift in frequency and is not assigned a special name. In the context of cosmology, due to the overall expansion of the universe, the observed cosmological photons almost always exhibit a redshift.

According to quantum mechanics, the energy  $E_\gamma$  of a photon is directly proportional to its frequency  $\nu$  [14]. Combining this relation with Equation 2.64 the connection between scale factor and redshift is obtained:

$$\frac{\nu}{\nu_0} = \frac{a_0}{a} = \frac{1}{a} \Rightarrow \boxed{1 + z = \frac{1}{a}}. \quad (2.66)$$

Some cosmologists use cosmological time ( $t$ ) as a reference for event occurrences in the universe, while others prefer to utilize redshift. The previously derived result establishes a connection between these two methods of recording events.<sup>6</sup>

### 2.3.3 Geodesic on flat FRW geometry using spatial spherical coordinates

In the last section, I used the geodesic equation for a flat FRW geometry in Euclidean space coordinates. Now, I will study the geodesic equation using polar coordinates. However, instead of using the geodesic expression given by Eq. 2.20, I will employ an alternative version of this equation.

First, let's recall that the four-velocity  $U^\mu$  is defined as  $dx^\mu/d\lambda$ , where  $\lambda$  is an affine parameter. With this definition, the geodesic equation becomes:

$$\frac{dU^\nu}{d\lambda} + \Gamma_{\alpha\beta}^\nu U^\alpha U^\beta = 0. \quad (2.67)$$

Multiplying this equation by  $g_{\nu\mu}$  and using the definition of the connections given in Eq. 2.21, I obtain the following result:

$$\frac{dU^\nu}{d\lambda} + \left( \partial_\alpha g_{\mu\nu} - \frac{1}{2} \partial_\mu g_{\alpha\beta} \right) U^\alpha U^\beta = 0. \quad (2.68)$$

This equation can be rewritten in a useful form as:

$$\boxed{\frac{dU_\mu}{d\lambda} = \frac{1}{2} (\partial_\mu g_{\alpha\beta}) U^\alpha U^\beta}. \quad (2.69)$$

This form of the geodesic equation is very powerful as it automatically yields the conserved components along the geodesic.

Now, I will apply the metric for a flat universe in spherical spatial coordinates,  $ds^2 = dt^2 - a^2[dr^2 + r^2(d\theta^2 + \sin^2\theta d\phi^2)]$ , to Eq. 2.69 in order to determine the conserved quantities along a geodesic path.

<sup>6</sup> The temperature of photons can also serve as a parameter to identify the timing of events. I will soon explore the connection between photons' energy and the scale factor.

Let's start with the  $\phi$  component:

$$\frac{dU_\phi}{d\lambda} = \frac{1}{2}(\partial_\phi g_{\alpha\beta})U^\alpha U^\beta = 0 \Rightarrow U_\phi = 0 \quad (2.70)$$

However,  $U_\phi$  is equivalent to  $g_{\phi\alpha}U^\alpha$ , which is the same as  $-a^2 r^2 \sin^2 \theta d\phi/d\lambda$ . Thus, this last expression represents the conserved quantity. In the Big Bang model, defined by setting  $a(0) = 0$ ,  $U_\phi(0) = 0$ . Therefore, the conclusion is that through the geodesic the  $\phi$  component is constant.

The calculations for the  $\theta$  component are very similar to the previous case:

$$\frac{dU_\theta}{d\lambda} = \frac{1}{2}(\partial_\theta g_{\alpha\beta})U^\alpha U^\beta = \frac{1}{2}(\partial_\theta g_{\phi\phi})U^\phi U^\phi = 0, \quad (2.71)$$

where the last identity holds because  $\phi$  is constant along the geodesic.

It was found that  $U_\theta$  is constant along the geodesic, which is the same as saying that  $g_{\theta\theta}U^\theta = -a^2 r^2 d\theta/d\lambda$  is also constant. Therefore, the Big Bang condition,  $a(0) = 0$  implies that  $\theta$  must be constant.

The constancy of the  $\theta$  and  $\phi$  components along the geodesic was initially deduced under the assumption of non-curvature. However, it is important to know that these conditions also hold in the curved cases of FRW geometries.

The calculations for  $U_r$  are straightforward and confirm that this quantity remains constant along the geodesic. In other words, this implies that  $a^2 dr/d\lambda$  remains constant as well.

## 2.4 Number density, energy density, and pressure

### 2.4.1 Equation of state

Cosmology usually deals with fluids whose pressure is proportional to energy density,

$$P = w\rho. \quad (2.72)$$

In the following subsections, I will show that a non-relativistic fluid has  $w = 0$  and a relativistic fluid has  $w = 1/3$ .<sup>7</sup> This kind of equation of state simplifies a lot the solution of Eq. 2.51, as you can see below.

$$\dot{\rho} + 3H(1+w)\rho = 0 \Rightarrow \rho \propto \frac{1}{a^{3(1+w)}} \Rightarrow \boxed{\begin{cases} \rho \propto \frac{1}{a^3}, & w = 0 \quad (\text{dust}) \\ \rho \propto \frac{1}{a^4}, & w = 1/3 \quad (\text{radiation}) \end{cases}} \quad (2.73)$$

Dark energy is a non-usual fluid that also follows the state of equation (2.72). In the dark energy case  $P = -\rho$ . I will explore more this point in Sect. 2.9.3.

<sup>7</sup> In many moments non-relativistic fluids are called dust or cold particles, and relativistic fluids are labeled radiation or hot particle. I will use all these nomenclatures in the scope of this thesis.

### 2.4.2 Equilibrium thermodynamics

In cosmology, we are usually concerned about the number density  $n$ , the energy density  $\rho$ , and the pressure  $P$  of some perfect fluid. To calculate these quantities we only need the energy spectrum  $E$ , the specie degeneracy  $g_s$ , and the function distribution  $f$  [15].

$$n(t, \mathbf{x}) = g_s \int \frac{d^3 \mathbf{p}}{(2\pi)^3} f(t, \mathbf{x}, \mathbf{p}) \quad (2.74)$$

$$\rho(t, \mathbf{x}) = g_s \int \frac{d^3 \mathbf{p}}{(2\pi)^3} E(\mathbf{p}) f(t, \mathbf{x}, \mathbf{p}) \quad (2.75)$$

$$P(t, \mathbf{x}) = g_s \int \frac{d^3 \mathbf{p}}{(2\pi)^3} \frac{\mathbf{p}^2}{3E(\mathbf{p})} f(t, \mathbf{x}, \mathbf{p}) \quad (2.76)$$

The distribution function  $f$  depends on the spin nature of the fluid constituent. For bosonic particles, it is necessary to use the Bose-Einstein distribution function

$$f_{BE} = \frac{1}{e^{(E-\mu)/T} - 1}, \quad (2.77)$$

where  $T$  is the temperature and  $\mu$  is the chemical potential.

For fermionic particles, it is mandatory to employ the Fermi-Dirac distribution function

$$f_{FD} = \frac{1}{e^{(E-\mu)/T} + 1}. \quad (2.78)$$

An essential case is a limit where  $e^{-\mu/T} \gg 1$ , in which the Bose-Einstein and Fermi-Dirac distribution functions have the same behavior [15]:

$$f_{BE,FD} \approx e^{-(E-\mu)/T}. \quad (2.79)$$

### 2.4.3 Equation of state for dust

Dust is a non-relativistic fluid, i.e., the energy-momentum relation of its constituent is  $E = \mathbf{p}^2/(2m) + m$ , where the rest energy  $m$  is much bigger than kinetic energy  $\mathbf{p}^2/(2m)$ . For dust, the distribution function provided by Eq. 2.79 is enough to obtain  $n$  (Eq. 2.74),  $\rho$  (Eq. 2.75), and  $P$  (Eq. 2.76).

The number density gives

$$\begin{aligned} n_{\text{dust}} &= g_s \int \frac{d^3 \mathbf{p}}{(2\pi)^3} \exp \left[ -\frac{1}{T} \left( \frac{\mathbf{p}^2}{2m} + m - \mu \right) \right] \\ &\Rightarrow \boxed{n_{\text{dust}} = g_s \left( \frac{mT}{2\pi} \right)^{3/2} \exp \left( \frac{\mu - m}{T} \right)}. \end{aligned} \quad (2.80)$$

The energy density requires more careful analysis.

$$\rho_{\text{dust}} = g_s \int \frac{d^3 \mathbf{p}}{(2\pi)^3} \left( \frac{\mathbf{p}^2}{2m} + m \right) \exp \left[ -\frac{1}{T} \left( \frac{\mathbf{p}^2}{2m} + m - \mu \right) \right] = \left( m + \frac{3T}{2} \right) n_{\text{dust}}. \quad (2.81)$$

The work is not done yet. First, notice that the condition  $e^{-\mu/T} \gg 1$  implies that  $-\mu/T \gg 1$ . In the above result the Boltzmann suppression factor  $\exp[-(m - \mu)/T]$  demands that  $m/T \gg 1$ , otherwise the factor  $m/T$  would not be relevant. In this condition,  $m + 3T/2 \approx m$ . Therefore the energy density of dust is

$$\boxed{\rho_{\text{dust}} = mn_{\text{dust}}}. \quad (2.82)$$

The last step is the pressure calculation.

$$P_{\text{dust}} = g_s \int \frac{d^3\mathbf{p}}{(2\pi)^3} \frac{\mathbf{p}^2}{3m} \exp\left[-\frac{1}{T} \left(\frac{\mathbf{p}^2}{2m} + m - \mu\right)\right] = \frac{\rho_{\text{dust}} T}{m}. \quad (2.83)$$

As I pointed out before,  $m \gg T$ , which implies that  $P_{\text{dust}} \ll \rho$ . This is the reason some books define dust as a pressureless fluid.

$$\boxed{P_{\text{dust}} \approx 0}. \quad (2.84)$$

Applying this result to Eq. 2.51, the cosmological evolution of dust energy density is obtained.

$$\dot{\rho}_{\text{dust}} + 3H\rho_{\text{dust}} = 0 \Rightarrow \frac{d}{dt}(\rho_{\text{dust}} a^3) \Rightarrow \boxed{\rho_{\text{dust}} \propto \frac{1}{a^3}} \quad (2.85)$$

The above equation and Eq. 2.82 gives

$$\boxed{n_{\text{dust}} \propto \frac{1}{a^3}}. \quad (2.86)$$

Which makes perfect sense since the number density is inversely proportional to the volume.

## 2.4.4 Equation of state for radiation

Let's suppose an ensemble of ultrarelativistic particles that forms a perfect fluid. Let's also assume that the chemical potential is irrelevant. The dispersion relation for this case is  $E = |\mathbf{p}|$ . Unlike cold particles, the spin nature of the hot particles is fundamental to obtaining the correct factor in the thermodynamic functions. An example of an ultrarelativistic boson fluid is a photon gas and an example of a fermionic one is a massless neutrino gas. Therefore, I will calculate  $n$ ,  $\rho$ , and  $P$  for bosonic and fermionic cases of hot fluid.

### 2.4.4.1 Ultrarelativistic bosonic gas

In the bosonic case, we must use the Bose-Einstein function distribution (Eq. 2.77). In this case, the number density of an ultrarelativistic gas (radiation) is

$$n_{\text{rad}}^{\text{BE}} = g_s \int \frac{d^3\mathbf{p}}{(2\pi)^3} \frac{1}{e^{|\mathbf{p}|/T} - 1} = \frac{g_s}{2\pi^2} \int_0^\infty dp \frac{p^2}{e^{p/T} - 1} = \frac{g_s T^3}{2\pi^2} \int_0^\infty \frac{x^2}{e^x - 1} \quad (2.87)$$

$$\Rightarrow \boxed{n_{\text{rad}}^{\text{BE}} = \frac{g_s \zeta(3)}{\pi^2} T^3.} \quad (2.88)$$

Where  $\zeta(x)$  is the zeta function and  $\zeta(3) \approx 1.20206$ .

The energy density is

$$\rho_{\text{rad}}^{\text{BE}} = g_s \int \frac{d^3 \mathbf{p}}{(2\pi)^3} \frac{|\mathbf{p}|}{e^{|\mathbf{p}|/T} - 1} = \frac{g_s}{2\pi^2} \int_0^\infty dp \frac{p^3}{e^{p/T} - 1} = \frac{gT^4}{2\pi^2} \int_0^\infty dx \frac{x^3}{e^x - 1} \quad (2.89)$$

$$\Rightarrow \boxed{\rho_{\text{rad}}^{\text{BE}} = \frac{\pi^2 g_s}{30} T^4.} \quad (2.90)$$

The pressure gives

$$P_{\text{rad}}^{\text{BE}} = g_s \int \frac{d^3 \mathbf{p}}{(2\pi)^3} \frac{\mathbf{p}^2}{3|\mathbf{p}|} \frac{1}{e^{|\mathbf{p}|/T} - 1} \Rightarrow \boxed{P_{\text{rad}}^{\text{BE}} = \frac{1}{3} \rho_{\text{rad}}^{\text{BE}}.} \quad (2.91)$$

#### 2.4.4.2 Ultrarelativistic fermionic gas

In the fermionic case, the application of Fermi-Dirac (Eq. 2.78) distribution is mandatory. As I did before, I start with the number density calculation.

$$n_{\text{rad}}^{\text{FD}} = g_s \int \frac{d^3 \mathbf{p}}{(2\pi)^3} \frac{1}{e^{|\mathbf{p}|/T} + 1} = \frac{g_s}{2\pi^2} \int_0^\infty dp \frac{p^2}{e^{p/T} + 1} = \frac{g_s T^3}{2\pi^2} \int_0^\infty \frac{x^2}{e^x + 1} \quad (2.92)$$

$$\Rightarrow \boxed{n_{\text{rad}}^{\text{FD}} = \frac{3g_s \zeta(3)}{4\pi^2} T^3.} \quad (2.93)$$

The next step is the energy density calculation.

$$\rho_{\text{rad}}^{\text{FD}} = g_s \int \frac{d^3 \mathbf{p}}{(2\pi)^3} \frac{|\mathbf{p}|}{e^{|\mathbf{p}|/T} + 1} = \frac{g_s}{2\pi^2} \int_0^\infty dp \frac{p^3}{e^{p/T} + 1} = \frac{gT^4}{2\pi^2} \int_0^\infty dx \frac{x^3}{e^x + 1} \quad (2.94)$$

$$\Rightarrow \boxed{\rho_{\text{rad}}^{\text{FD}} = \frac{7\pi^2 g_s}{240} T^4.} \quad (2.95)$$

The pressure is

$$P_{\text{rad}}^{\text{FD}} = g_s \int \frac{d^3 \mathbf{p}}{(2\pi)^3} \frac{\mathbf{p}^2}{3|\mathbf{p}|} \frac{1}{e^{|\mathbf{p}|/T} + 1} \Rightarrow \boxed{P_{\text{rad}}^{\text{FD}} = \frac{1}{3} \rho_{\text{rad}}^{\text{FD}}.} \quad (2.96)$$

#### 2.4.4.3 Effective energy density and pressure for radiation

The total radiation energy density is the sum of the contribution due to ultrarelativistic fermions and bosons:

$$\rho_{\text{rad}} = \sum_b \frac{\pi^2 g_b}{30} T_b^4 + \sum_f \frac{7\pi^2 g_f}{240} T_f^4. \quad (2.97)$$

Which can be rewritten as

$$\rho_{\text{rad}} = \frac{\pi^2}{30} \left[ \sum_b g_b \left( \frac{T_b}{T} \right)^4 + \frac{7}{8} \sum_f g_f \left( \frac{T_f}{T} \right)^4 \right] T^4. \quad (2.98)$$

Where  $T$  is the temperature of the photons.

It is common to define the effective number of relativistic degrees of freedom as

$$g_*(T) \equiv \sum_b g_b \left( \frac{T_b}{T} \right)^4 + \frac{7}{8} \sum_f g_f \left( \frac{T_f}{T} \right)^4, \quad (2.99)$$

to rewrite

$$\rho_{rad} = \frac{\pi^2 g_*}{30} T^4. \quad (2.100)$$

It is not easy to calculate  $g_*(T)$  at any temperature due to the QCD phase transition [16]. However, this is not relevant to this work, so I will not explore it in depth. The important thing to keep in mind is that in thermal equilibrium, all species have the same temperature, and only after some species decouple from the fundamental plasma does the temperature ratio become relevant.

The pressure generated by the amount of radiation is simply one-third the energy density, i.e.,

$$P_{rad} = \frac{1}{3} \rho_{rad} = \frac{\pi^2 g_*}{90} T^4. \quad (2.101)$$

#### 2.4.4.4 Radiation

For bosonic or fermionic radiation we have  $n \propto T^3$  and  $\rho \propto T^4$ , in which the only difference between both cases is just the proportional constant. In the two situations was obtained  $P = \rho/3$ , and this is the equation of state that defines a radiation fluid.

Let's apply the radiation equation of state in Eq. 2.51.

$$\dot{\rho}_{rad} + 3H \left( 1 + \frac{1}{3} \right) \rho_{rad} = 0 \Rightarrow \frac{d}{dt} (\rho_{rad} a^4) \Rightarrow \rho_{rad} \propto \frac{1}{a^4}. \quad (2.102)$$

Both equations 2.90 and 2.95 demand that  $\rho_{rad} \propto T^4$ . Connecting this result with the above equation provides one of the most important results in cosmology, that the temperature of a source of radiation is inversely proportional to the scale factor, i.e.,

$$T_{rad} \propto \frac{1}{a}. \quad (2.103)$$

Both BE and FD radiation fluid obeys  $n_{rad} \propto T^3$ . That information together with the above equation gives

$$n_{rad} \propto \frac{1}{a^3}. \quad (2.104)$$

Corroborating the idea that the number density must be inversely proportional to the volume.



### 2.4.5 Mass and temperature comparison

I pointed out that particles of cold matter (dust) are non-relativistic and the mass is the main contribution to the mean energy. On the other hand, hot matter (radiation) particles are ultrarelativistic and the mass contribution to the energy is completely suppressed by the momentum. But, in an expanded universe the scale factor increase in time, therefore if a particle is massive and relativist it will lose energy and become a cold particle. Therefore it is important to have a clear criterion to classify a particle as hot or cold at a such moment. I anticipate that this is related to the comparison between the mass and the temperature, i.e., cold gas is one that  $m \gg T$  and a hot gas has  $m \ll T$  [16].

First, let's consider a Bose-Einstein gas with energy density

$$\begin{aligned}\rho_{BE} &= g_s \int \frac{d^3\mathbf{p}}{(2\pi)^3} E(\mathbf{p}) f_{BE}(t, \mathbf{x}, \mathbf{p}) = g_s \int \frac{d^3\mathbf{p}}{(2\pi)^3} \frac{\sqrt{\mathbf{p}^2 + m^2}}{\exp\left[\frac{1}{T}(\sqrt{\mathbf{p}^2 + m^2})\right] - 1} \\ &= \frac{g_s m}{2\pi^2} \int_0^\infty dp \frac{p^2 \sqrt{1 + (p/m)^2}}{\exp\left[\frac{m}{T} \sqrt{1 + (p/m)^2}\right] - 1} = \frac{g_s T^4}{2\pi^2} \int_{m/T}^\infty dx \frac{x^2 \sqrt{x^2 - (m/T)^2}}{e^x - 1}.\end{aligned}\quad (2.105)$$

Where the substitution  $x \equiv (m/T)\sqrt{1 + (p/m)^2}$  was used.

Using the expression (2.90) the above equation can be rewrite as follow:

$$\frac{\rho_{BE}}{\rho_{\text{rad}}^{BE}} = \frac{15}{\pi^4} \int_{m/T}^\infty dx \frac{x^2 \sqrt{x^2 - (m/T)^2}}{e^x - 1}.\quad (2.106)$$

This is not an easy integral to calculate analytically. But in Fig 1 you can see that for  $m \ll T$  the right-hand side of the above equation is equal to 1. Therefore, the criteria for a bosonic gas to be hot is that its temperature is much larger than the mass of particles that compose the gas.

The energy density for a fermionic gas gives

$$\rho_{FD} = \frac{g_s T^4}{2\pi^2} \int_{m/T}^\infty dx \frac{x^2 \sqrt{x^2 - (m/T)^2}}{e^x + 1} \Rightarrow \frac{\rho_{FD}}{\rho_{\text{rad}}^{FD}} = \frac{120}{7\pi^4} \int_{m/T}^\infty dx \frac{x^2 \sqrt{x^2 - (m/T)^2}}{e^x + 1}.\quad (2.107)$$

Where I used the expression (2.95).

Again, the analytical expression is not easy to obtain. But, I put the numerical solution in Fig. 1. As in the bosonic case, the right-hand side of the above equation is equal to 1 when  $m \ll T$ .

The conclusion is: A fluid is considered hot (radiation) if the mass of its particle components is much smaller than the fluid temperature [16].

To study the criteria for classifying a cold fluid, I follow the procedure sketched in

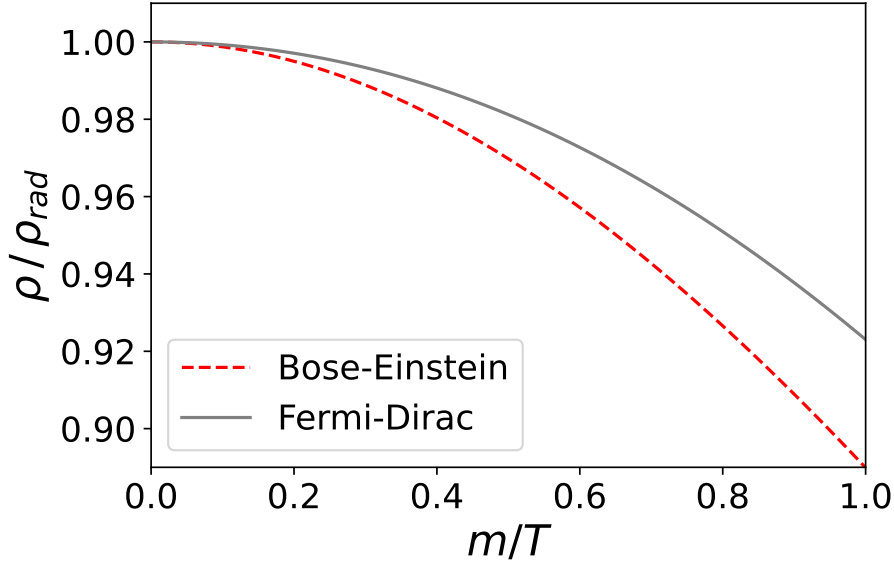


Figure 1 – Ratio between the energy density and the ultrarelativistic energy density for a generic bosonic and a fermionic fluid. For  $m \ll T$  both densities are equivalent.

[16]. First, I rewrite the number density in the following way:

$$\begin{aligned}
 n_{\pm} &= g_s \int \frac{d^3\mathbf{p}}{(2\pi)^3} \frac{1}{\exp\left[\frac{1}{T}\sqrt{\mathbf{p}^2 + m^2} \pm 1\right]} \\
 &= \frac{g_s}{2\pi^2} \int_0^\infty \frac{d^3\mathbf{p}}{(2\pi)^3} \frac{p^2}{\exp\left[\frac{m}{T}\sqrt{1 + (p/m)^2} \pm 1\right]} \\
 &= \frac{g_s T^3}{2\pi^2} \int_{m/T}^\infty dx \frac{x\sqrt{x^2 - (m/T)^2}}{e^x \pm 1}.
 \end{aligned} \tag{2.108}$$

Where  $n_-$  is the BE number density,  $n_+$  is the FD number density, the substitution  $x \equiv (m/T)\sqrt{1 + (p/m)^2}$  was applied, and the chemical potential was disregarded.

I showed previously that

$$\rho_{\pm} = \frac{g_s m}{2\pi^2} \int_0^\infty dp \frac{p^2 \sqrt{1 + (p/m)^2}}{\exp\left[\frac{m}{T}\sqrt{1 + (p/m)^2}\right] \pm 1} = \frac{g_s T^4}{2\pi^2} \int_{m/T}^\infty dx \frac{x^2 \sqrt{x^2 - (m/T)^2}}{e^x \pm 1}. \tag{2.109}$$

Therefore, the ratio

$$\frac{\rho_{\pm}}{mn_{\pm}} = \frac{1}{m/T} \frac{\int_{m/T}^\infty dx \frac{x^2 \sqrt{x^2 - (m/T)^2}}{e^x \pm 1}}{\int_{m/T}^\infty dx \frac{x \sqrt{x^2 - (m/T)^2}}{e^x \pm 1}} \tag{2.110}$$

is the quantity that needed to be analyzed numerically. As you can see in Fig. 2, for  $m \gg T$  the approximation  $\rho \approx mn$  becomes more and more accurate. We can conclude that a fluid is considered cold (dust) if the mass of its particle components is much greater than the fluid temperature [16].

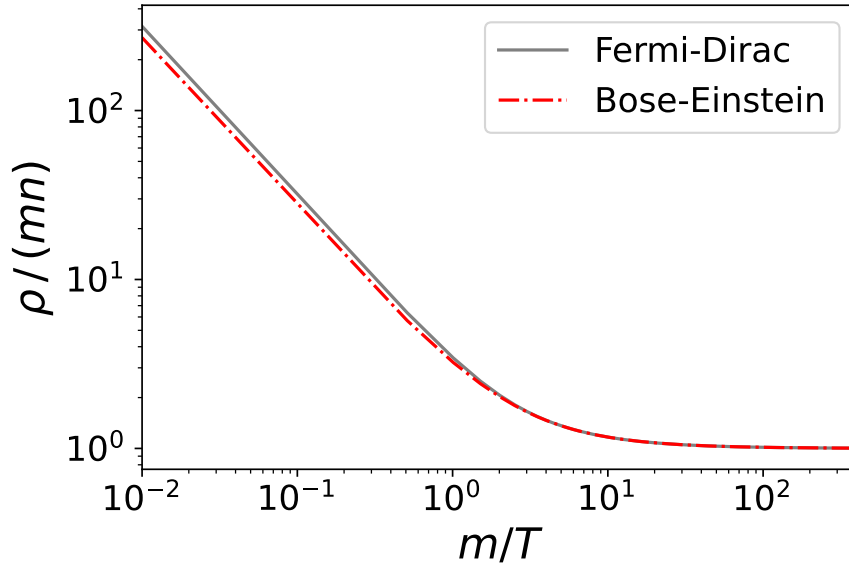


Figure 2 – Ratio between the energy density of a generic fluid and the dust energy density. When  $m \gg T$  the ratio is 1, which shows that in this regime the fluid is cold. This behavior is valid for a generic bosonic and fermionic gas.

#### 2.4.6 Equation of state for dark energy

In the standard cosmological model, dark energy is the energy due to the presence of the cosmological constant  $\Lambda$  in Einstein's equation (Eq. 2.34). Here, I will not explore possible interpretations of dark energy. In this text, I follow a very pragmatic use of this concept where this energy is necessary to describe well the universe and its energy density is defined by Eq. 2.47. Therefore, the dark energy density is constant. Applying this constancy to Eq. 2.51 the dark energy pressure is obtained:

$$\boxed{P_\Lambda = -\rho_\Lambda.} \quad (2.111)$$

This is a very strange state of the equation because if  $\rho_\Lambda > 0$  implies a negative pressure. Planck 2018 mission [17] provides a positive value for the dark energy density, therefore adopting the standard cosmological model, it is necessary to consider the existence of such a weird equation of state.<sup>8</sup>

## 2.5 Entropy

The first law of thermodynamics states that, for a system with a negligible chemical potential ( $\mu \approx 0$ ), the entropy variation is expressed as

$$dS = \frac{1}{T}dU + \frac{P}{T}dV, \quad (2.112)$$

<sup>8</sup> I explore deeply the Planck 2018 results in Sect. 2.8.

where  $U$  is the internal energy and  $V$  is the volume of the thermodynamic system [15].

Expressing the internal by  $U = \rho V$  rewrites the thermodynamics first law in the following way:

$$TdS = d(\rho V) + PdV = V \frac{d\rho}{dT} dT + (\rho + P)dV \Rightarrow dS = \frac{V}{T} \frac{d\rho}{dT} dT + \frac{\rho + P}{T} dV. \quad (2.113)$$

Entropy is a state function, so  $dS$  is an exact differential [15], which gives the relation

$$\begin{aligned} \frac{\partial}{\partial V} \left( \frac{V}{T} \frac{d\rho}{dT} \right)_T &= \frac{\partial}{\partial T} \left( \frac{\rho + P}{T} \right)_V \Rightarrow \frac{1}{T} \frac{d\rho}{dT} = \frac{1}{T^2} \left[ \left( \frac{d\rho}{dT} + \frac{dP}{dT} \right) T - (\rho + P) \right] \\ &\Rightarrow \frac{dP}{dT} = \frac{\rho + P}{T}. \end{aligned} \quad (2.114)$$

The next step is to apply the above equation to the first law of thermodynamics (Eq. 2.112) to obtain the entropy variation.

$$\begin{aligned} TdS &= d(\rho V) + PdV \\ &= d(\rho V) + d(PV) - VdP \\ &= d[(\rho + P)V] - V \frac{dP}{dT} dT \\ &= d[(\rho + P)V] - V \left( \frac{\rho + P}{T} \right) dT \\ &\Rightarrow dS = \frac{1}{T^2} \{ Td[(\rho + P)V] - V(\rho + P)dT \} \\ &= d \left( \frac{\rho + P}{T} V \right) \end{aligned}$$

Defining the entropy density as  $s = S/V$ , the above result provides

$$\boxed{s = \frac{\rho + P}{T}}. \quad (2.115)$$

The universe is an expanding system, therefore, a region of volume  $V_{ref}$  at reference time  $t_{ref}$  has energy  $U = \rho a^3 V_{ref}$  and volume  $V = a^3 V_{ref}$  at time  $t$ . Applying these reparametrizations to the right-handed side of  $TdS$  equation gives

$$\begin{aligned} dU + PdV &= d(\rho a^3 V_{ref}) + Pd(a^3 V_{ref}) \\ &= V_{ref} [a^3 d\rho + 3\rho a^2 da + 3Pa^2 da] \\ &= V_{ref} \left[ \frac{d\rho}{dt} + \frac{3}{a} \frac{da}{dt} (\rho + P) \right] dt \\ &= [\dot{\rho} + 3H(\rho + P)] V_{ref} dt \end{aligned}$$

The expression  $\dot{\rho} + 3H(\rho + P)$  vanishes (see Eq. 2.51), which provides  $dU + PdV = 0$ , i.e., the entropy of the homogeneous and isotropic universe must be constant,  $dS = 0$  [16, 12].

The entropy conservation and the relation  $S = sV = sa^3V_{ref}$  informs how the entropy density changes with time.

$$dS = 0 \Rightarrow d(sa^3) = 0 \Rightarrow \boxed{s \propto \frac{1}{a^3}} \quad (2.116)$$

Realize that this means a decrease in the entropy density, as the universe expands.

In a phase where the universe is dominated by radiation the density entropy due to one relativistic bosonic specie is

$$\frac{1}{T}(\rho + P) = \frac{1}{T} \left( \rho + \frac{1}{3}P \right) = \frac{4\rho}{3T} = \frac{4}{3T} \times \frac{\pi^2 g}{30} T^4 = \frac{2\pi^2 g}{45} T^3,$$

while to a fermionic specie is

$$\frac{4\rho}{3T} = \frac{4}{3T} \times \frac{7\pi^2 g}{240} T^4 = \frac{7}{8} \left( \frac{2\pi^2 g}{45} T^3 \right).$$

Where Eqs. 2.90 and 2.95 was used.

The total density is the sum of fermionic and bosonic contribution, i.e.,

$$s_{rad} = \sum_b \frac{2\pi^2 g_b}{45} T_b^3 + \frac{7}{8} \sum_f \frac{2\pi^2 g_f}{45} T_f^3. \quad (2.117)$$

Defining

$$\boxed{g_{*s}(T) = \sum_b g_b \left( \frac{T_b}{T} \right)^3 + \frac{7}{8} \sum_f g_f \left( \frac{T_f}{T} \right)^3}, \quad (2.118)$$

rewrites the total radiation entropy density in the following way:

$$\boxed{s_{rad} = \frac{2\pi^2 g_{*s}}{45} T^3}. \quad (2.119)$$

Notice that only when all relativistic particles are in thermal equilibrium does the identity  $g_* = g_{*s}$  hold, i.e., if only one relativistic particle is decoupled, the equivalence fails.

## 2.6 Density parameter

Let's return the attention to Eq. 2.50,

$$H^2 = \frac{H_0^2}{\rho_{crit,0}} \left[ \rho + \rho_\Lambda - \left( \frac{3}{8\pi} \right) \frac{k}{R^2} \right]. \quad (2.120)$$

It is enough to assume that energy density  $\rho$  is the sum of the matter and radiation energy density [8]. Which implies

$$H^2 = \frac{H_0^2}{\rho_{crit,0}} \left[ \rho_m + \rho_{rad} + \rho_\Lambda - \left( \frac{3}{8\pi} \right) \frac{k}{R^2} \right]. \quad (2.121)$$

Eq. 2.85 provides  $\rho_m = \rho_{m,0}/a^3$  and Eq. 2.102 gives  $\rho_{rad} = \rho_{m,0}/a^4$ . Thus

$$H^2 = \frac{H_0^2}{\rho_{crit,0}} \left[ \frac{\rho_{rad,0}}{a^4} + \frac{\rho_{m,0}}{a^3} + \rho_\Lambda - \left( \frac{3}{8\pi} \right) \frac{k}{R^2} \right]. \quad (2.122)$$

The above equation prompts the natural definition of density parameter  $\Omega$  as the ration between the energy density and the critical density, i.e.,

$$\Omega_m \equiv \frac{\rho_m}{\rho_{crit}}, \quad (2.123a)$$

$$\Omega_{rad} \equiv \frac{\rho_{rad}}{\rho_{crit}}, \quad (2.123b)$$

$$\Omega_\Lambda \equiv \frac{\rho_\Lambda}{\rho_{crit}}. \quad (2.123c)$$

It is also useful to define [8]

$$\Omega_k \equiv -\frac{k}{R^2 H^2}. \quad (2.124)$$

All these number density definitions provide another very usual way of the Friedmann equation:

$$H^2 = H_0^2 \left[ \frac{\Omega_{rad,0}}{a^4} + \frac{\Omega_{m,0}}{a^3} + \frac{\Omega_{k,0}}{a^2} + \Omega_{\Lambda,0} \right]. \quad (2.125)$$

Setting  $t = t_0$  this equation provides the constraint

$$\Omega_{rad,0} + \Omega_{m,0} + \Omega_{k,0} + \Omega_{\Lambda,0} = 1. \quad (2.126)$$

Assuming  $k = -1$  implies in  $\Omega_{k,0} > 0$ , therefore the above constraint demands  $\Omega_{rad,0} + \Omega_{m,0} + \Omega_{\Lambda,0} < 1$ . If  $k = 0$ , the equality  $\Omega_{rad,0} + \Omega_{m,0} + \Omega_{\Lambda,0} = 1$  must hold. In case  $k = +1$ , it holds  $\Omega_{k,0} < 0$ , which implies in  $\Omega_{rad,0} + \Omega_{m,0} + \Omega_{\Lambda,0} > 1$ . This means that knowing the numerical value of the sum  $\Omega_{rad,0} + \Omega_{m,0} + \Omega_{\Lambda,0}$  gives the geometry of the universe!

## 2.7 Cosmic catalogue

### 2.7.1 Photons

In the early universe, all standard model particles were in thermal equilibrium with each other, forming the fundamental plasma. Over time, some particles decoupled from fundamental plasma, in a process called freeze-out. In the very early universe, the photons had a very small free path, i.e., the photons' interaction rate was so huge that universe was opaque for this kind of radiation. Around 350 000 years after the Big Bang, the photons were not able to interact efficiently with other particles, then the universe

became transparent to them. Therefore the photons became free particles and generate a background of electromagnetic radiation. This background is very close to a perfect black body, having a present-day temperature  $T_0 = 2.7255(6)$  K [13], which provides radiation in the microwave wavelength. For these reasons, this radiation is called cosmic microwave background (CMB). The CMB is the richest source of cosmological information we have. Its small deviations from a perfect black body provide all the cosmological parameters [10, 12].

Photons are bosons without mass with two polarization states ( $g_\gamma = 2$ ), which allows us to make use of Eq. 2.88 to calculate the photon present-day number density.

$$n_{\gamma,0} = \frac{2\zeta(3)}{\pi^2} T_0^3 = \frac{2\zeta(3)}{\pi^2} T_0^3 \times \frac{1}{(T_P l_P)^3} \approx 412 \text{cm}^{-3}. \quad (2.127)$$

Where the Planck temperature  $T_P$  and the Planck length  $l_P$  were used to provide the result in a more experimental unity.<sup>9</sup>

The above result tells us that there is a huge concentration of cosmological photons in current days.

I want also to calculate the present-day photons density parameter  $\Omega_{\gamma,0}$ . To do this I use Eq. 2.90 and Eq. 2.49.

$$\Omega_{\gamma,0} = \frac{8\pi^3 T_0^4}{45 H_0^2} \quad (2.128)$$

Unfortunately, there isn't a consensus about the value of the Hubble constant. CMB adopting the standard cosmological model demands  $H_0 = 67.4(5) \text{km s}^{-1} \text{Mpc}^{-1}$  [17, 13], while cosmic distance-ladder estimates  $H_0 = 0.732 \pm 0.013 \text{km s}^{-1} \text{Mpc}^{-1}$  [13]. In fact, the problem is worse than I sketched, because many  $H_0$  measure methods don't agree with each other, generating the so-called Hubble tension. That is one of the most important subjects of this thesis, therefore I will dedicate an entire chapter, Ch. 3, to discussing this subject.

The Hubble tension leads us to write the Hubble constant in the following way:

$$H_0 = 100h \text{km s}^{-1} \text{Mpc}^{-1}. \quad (2.129)$$

Applying the above result to Eq. 2.128 gives

$$\Omega_{\gamma,0} h^2 = \frac{8\pi^3 T_0^4}{45 (100 \text{km s}^{-1} \text{Mpc}^{-1})^2} \times \frac{1}{T_P^4 t_P^2} \Rightarrow \boxed{\Omega_{\gamma,0} h^2 \approx 2.49 \times 10^{-5}}. \quad (2.130)$$

In Tab. 1 there is the  $\Omega_{\gamma,0}$  value, adopting CMB data.

<sup>9</sup> In App. A I review the Planck units, natural units, and how to convert one to another.

## 2.7.2 Baryons

Cosmology is the kingdom of weird nomenclatures. For example, in this theory, all ordinary matter is called baryons, i.e., the matter that forms stars, planets, diffuse gas around galaxies, hot ionized gas, light elements like hydrogen, deuterium, helium, lithium, and even electrons are labeled as baryons [12].<sup>10</sup> It is not easy to measure the baryon energy density in the universe directly, but the formation of light elements in the early universe, called big bang nucleosynthesis theory (BBN) together with the analyses of the small perturbations in the CMB spectrum provides strong bounds on it.

Planck Collaboration 2018 [17] sets the baryon density parameter to be

$$\boxed{\Omega_{b,0}h^2 = 0.0225 \pm 0.0003.} \quad (2.131)$$

Comparing this numerical value with Eq. 2.130, we infer that the present-day energy of baryons is much more relevant than the photons' energy density. However, there are much more photons than barons in current days, i.e., the current number density of photons is much greater than that of baryons. To show this I will calculate the baryon-to-photon ratio  $\eta_b$ .

Baryons are usually very massive, in such a way that they can be considered cold particles in almost every moment I will treat them. Adopting this point of view, I use Eq. 2.82 to write  $n_b = \rho_b/m_b$ . I also use Eq. 2.85 and Eq. 2.104 to write  $\rho_b = \rho_{b,0}/a^3$  and  $n_\gamma = n_{\gamma,0}/a^3$ . Applying all this in  $\eta_b$  provides that the baryon-to-photon ratio is constant.

$$\eta_b = \frac{n_b}{n_\gamma} = \frac{\rho_b/m_b}{n_\gamma} = \frac{1}{m_b} \frac{\rho_{b,0}}{a^3} \frac{1}{n_\gamma} = \frac{1}{m_b} \frac{\rho_{b,0}}{a^3} \frac{a^3}{n_{\gamma,0}} = \frac{\rho_{b,0}}{m_b n_{\gamma,0}}. \quad (2.132)$$

Protons and neutrons yield the mean contribution to the baryon density [16, 12], which allows writing  $\rho_b \approx m_p n_p + m_n n_n$ . Proton mass is  $m_p = 938.272 \text{ MeV}$  and the neutron mass is  $m_n = 939.565 \text{ MeV}$  [13], therefore the approximation  $m_p = m_n = m_p$  together with  $n_b = n_p + n_n$  is good enough for the current purpose.

$$\eta_b = \frac{\rho_{b,0}}{m_p n_{\gamma,0}} \quad (2.133)$$

Another step for the  $\eta_b$  calculation is using the parameter density definition to make the substitution  $\rho_{b,0} = \Omega_{b,0} \rho_{\text{crit},0}$ . Other substitution comes from the comparison between Eq. 2.49, Eq. 2.88, and Eq. 2.128, that provides the relation  $n_{\gamma,0}/\rho_{\text{crit},0} = (30\zeta(3)\Omega_{\gamma,0})/(\pi^4 T_0)$ .

Thus, the baryon-to-photon ratio gives [13]

$$\eta_b = \frac{\pi^4 T_0}{30 m_p \zeta(3)} \left( \frac{\Omega_{b,0} h^2}{\Omega_{\gamma,0} h^2} \right) \Rightarrow \boxed{\eta_b = 6.14(19) \times 10^{-10}.} \quad (2.134)$$

There are approximately  $10^9$  cosmological photons to each baryon in the universe!

<sup>10</sup> In particle physics jargon electrons are leptons, not baryons. But, as I said, cosmology is the kingdom of weird nomenclatures.



### 2.7.3 Dark matter

Here I will sketch the history of dark matter, a fundamental concept to understand the standard cosmological model.

In 1933 the Swiss astronomer Fritz Zwicky applied the virial theorem to calculate the velocity of the galaxies in the Coma galaxy cluster. He found that the virial velocity distribution is considerably smaller than the observed velocity, concluding that dark matter (“non-luminous matter”) is much more abundant than luminous matter [18, 19]. In 1937, Zwicky deepened his analysis of the Coma galaxy cluster, concluding that the mass and the non-luminous mass ratio was about 500, concluding again that dark matter is much more abundant than the luminous matter in the cluster [18, 20].

In 1936 the American astronomer Sinclair Smith published his study of the Virgo Cluster. He assumed that the outer galaxies were in a circular motion, and he concluded that the average mass per galaxy was two orders of magnitude greater than the estimates made by Edwin Powell Hubble [18], providing strong evidence of dark matter.

Zwicky and Sinclair advocate that the “non-luminous” matter were cold stars and low luminous clouds [18]. Neville Woolf in 1967 suggested that dark matter was an ionized gas capable to emit X-rays [18, 21]. In 1970, Barry E. Turnrose and Herbert J. Rood concluded that X-ray emission gas is less than 2% of the required mass needed to keep the system bounded [18, 22]. Which ruled out ionized gas as a solution to the “missing mass” problem [18].

The 1970s was a revolutionary decade in dark matter research. Kent Ford and Vera Rubin used a new kind of spectroscope to observe the rotation curve of the Andromeda Galaxy (M31), with high quality when compared with the previous observations. They found that the velocity shape of stars around the galaxy has a non-Newtonian behavior in the outermost radius region [18, 23]. A few years later, they jointly with Norbert Thonnard showed that ten high-luminous spiral galaxies had flat rotation curves in their outermost regions [18, 24].

In 1970, K. C. Freeman found that galaxies M33 and NGC 300 had rotation curve peak at larger radii than expected, providing another clue that an amount of non-luminous matter exists and it is distributed in a different way than the ordinary mass [18].

The conclusion of the amount of rotation galaxies studies was that the velocity curves have a flat shape in the outermost radii region, the spiral galaxies must be bigger than indicated by photometric measurements methods, the mass of a galaxy continues to grow beyond the region populated by stars, and the luminous matter is a small contribution to the galaxy mass [18]. This is the essence of the dark matter halo proposal, in which galaxies and clusters are embedded within a large distribution of dark matter.

For a long time, there were proponents of the idea that the dark matter halo could

be composed of very low-luminosity, massive astrophysical objects such as planets, brown dwarfs, red dwarfs, white dwarfs, neutron stars, and black holes. However, investigations of microlensing events by the EROS Collaboration have placed an upper limit on the contribution of these massive astrophysical compact halo objects (MACHOs) to the dark matter halo mass, which is less than 8% [25, 18].

In the 1950s, the astrophysics community realized that stellar processes were unable to account for the observed abundance of helium. Subsequently, in the 1970s, the detection of deuterium in the interstellar medium further reinforced the notion that these light elements could not be solely produced within stars. These challenges provided strong evidence for the need of a cosmological mechanism for the formation of light elements. Big Bang nucleosynthesis (BBN) emerged as the most plausible explanation for the observed abundance of helium and deuterium. According to BBN, baryonic matter constitutes less than 10% of the present-day critical density, which indicates that the matter of the universe is mostly of non-baryonic origin. This conclusion was supported by the WMAP [26] and the Planck Collaboration [17], which analyzed the cosmic microwave background (CMB) power spectrum and demonstrated that baryonic matter does not constitute the majority of the overall matter abundance.

BBN and CMB measurements constrain the baryon density parameter to be  $\Omega_{b,0} = 0.0493(6)$ , while the CMB analysis determines  $\Omega_{m,0} = 0.315(7)$  [13, 17]. This indicates that baryonic matter constitutes only about one-sixth of the total matter content in the universe. However, this does not necessarily imply that the standard cosmological model is incorrect or that our understanding of the universe needs to be revised. As I mentioned earlier, numerous independent methods and observations consistently suggest a much smaller fraction of non-baryonic matter compared to baryonic matter.

Throughout the history of dark matter research, numerous candidates have been proposed, with some being ruled out by experimental data while others remain viable. Primordial black holes are among the candidates that have been considered. These black holes are believed to have formed before the BBN and should have a mass below the detectability threshold of microlensing experiments. However, in order to produce a sufficiently abundant population of primordial black holes, it would require the presence of non-Gaussianity in the primordial power spectrum [18].

Another candidate is the modified Newtonian dynamics (MOND), which introduces modifications to Newton's second law at large scales. MOND is able to explain the observed rotation curves of galaxies. However, it encounters difficulties when applied to the scale of galaxy clusters, where the introduction of a dark matter component is still necessary to reconcile with observational data. Additionally, providing a relativistic version of MOND poses challenges that require careful consideration and additional theoretical developments [18].

In the realm of particle physics, there exist various candidates for dark matter, including supersymmetric particles, axion-like particles, and a multitude of particles beyond the standard model. Among these, the most prominent class of dark matter candidates is the weakly interacting particles (WIMPs). WIMPs are characterized by a freeze-out mechanism that generates their present-day abundance, and their interaction cross-section is typically on the order of the weak scale [18, 27].

Collisions between galaxy clusters lead to non-baryonic mass distributions within the clusters, providing additional evidence for the non-baryonic nature of dark matter [18].

Computational simulations provide additional fundamental evidence for dark matter. These simulations demonstrate that the growth of small-scale structures is suppressed if dark matter is hot, indicating that hot dark matter is not a suitable candidate. They also reveal that galaxies would be unstable systems without cold dark matter, contradicting observational data. Simulations support the idea that a galaxy is surrounded by a massive spherical cold dark matter halo, with rotation curves that align with observed data. Interestingly, the results of cosmological simulations are relatively insensitive to the specific interactions of dark matter, whether they are electroweak or non-gravitational. However, the initial velocity distribution of dark matter particles has a significant influence on the simulation outcomes [18].

In summary, based on the evidence presented, the majority of the scientific community believes in the existence of dark matter. It is widely accepted that dark matter must be cold at structure formation, and it is significantly more abundant than baryonic matter. The exact nature of dark matter remains an open problem. However, in this thesis, I join in with those who defend that dark matter is a beyond-standard model particle that exhibits extremely weak interactions with known particles, lacks an electric charge, and is stable.

#### 2.7.4 Neutrinos

Neutrinos are particles that interact only by the weak force, i.e., they do not have electric and color charges. In the standard model of particles (SM), the neutrinos are massless and there are three neutrinos flavors: electron ( $\nu_e$ ), muon ( $\nu_\mu$ ), and tau neutrino ( $\nu_\tau$ ). All of them are fermions and classified as leptons [28]. It is now clear that the assumption that neutrinos are massless is incorrect, as it has been discovered that they oscillate between flavors, which implies that they have mass [28]. The mechanism that generates their mass is a matter of debate and the value of an individual neutrino is unknown until this moment. Neutrinos oscillation provides that the sum of the three neutrinos' mass is bigger than 0.06 eV, while cosmology provides that this sum has an upper limit of 0.12 eV, i.e.,  $0.06 \text{ eV} \leq \sum_i m_{\nu_i} < 0.12 \text{ eV}$  [13]. This implies that cosmology provides the most stringent constraint on the total mass of neutrinos [16, 13, 12].

To prove the cosmological constraints on the total mass of neutrinos is necessary to calculate the temperature at that neutrinos decouple from the fundamental plasma and the present-day number density of neutrinos. Detailed calculations show that neutrino decoupling occurred before electron-positron annihilation [12, 10]. This fact, together with entropy conservation, can be used to determine the ratio of neutrino temperature to photon temperature after the neutrino decoupling.

Just before the neutrino decoupling only electrons ( $e^-$ ), neutrinos ( $\nu$ ), photons ( $\gamma$ ), and their antiparticles ( $e^+$ ,  $\bar{\nu}$ ) were relativistic and in thermal equilibrium, with temperature  $T_1$ . Therefore, Eq. 2.119 shows that at  $T_1$  the entropy density is

$$s_1 = \frac{2\pi^2}{45} \left\{ g_\gamma + \frac{7}{8} [N_\nu(g_\nu + g_{\bar{\nu}}) + g_{e^-} + g_{e^+}] \right\} T_1^3 = \frac{2\pi^2}{45} \left( 2 + \frac{7}{2} + \frac{7}{4} N_\nu g_\nu \right) T_1^3. \quad (2.135)$$

Immediately before the electron-positron annihilation, the entropy density gives

$$s_2 = \frac{2\pi^2}{45} \left( g_\gamma T_\gamma^3 + \frac{7}{4} N_\nu g_\nu T_\nu^3 \right) = \frac{2\pi^2}{45} \left[ 2 \left( \frac{T_\gamma}{T_\nu} \right)^3 + \frac{7}{4} N_\nu g_\nu \right] T_\nu^3. \quad (2.136)$$

Entropy conservation implies that  $sa^3$  is constant. Therefore, I can equate  $s_1 a_1^3$  to  $s_2 a_2^3$ , i.e.,

$$\left( 2 + \frac{7}{2} + \frac{7}{4} N_\nu g_\nu \right) (T_1 a_1)^3 = \left[ 2 \left( \frac{T_\gamma}{T_\nu} \right)^3 + \frac{7}{4} N_\nu g_\nu \right] (T_\nu a_2)^3. \quad (2.137)$$

When decoupled, the neutrinos behave like radiation, having temperature inversely proportional to the scale factor,  $T \propto a^{-1}$ . This fact rules out the factors  $(T_1 a_1)^3$  and  $(T_\nu a_2)^3$  in the above equation, and provides the following value for the neutrino-photon temperature ratio:

$$2 \left( \frac{T_\gamma}{T_\nu} \right)^3 = 2 + \frac{7}{2} \Rightarrow \boxed{\frac{T_\nu}{T_\gamma} = \left( \frac{4}{11} \right)^{1/3}}. \quad (2.138)$$

This important result is independent of both the number of neutrino flavors ( $N_\nu$ ) and the number of neutrino helicity states ( $g_\nu$ ).

According to Eq. 2.93, the number density of neutrinos in the hot stage is

$$n_\nu = (2 \times 3) \times \frac{3\zeta(3)}{4\pi^2} T_\nu^3, \quad (2.139)$$

where factor 2 comes from the neutrino and antineutrino contribution, and factor 3 is due to the three neutrinos flavors.

Dividing this result by  $n_\gamma$  gives

$$\frac{n_\nu}{n_\gamma} = \frac{9\zeta(3)T_\nu^3}{2\pi^2} \times \frac{\pi^2}{2\zeta(3)T^3} = \frac{9}{4} \times \frac{4}{11} = \frac{9}{11}. \quad (2.140)$$

This ratio is valid for any moment after the neutrinos decouple, even when neutrinos are no more relativistic. This holds because any number density of decoupled particles is

inversely proportional to the scale factor, therefore the ratio between two number densities is constant.

The present-day density parameter for massive neutrinos gives:

$$\begin{aligned}
 \Omega_{\nu,0} &= \frac{1}{\rho_{\text{crit},0}} \times \sum_i m_{\nu_i} \frac{n_{\nu,0}}{3} \\
 &= \frac{8\pi}{9H_0^2} \left( \sum_i m_{\nu_i} \right) \frac{n_{\nu,0}}{n_{\gamma,0}} n_{\gamma,0} \\
 &= \frac{8\pi}{9H_0^2} \left( \sum_i m_{\nu_i} \right) \times \frac{9}{11} \times \frac{412}{\text{cm}^3} \times \frac{l_P^3}{t_P^2 m_P} \\
 &\Rightarrow \boxed{\Omega_{\nu,0} h^2 = \frac{\sum_i m_{\nu_i}}{94 \text{ eV}}}. \tag{2.141}
 \end{aligned}$$

Where I made use of Planck units to restore  $G$ s,  $\hbar$ s, and  $c$ s. The numerical value for the present-day number density for photons comes from Eq. 2.127, and the Hubble constant was used in the form  $H_0 = 100h \text{ km s}^{-1} \text{ Mpc}^{-1}$ . It was also necessary to use that 1 Mpc is equivalent to  $3.086 \times 10^{22} \text{ m}$  [11] and 1 Kg is equal to  $5.60959 \times 10^{26} \text{ GeV}$ .

Using the CMB power spectrum limit of  $\Omega_{\nu,0} < 0.03$  [13, 17] in the above expression gives  $\sum_i m_{\nu_i} < 0.13 \text{ eV}$ . It is worth noting that the limit provided in [13] is  $\sum_i m_{\nu_i} < 0.12 \text{ eV}$ , as the numerical truncation used there is more precise than the calculations performed here.

### 2.7.5 Dark energy

Standard candles, like supernovae type Ia, and standard rulers show that at present, the universe is expanding at an accelerated phase. Considering that for a radiation-dominated and a matter-dominated universe, the expansion is slowed down, the accelerated phase implies the necessity of an extra fluid with a negative state equation, i.e., it must exist a fluid obeying  $P = w\rho$  with  $w < 0$  [11, 12].<sup>11,12</sup> This new fluid is called dark energy, a pompous name that indicates our ignorance of its physical nature.

In the standard cosmological model, the dark energy is due to the presence of the cosmological constant  $\Lambda$  in Einstein's equation (Eq. 2.34). It is interesting to note that even in the absence of an energy-momentum tensor in Einstein's equation, the universe still exhibits dynamics because of the cosmological constant. Thus, it is common to refer to the energy associated with the cosmological constant as vacuum energy.

<sup>11</sup> In Sec. 2.9, I show why a radiation-dominated phase and a matter-dominated phase can not generate an accelerated expanding universe. In this section, I also prove that a universe with a cosmological constant enables an accelerated expanding behavior.

<sup>12</sup> The sentence "it must exist a fluid obeying  $P = w\rho$  with  $w < 0$ " is a very strong statement, because there is still a chance that modification to general relativity generates corrections in the cosmological equations that explain the accelerated expanding phase [13, 29]. In this thesis, I consider that general relativity provides the correct description for cosmology, which justifies my assertion.

Type Ia supernovae and CMB data provide that the present-day dark energy density parameter is

$$\boxed{\Omega_{\Lambda,0} \approx 0.7}, \quad (2.142)$$

being the biggest contribution to the current parameter density [13, 12, 29].

## 2.8 $\Lambda$ CDM: the benchmark model

A huge set of astrophysical and cosmological data give the conclusion that the present-day universe is flat and is basically dominated by dark energy and dark matter. In the current era, radiation and neutrinos do not contribute significantly to the universe's energy budget, being relevant only in early times. The main part of the contribution of the matter density parameter comes from cold dark matter (CDM). For these reasons, the standard cosmological model is called  $\Lambda$ CDM. Remarkably, almost 95% of the present-day total energy has unknown sources. All planets, stars, visible galaxies, clouds of dust, light, and neutrinos represent about 5% of the content of the universe. The necessity for these energy sources is clear, but their physical nature is an open problem.

For quick future checks, I summarize in Tab. 1 the cosmological parameters that appear in the Friedmann equation for the standard cosmological model.

| Cosmological parameter                         | Symbol               | Numerical Value [13]                         |
|--|----------------------|--|
| Present-day CMB temperature                    | $T_0$                | 2.7255(6) K                                  |
| Hubble constant                                | $H_0$                | 67.4(5) km s <sup>-1</sup> Mpc <sup>-1</sup> |
| Present-day photon density parameter           | $\Omega_{\gamma,0}$  | $5.38(15) \times 10^{-5}$                    |
| Present-day baryon density parameter           | $\Omega_{b,0}$       | 0.0493(6)                                    |
| Present-day matter density parameter           | $\Omega_{m,0}$       | 0.315(7)                                     |
| Present-day cold dark matter density parameter | $\Omega_{c,0}$       | 0.265(7)                                     |
| Present-day neutrino density parameter         | $\Omega_{\nu,0}$     | [0.0012, 0.003]                              |
| Present-day curvature density parameter        | $\Omega_{k,0}$       | 0.0007(19)                                   |
| Present-day dark energy density parameter      | $\Omega_{\Lambda,0}$ | 0.685(7)                                     |

Table 1 – Present-day density parameter for photons, baryonic matter, matter, cold dark matter, neutrinos, curvature, and dark energy. The table also has the CMB inferred value for the Hubble constant and the present-day CMB temperature.

## 2.9 Cosmological eras

In a simplified way, the universe has first a radiation-dominated phase, followed by a matter-domination phase, and after that, it is dominated by dark-energy [12]. The transitions between these stages are calculated by the Friedmann equation (Eq. 2.125). The matter-radiation equality happens when

$$\rho_{rad} = \rho_m \Rightarrow \frac{\Omega_{rad,0}}{a_{emr}^4} = \frac{\Omega_{m,0}}{a_{emr}^3} \Rightarrow 1 + z_{emr} = \frac{\Omega_{m,0}}{\Omega_{rad,0}} \Rightarrow z_{emr} \approx 3600. \quad (2.143)$$

The equivalence between dark energy and matter happens when

$$\rho_m = \rho_\Lambda \Rightarrow \frac{\Omega_{m,0}}{a_{e\Lambda m}^3} = \Omega_{\Lambda,0} \Rightarrow (1 + z_{e\Lambda m})^3 = \frac{\Omega_{\Lambda,0}}{\Omega_{m,0}} \Rightarrow z_{e\Lambda m} \approx 0.3. \quad (2.144)$$

In Fig. 3 are shown the energy density evolution for radiation, matter, and dark energy. The radiation era is the shortest, lasting about 47,000 years. The universe was dominated by matter for approximately 10 Gy. After the equivalence between dark energy and matter, the universe starts to be dominated by dark energy, and it will spend all eternity in this stage.<sup>13</sup>

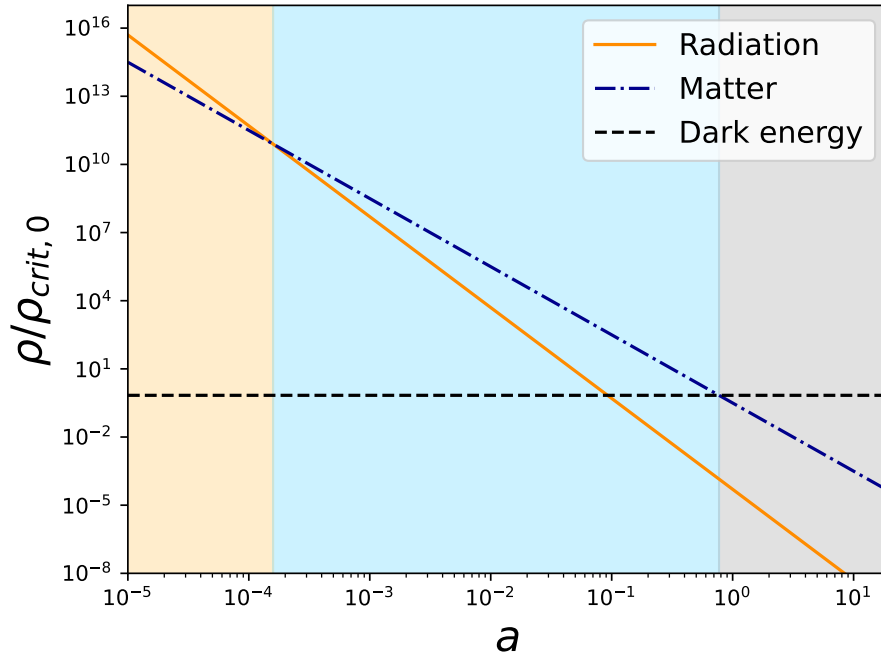


Figure 3 – Energy density evolution for radiation, matter, and dark energy. The energy density ( $\rho$ ) is normalized by the present-day critical density ( $\rho_{\text{crit},0}$ ). The horizontal axis is the scale factor, and the orange region represents the radiation phase, the blue region represents the matter phase, and the gray region represents the dark energy phase.

My next step is to calculate the analytical expression for the scale factor,  $a(t)$ , in each one of the three domination phases, and also calculate the scale factor for a universe dominated by matter and dark energy, which provides a good approximation for the majority of the history of the universe.

<sup>13</sup> The calculation of the equivalence moments between radiation and matter, and between matter and dark energy are well explained in [8].

### 2.9.1 Radiation era

To find the scale factor in the radiation-dominated phase, it is necessary to solve the equation

$$H^2 = H_0^2 \frac{\Omega_{\text{rad},0}}{a^4}. \quad (2.145)$$

The solution to this is

$$a(t) = \sqrt{2H_0 \sqrt{\Omega_{\text{rad},0}} t}. \quad (2.146)$$

Here, I used the big-bang condition  $a(0) = 0$ .

Realize that for the radiation phase  $a \propto t^{1/2}$  and  $H = 1/(2t)$ . The deceleration parameter  $q \equiv -\ddot{a}a/\dot{a}^2$  in this period is  $q = 1$ , which implies a decelerating expansion [8, 12].<sup>14</sup>

### 2.9.2 Matter era

Finding the scale factor for the matter-domination phase involves solving the ODE

$$H^2 = H_0^2 \frac{\Omega_{m,0}}{a^3}. \quad (2.148)$$

Whose solution is

$$a(t) = \left( \frac{3}{2} H_0 \sqrt{\Omega_{m,0}} t \right)^{2/3}. \quad (2.149)$$

Again, the big-bang condition  $a(0) = 0$  was used. This approximation is valid because the radiation-dominated phase lasts for less than 50,000 years, while the matter-dominated era lasts until around 10 billion years.

In this case,  $a \propto t^{2/3}$ ,  $H = 2/(3t)$ , and  $q = 1/2$ , which implies in a decelerating phase [8, 12].

---

<sup>14</sup> I did not create a section discussing the deceleration parameter deeply because it is a concept that I do not frequently use in this thesis. But, I can provide a fast explanation for it. If  $q < 0$ , the universe is in an accelerating expansion phase, while  $q = 0$  the universe is static, and  $q > 0$  is a decelerating stage.

The deceleration parameter is not an independent quantity. Using the acceleration equation, Eq. 2.44, and the critical density definition, Eq. 2.49,  $q$  can be related to the matter, radiation, and dark energy density parameter:

$$\begin{aligned} q &= -\frac{\ddot{a}a}{\dot{a}^2} \\ &= -\frac{a}{\dot{a}^2} \times \left[ -\frac{4\pi}{3} (\rho_m + 2\rho_{\text{rad}} - 2\rho_{\Lambda}) a \right] \\ &= \frac{4\pi}{3H^2} (\rho_m + 2\rho_{\text{rad}} - 2\rho_{\Lambda}) \\ &= \frac{1}{2\rho_{\text{crit}}} (\rho_m + 2\rho_{\text{rad}} - 2\rho_{\Lambda}) \\ &= \frac{1}{2} (\Omega_m + 2\Omega_{\text{rad}} - 2\Omega_{\Lambda}). \end{aligned} \quad (2.147)$$



### 2.9.3 Dark energy era

The last phase is the dark-energy domination era, where the scale factor is determined by solving the ODE

$$H^2 = H_0^2 \Omega_{\Lambda,0} \Rightarrow H = \sqrt{\frac{\Lambda}{3}}. \quad (2.150)$$

Whose the solution is

$$a \propto \exp \left( \sqrt{\frac{\Lambda}{3}} t \right). \quad (2.151)$$

This scale factor provides  $q = -1$ , implying an accelerating phase [8, 12].



## 3 The Hubble tension

In this chapter, I will provide an overview of the methods employed to measure the Hubble constant. Through an examination of these techniques, it will become clear the reasons why determining  $H_0$  gave rise to a cosmological challenge known as the Hubble tension. Understanding the nature of this tension is crucial as it sets the stage for the subsequent chapter, where I will present a potential solution to this intriguing problem.

### 3.1 The many definitions of distance in cosmology

Many cosmological parameters can be determined by studying the distance-redshift relation of astrophysical objects. However, the question arises: what concept of distance should be used? The natural approach is to define distance in terms of proper distance ( $d_p$ ). However, it is impossible to directly measure the proper distance of an object on the cosmological scale. As a result, alternative distance concepts have been developed, such as luminosity distance ( $d_L$ ) and angular distance ( $d_A$ ). In this section, I present a review of the proper distance and the luminosity distance.<sup>1</sup>

#### 3.1.1 Proper distance and Hubble's law

The non-normalized scale factor,  $R(t)$ , can be expanded around the present-day time as follows [8]:

$$R(t) = R_0 + \dot{R}_0(t - t_0) + \frac{1}{2}\ddot{R}_0(t - t_0)^2 + \dots \quad (3.1)$$

By factoring out  $R_0$  and using the definitions of the Hubble parameter ( $H = \dot{R}/R = \dot{a}/a$ ) and the deceleration parameter ( $q = -\ddot{R}R/\dot{R}^2 = -\ddot{a}a/\dot{a}^2$ ), the above equation can be rewritten as [11]:

$$a(t) = 1 - H_0(t_0 - t) - \frac{1}{2}q_0H_0^2(t_0 - t)^2 + \dots \quad (3.2)$$

Applying the scale factor and redshift relation,  $1 + z = 1/a$ , to Equation 3.2, the connection between  $z$  and the time difference  $t_0 - t$  is obtained:

$$z = H_0(t_0 - t) + \left(1 + \frac{q_0}{2}\right)H_0^2(t_0 - t)^2 + \dots \quad (3.3)$$

---

<sup>1</sup> The angular distance is an interesting subject, but for the future discussions contained in this thesis, it is a concept that will not be necessary. Therefore, I consider it beyond the scope of this text, and I will not discuss this concept in depth.

This equation can be inverted to solve for  $t_0 - t$ :

$$t_0 - t = \frac{1}{H_0} \left[ z - \left( 1 + \frac{q_0}{2} \right) z^2 + \mathcal{O}(z^3) \right] \quad (3.4)$$

Equation 3.4 indicates that knowing the redshift of a light source provides information about the time  $t$  at which the light was emitted.

As shown in Subsection 2.3.3, light travels along a geodesic with  $\phi$  and  $\theta$  constant, implying that its geodesic is given by:

$$dr = -\frac{dt}{a} \quad (3.5)$$

The proper distance, or physical distance, of a light emitter is defined as the length of the null geodesic that the light travels to reach the Earth. It can be expressed as [11]:

$$l_p = \int_t^{t_0} \frac{dt}{a} \quad (3.6)$$

Using the scale factor expansion from Equation 3.2,  $l_p$  can express as:

$$l_p = \int_t^{t_0} \frac{dt}{1 - H_0(t_0 - t) - \frac{1}{2}q_0 H_0^2(t_0 - t)^2 + \dots} \quad (3.7)$$

Performing the integration yields:

$$l_p = (t_0 - t) + \frac{1}{2}H_0(t_0 - t)^2 + \dots \quad (3.8)$$

By applying Equation 3.4, relationship between the proper distance and the redshift is given:

$$\boxed{l_p = \frac{1}{H_0} \left[ z - \frac{1}{2}(1 + q_0)z^2 + \mathcal{O}(z^3) \right]} \quad (3.9)$$

For small redshift values, this result yields Hubble's law:

$$z = H_0 l_p \quad (3.10)$$

This interpretation is straightforward: the greater the distance of a galaxy, the greater the redshift detected on Earth. The observation of this behavior was the first evidence of the expansion of the universe.

There is another way to express Hubble's law by associating the redshift with a Doppler effect. In special relativity, the ratio of the emitted radiation frequency ( $\nu$ ) to the received frequency ( $\nu_0$ ) for a source moving at a low speed ( $v$ ) is approximately  $\nu/\nu_0 \approx 1 + v$  [8, 9]. By comparing this equation with the cosmological redshift  $\nu/\nu_0 = 1 + z$  (Eq. 2.65), the approximation  $v \approx v$  holds, which provides an alternative formulation of Hubble's law:

$$v = H_0 l_p \quad (3.11)$$

The linear dependence of  $H_0$  in Hubble's law was the first method used to determine the numerical value of the Hubble constant.

### 3.1.2 Luminous distance

In a Euclidean space, a radiation source has a luminosity denoted by  $L$ , representing the energy released per unit of time. This energy propagates spherically, resulting in a flux  $F = L/4\pi d^2$  when detected at a distance  $d$  [8]. Therefore, it is natural to define the luminosity distance as:

$$d_L = \sqrt{\frac{L}{4\pi F}}. \quad (3.12)$$

Extending this concept to a null-curvature FRW geometry involves accounting for the decrease in received radiation due to cosmological expansion. Suppose that at time  $t_E$ , a radiation source emits a photon with frequency  $\nu_E$ , and after a time interval  $\Delta t_E$ , the same amount of energy is emitted. The emitted luminosity is thus given by  $L_E = 4\pi\nu_E/\Delta t_E$ , utilizing the energy-frequency relation  $E = 2\pi\nu$  [14]. If these two photons are detected by an observer on Earth with a time difference of  $\Delta t_R$ , the detected luminosity is represented by  $L_R = 4\pi\nu_R/\Delta t_R$ . Consequently, the ratio between the emitted luminosity  $L_E$  and the detected luminosity  $L_R$  is given by:

$$\frac{L_E}{L_R} = \frac{\nu_E/\Delta t_E}{\nu_R/\Delta t_R} = \frac{\nu_E^2}{\nu_R^2} = (1+z)^2, \quad (3.13)$$

where the redshift-frequency relation from Eq. 2.65 is employed.

The flux detected at a physical distance  $l_p$  from the source is simply:

$$F = \frac{L_R}{4\pi l_p^2}. \quad (3.14)$$

The luminosity distance for an FRW geometry is defined in a similar manner as Eq. 3.12, replacing  $L$  with emitted luminosity and  $F$  with detected flux. This yields:

$$d_L = \sqrt{\frac{L_E}{4\pi F}} \Rightarrow d_L = l_p(1+z). \quad (3.15)$$

By employing the approximation of proper distance  $l_p$  for small redshift, as given by Equation 3.9, the expression for the luminosity distance is derived [11, 30]:

$$\boxed{d_L = l_p(1+z) = \frac{1}{H_0} \left[ z + \frac{1}{2}(1-q_0)z^2 + \mathcal{O}(z^3) \right]}. \quad (3.16)$$

This equation represents the core of late measurements of the Hubble constant  $H_0$  and the deceleration parameter  $q_0$ . Here, "late" refers to small redshifts, corresponding to a more recent epoch in the universe.

The key idea is to identify a population of astrophysical objects whose luminosity is well-known. They are called standard candles. After identifying these objects, it is necessary to measure their redshift and flux. Using the relation  $d_L = [L/(4\pi F)]^{1/2}$ , the

luminosity distance is calculated. After completing these steps, the curve of  $z$  versus  $d_L$  must be plotted, and its slope gives  $H_0$  and  $q_0$  [11].

The difficult task is to identify suitable candidates for standard candles. This objective will be further explored in the following section.

## 3.2 Standard candles for local measurements

### 3.2.1 Cepheids

Cepheids are pulsating stars with a luminosity that is proportional to their pulsation period. This class of stars exhibits a well-established period-luminosity relationship. By comparing the observed luminosity of Cepheids with their intrinsic luminosity, astronomers can determine their distances [31, 30]. However, the calibration of this technique is necessary, which involves accurately measuring the distances of nearby Cepheids using independent methods.

Using Cepheids, Edwin Powell Hubble applied the relation between redshift and distance (Eqs. 3.10 and 3.11) to estimate  $H_0$ . Although his numerical estimation of  $H_0$  was significantly different from the values accepted today, his work was revolutionary.

### 3.2.2 Type Ia Supernovae

A supernova is a powerful stellar explosion that can shine as an entire galaxy at its luminous peak [30]. It is a rare event; for example, in the Milky Way, a supernova occurs, on average, once per century [11]. There are two types of supernovae: Type I and Type II. Type I supernovae do not have hydrogen absorption lines in their spectra, while Type II supernovae do [31, 11]. Type I can be further divided into two classes: Type Ia and Type Ib. Type Ia supernovae are excellent standard candles. They originate from white dwarfs that accrete an excessive amount of matter from an orbiting companion star, reaching the Chandrasekhar limit. When this occurs, their core becomes unstable, triggering a runaway fusion process and releasing a tremendous amount of energy in an explosion. The maximum luminosity of Type Ia supernovae varies between  $(3 - 5) \times 10^9 L_\odot$  [11, 31]. The formation process of this type of supernova is highly uniform, making it an excellent characteristic of a standard candle. Its intrinsic luminosity is well understood, and by comparing it with the observed luminosity, astronomers can estimate their distances. With knowledge of the distance and redshift, the Hubble constant can be estimated, as explained earlier.

### 3.3 Standard sirens

A standard siren refers to the use of gravitational waves for measuring cosmic distances. The merger of black holes or neutron stars represents highly energetic events that disturb the fabric of space-time and generate gravitational waves, making them excellent candidates for this purpose. These waves propagate through space, carrying valuable information about the objects that gave rise to them and the dynamics of their interactions. The idea behind standard sirens is to detect the gravitational waves generated and utilize the information obtained from the detection to determine the luminosity of the source [30].

The process of measuring distances using standard sirens involves several steps. Initially, the gravitational wave signal captured by ground-based or space-based detectors, such as the Laser Interferometer Gravitational-Wave Observatory (LIGO) or the Virgo detector, is analyzed to extract relevant information regarding the merging objects. The gravitational wave signal contains encoded details about the masses, spins, and orbital dynamics of the involved objects [32].

In cases where the gravitational wave source can also be detected electromagnetically, such as in the scenario of a binary neutron star merger, combining the gravitational and electromagnetic analyses allows for the generation of precise information about the distance of the source.

### 3.4 Measurement from the Early Universe: Cosmic Microwave Background

The measurement of the Hubble constant from the early universe relies on observations of temperature anisotropies in the cosmic microwave background (CMB). This anisotropy arises due to scalar perturbations on the FRW metric with null curvature. These geometric perturbations induce tiny deformations in the energy density spectra of photons, neutrinos, baryons, and dark matter [12].

The CMB anisotropy serves as a rich source of information, providing insights into the spatial geometry of the universe, the present-day density parameters of the universe's energy components, and the Hubble constant itself [2, 33, 12, 10]. Two notable missions that have analyzed the CMB power spectrum are the Wilkinson Microwave Anisotropy Probe (WMAP), which provided measurements of the Hubble constant, and the Planck Collaboration [4], which has furnished the most precise information regarding the CMB.

Another important cosmological probe is the Baryon Acoustic Oscillation (BAO), which manifests as a perturbation in the matter power spectrum. This phenomenon generates pressure waves in the primordial plasma, leading to additional constraints on

the Hubble constant.

Projects like the Baryon Oscillation Spectroscopic Survey (BOSS) [34] and the Dark Energy Survey (DES) [35] have undertaken extensive galaxy surveys on large scales to precisely measure the BAO scale. These measurements, when combined with CMB data and other cosmological probes, contribute significantly to the determination of the Hubble constant.

### 3.5 The Hubble tension

Knowing the theory behind measuring distance and the cosmological and astrophysical phenomena used, it is time to delve into the numerical results of these techniques.

The SH0ES team utilized data from the Hubble Space Telescope (HST) and Gaia to refine the determination of the Hubble constant [36]. They studied 75 Milky Way Cepheids and achieved precise calibration of their luminosities by combining different calibration sources. Applying this calibration to Type Ia supernovae, they measured the Hubble constant as  $H_0 = 73.2 \pm 1.3 \text{ km s}^{-1} \text{ Mpc}^{-1}$ , reaching a precision of 1.8%. The study confirmed the agreement of Cepheid properties in the Milky Way with those in other galaxies.

The Carnegie–Chicago Hubble Programme (CCHP) combines calibration of the tip of the red-giant branch with Type Ia supernovae to determine a value for the Hubble constant of  $H_0 = 69.8 \pm 0.6(\text{stat}) \pm 1.6(\text{sys}) \text{ km s}^{-1} \text{ Mpc}^{-1}$  [37]. Their method shows consistency with other calibrations and does not require new physics beyond the standard cosmological model.

The HOLiCOW collaboration [38] presents a measurement of the Hubble constant using six gravitationally lensed quasars with measured time delays. In a flat  $\Lambda$ CDM cosmology,  $H_0$  is determined to be  $73.3 \pm 1.7 \text{ km s}^{-1} \text{ Mpc}^{-1}$ , which is consistent with other local measurements. The method used is independent of supernovae and CMB analyses. The study explores different cosmological models and shows the complementarity of time-delay cosmography with other methods.

LIGO and Virgo detected a gravitational-wave event resulting from a binary neutron-star merger, and the Hubble constant was measured directly from the gravitational wave and redshift data, yielding a value of  $H_0 = 70_{-8}^{+12} \text{ km s}^{-1} \text{ Mpc}^{-1}$  [39]. In [40], the same gravitational wave event was studied, but two extra standard sirens were added, resulting in  $H_0 = 72_{-8}^{+12} \text{ km s}^{-1} \text{ Mpc}^{-1}$ .

There are many other direct measurement values for the Hubble constant. To continue the discussion, I will briefly cite some of them. Parallax measurements of Cepheids provide  $H_0 = 73.24 \pm 1.74 \text{ km s}^{-1} \text{ Mpc}^{-1}$  [33]. The overlap of cepheids and Type Ia



supernovae (SNIa) yields  $H_0$  in the range of  $70.1 - 77.1 \text{ km s}^{-1} \text{ Mpc}^{-1}$  [5]. Combining the tip of the red giant branch (TRGB) with SNIa results in  $H_0$  in the range of  $67.7 - 74.2 \text{ km s}^{-1} \text{ Mpc}^{-1}$  [5]. The Tully-Fisher relation (TRF), which relates the luminosity of a galaxy to its rotational velocity, has also been used to estimate  $H_0$ , yielding a range of  $72.3 - 78.6 \text{ km s}^{-1}$  [5].<sup>2</sup>

The main source of early measurements of the Hubble constant is the CMB. Considering the  $\Lambda$ CDM model and CMB power spectrum, Planck data favors  $H_0 = 67.27 \pm 0.6 \text{ km s}^{-1} \text{ Mpc}^{-1}$  [4]. Other early methods, whether they use the CMB or not, yield results very close to the Planck measurement [5].

In summary, early measurements of the Hubble constant favor  $H_0 < 69 \text{ km s}^{-1} \text{ Mpc}^{-1}$ , while local measurements yield  $H_0 > 70 \text{ km s}^{-1} \text{ Mpc}^{-1}$  [2, 5]. The discrepancy between these values is known as the Hubble tension, and its magnitude varies depending on the dataset used. Table 2 presents some of these measurements, highlighting the discrepancy between late and early universe data. Overall, it is evident that local measurements do not align with CMB-inferred values for  $H_0$ .

| EARLY UNIVERSE  | Dataset                |
|---|------------------------|
| $H_0 = 70.0 \pm 2.2 \text{ km s}^{-1} \text{ Mpc}^{-1}$   | WMAP9 [41]             |
| $H_0 = 67.36 \pm 0.54 \text{ km s}^{-1} \text{ Mpc}^{-1}$ | CMB 2018 [4]           |
| $H_0 = 67.36 \pm 0.54 \text{ km s}^{-1} \text{ Mpc}^{-1}$ | SPT 2021 [42]          |
| $H_0 = 69.72 \pm 1.63 \text{ km s}^{-1} \text{ Mpc}^{-1}$ | ACT 2019 [43]          |
| $H_0 = 67.9 \pm 1.1 \text{ km s}^{-1} \text{ Mpc}^{-1}$   | BOSS data [44]         |
| $H_0 = 69.6 \pm 1.8 \text{ km s}^{-1} \text{ Mpc}^{-1}$   | eBOSS Collab. [45]     |
| LATE UNIVERSE   | Dataset                |
| $H_0 = 73.8 \pm 2.1 \text{ km s}^{-1} \text{ Mpc}^{-1}$   | SN1a 2021 [46]         |
| $H_0 = 75.4 \pm 1.7 \text{ km s}^{-1} \text{ Mpc}^{-1}$   | Pantheon 2019 [47]     |
| $H_0 = 72.8 \pm 1.9 \text{ km s}^{-1} \text{ Mpc}^{-1}$   | Gaia 2020 [48]         |
| $H_0 = 73.2 \pm 1.3 \text{ km s}^{-1} \text{ Mpc}^{-1}$   | Gaia and HST 2020 [36] |
| $H_0 = 69.8 \pm 2.5 \text{ km s}^{-1} \text{ Mpc}^{-1}$   | Red Giants 2019 [49]   |

Table 2 – Early and late universe measurements of the Hubble constant and their respective data sets.

Although the measurement of the luminosity of a standardized star is a direct task, it is more susceptible to systematic errors compared to early universe measurements. This fact is evident in the last measurement presented in Table (2). It utilizes Red Giants instead of Cepheids or Supernovae to assess the distance-redshift relation, and the inferred value for  $H_0$  is slightly larger but compatible with the early universe evaluations, considering the

<sup>2</sup> The Tully-Fisher relation is based on the observation that spiral galaxies with higher rotational velocities tend to have greater luminosities. The Tully-Fisher relation has been widely used in cosmology and extragalactic astronomy to estimate the distances to galaxies, particularly when other distance indicators, such as Cepheid variable stars or Type Ia supernovae, are not available or applicable. It is important to note that the Tully-Fisher relation is an empirical relationship based on observations, and its physical mechanism is still the subject of ongoing research and investigation [13, 5].

error bars. In many cases, the Red Giants and Cepheids used to obtain the different data sets are located in the same galaxies. The discrepancy in the results indicates the presence of a significant systematic error in one or both of these measurements. It is possible that new observations using the James Webb telescope may resolve this issue in the coming years. For a detailed discussion of this conflict, refer to Ref. [37].

Both late and early results have such significant statistical discrepancies that they can no longer agree with each other. In many cases, there is no overlap between their uncertainties, highlighting the essence of the Hubble tension. If the early measurements are correct, it implies that the methods astronomers use to calculate distances to very distant objects need improvement. On the other hand, if the late measurements are correct, it suggests that something must be added to the cosmological equation to resolve the discrepancy.

### 3.6 Possible solutions for the Hubble tension

One possible way to alleviate the Hubble tension is by extending the standard cosmological model. One popular alternative extension is to consider non-standard dark energy models, such as quintessence. Another approach is to modify the theory of gravity. These models introduce additional parameters that can influence the expansion rate and potentially reconcile the conflicting measurements [5].

It is also common in the literature to propose modifications to early universe physics with the intention of addressing the Hubble tension. This includes scenarios where the early universe underwent a phase transition or experienced non-standard inflationary dynamics. Such modifications can have an impact on the expansion rate and result in different predictions for the Hubble constant [5].

The Hubble tension has also given rise to speculations about new physics and potential variations in fundamental constants. Some hypotheses suggest that the tension could be resolved by considering a time-varying speed of light or variations in the fine-structure constant. These ideas introduce fundamental changes to our understanding of physics and cosmology and are actively being explored through theoretical and observational studies [5].

Extensive investigations have been conducted to understand the systematic effects and biases in measurement methods that contribute to the Hubble tension. These investigations encompass various factors, including uncertainties in distance indicator calibration, variations in dust extinction treatment, and assumptions within the cosmological framework. Ongoing efforts are focused on refining the calibration of distance indicators, particularly Cepheid variable stars and Type Ia supernovae, to reduce systematic uncertainties. Additionally, careful examination is being given to the impact of local variations in

matter distribution and peculiar motions, as these factors can introduce biases that affect the determination of the Hubble constant. Another perspective in the literature suggests that the tension may arise from statistical anomalies or unaccounted-for systematic effects, emphasizing the need for continued investigation and methodological refinement to address and resolve the tension conclusively [5].

Two mechanisms have emerged as potential solutions to alleviate the Hubble tension, which will be further explored in the following chapter. The first involves the addition of extra radiation energy during the early universe, while the second entails considering a non-standard dark matter fluid. These approaches offer promising avenues for addressing the tension and will be the focus of in-depth analysis in subsequent discussions.

One possibility to increase the Hubble constant inferred from CMB probes is to add some amount of radiation at early times. A plausible way to accomplish this is via the introduction of new light species that were in thermal equilibrium much before CMB decoupling [2, 50, 51]. Such light species will contribute to the effective number of relativistic particles,  $N_{\text{eff}}$ , which is positively correlated with the Hubble rate [4, 6, 2]. An alternative way to increase  $N_{\text{eff}}$  is to introduce a relativistic production mechanism of dark matter particles, which in turn mimic the effect of a neutrino species [52]. The relation between the variation in the Hubble constant  $\Delta H_0$  induced by  $N_{\text{eff}}$  in the  $\Lambda$ CDM model is estimated to be  $\Delta H_0 = 6.2(N_{\text{eff}} - 3.046)$  [6], i.e.,  $N_{\text{eff}} > 3.046$  can alleviate the Hubble tension. Unfortunately, this alleviation is not too high, because CMB power spectrum does not allow enough  $N_{\text{eff}}$  to the early and late measurement of  $H_0$  be compatible [6, 2]. I will explore deeply this limitation in the next chapter.

As mentioned earlier, another intriguing path for alleviating the Hubble tension is the exploration of non-standard dark energy scenarios. One possibility involves considering the dark energy contribution in the Friedmann equation with the following form [2]:

$$\Omega_{\text{DE},0} \exp \left( 3 \int_0^z dz' \frac{1+w}{1+z'} \right), \quad (3.17)$$

Here,  $w$  represents a constant associated with an equation of state  $P = w\rho$ . In the  $\Lambda$ CDM model, the traditional dark energy corresponds to the case where  $w = -1$ . Another class of dark energy models involves the existence of a scalar fluid that slowly rolls towards the minimum of its potential, leading to a range of models with  $-1 < w < -1/3$ . The phantom-like fluid is characterized by  $w < -1$  [53, 54, 55]. Interestingly, phantom dark energy has the potential to alleviate the Hubble tension [7]. The relationship between the variation in the Hubble constant  $\Delta H_0$  induced by a non-standard dark energy fluid is estimated to be  $\Delta H_0 = -18.5(1+w)$  when  $N_{\text{eff}}$  is fixed at the value 3.046 [6].



## 4 Alleviating the Hubble tension with dark matter and non-standard cosmologies

In this chapter, I use a non-thermal production mechanism of dark matter to increase the relativistic energy density in the early universe, which has the potential to raise  $H_0$  [52, 56] and then alleviate the Hubble tension.

The main idea is considering a heavy particle  $\chi'$  that is thermally decoupled from the fundamental plasma in the early universe. This particle decays into dark matter  $\chi$  and another source of radiation, which may be photons or neutrinos, i.e.,  $\chi' \rightarrow \chi + \nu$  and/or  $\chi' \rightarrow \chi + \gamma$ . I will assume that  $m_{\chi'} \gg m_\chi$  and that the neutrino mass is negligible when compared with  $\chi'$  and  $\chi$  masses. Thus the dark matter particle will be relativistic at first but as the universe expands it cools and becomes a standard cold relic at the matter-radiation equality for structure formation purposes.

It is crucial to assume that only a small fraction of present-day dark matter abundance is due to this mechanism. If a large fraction of the overall dark matter abundance comes from the  $\chi'$ , the changes in the matter power spectrum are sufficiently large, in disagreement with Lyman- $\alpha$  observations [57]. This fact is also important to avoid conflict with structure formation [58]. The small fraction consideration also prevents possible problems with light element formations in the early universe [59, 60].

The small fraction of relativistic dark matter contributes to the energy density in the radiation-dominated phase, generating an effective relativistic degree of freedom,  $N_{\text{eff}}$ . This parameter is positively correlated with the Hubble constant ( $H_0$ ) [17, 2, 33, 6], therefore increasing in  $N_{\text{eff}}$  translates into a larger  $H_0$ .

Introducing  $N_{\text{eff}}$  into  $\Lambda$ CDM model is not enough to increase  $H_0$  to a point where the Hubble tension is alleviated. However, adding a phantom-like fluid and the extra source of radiation made the job [2, 6, 61], i.e., physics beyond the  $\Lambda$ CDM is needed. Having that in mind, I use combined data from Planck, BAO, and Supernovae IA observations to determine what is the parameter region in which the proposed mechanism can increase  $H_0$  and reconcile CMB and local measurements.

I emphasize that in  $\chi'$  decay, the neutrino and/or photon appearing in the final state is a pragmatic choice. Other decay channels involving further SM particles or particles beyond the SM are possible, but I do not consider these cases here.

I will start explaining the mechanism in a model-independent way, and later I use effective theories to describe the  $\chi'$  decay channels, considering cases where dark matter and dark matter mother ( $\chi'$ ) are spin 0, spin 1, and spin 1/2 particles. In the primer

approach, the important quantities are the ratio  $m_{\chi'}/m_{\chi}$  and the fraction of dark matter provided by the non-thermal decay,  $f$ . While in the former, the relevant quantities are the masses of the particles and the energy scale of the effective operator,  $\Lambda$ . With this at hand, I delimit the region of parameter space which offers a solution to the  $H_0$  trouble.

## 4.1 Dark matter particles as the source of dark radiation: a particle physics model-independent approach

I am considering a stage where the universe is dominated by radiation. In this period of time, the radiation energy density ( $\rho_{rad}$ ) is a function of the photon's temperature ( $T$ ) and the relativistic degrees of freedom ( $g_*$ ),

$$\rho_{rad} = \frac{\pi^2}{30} g_* T^4. \quad (4.1)$$

To calculate the  $g_*$  factor I consider the case where only photons and neutrinos are ultrarelativistic, which implies that the neutrinos-to-photons temperature ratio is  $T_\nu/T_\gamma = (4/11)^{1/3}$ . It is well known that photons have two polarization states, providing  $g_\gamma = 2$ . Standard model neutrinos are only left-handed, which sets  $g_\nu = 1$ . Therefore,

$$g_* = g_\gamma + \frac{7}{8} (g_\nu + g_{\bar{\nu}}) N_{\text{eff}} \left( \frac{T_\nu}{T_\gamma} \right)^4 = 2 + \frac{7}{4} \left( \frac{4}{11} \right)^{4/3} N_{\text{eff}}. \quad (4.2)$$

Where  $N_{\text{eff}}$  is the effective number of relativistic neutrino species.

In the standard model, there are three neutrinos species: electron, muon, and tau neutrino. Thus it is expected to have  $N_{\text{eff}}$  close to three, not precisely three, because of some temperature dependence.<sup>1</sup> However, it is useful to write  $N_{\text{eff}} = 3 + \Delta N_{\text{eff}}$ , where  $\Delta N_{\text{eff}}$  refers to the extra number of relativistic degrees of freedom, which may come from new light species or other mechanisms that mimic the neutrino effects.

Denoting the energy density of a single kind of standard model neutrino as

$$\rho_{1\nu} \equiv \frac{\pi^2}{30} \left[ \frac{7}{4} \left( \frac{4}{11} \right)^{4/3} \right] T^4, \quad (4.3)$$

the standard model radiation energy density can be split into two parts:

$$\rho_{rad}^{SM} \equiv \rho_\gamma + 3\rho_{1\nu}. \quad (4.4)$$

Which provides a natural justification to define the extra radiation energy density as

$$\rho_{\text{extra}} \equiv \rho_{rad} - \rho_{rad}^{SM}. \quad (4.5)$$

<sup>1</sup> The standard model predicts a value for the effective number of neutrino species,  $N_{\text{eff}}$ , slightly different from 3 [62, 10, 13]. However, for the purposes of this text, this correction is negligible and can be safely ignored.

Using all these definitions and notations, I can write

$$\boxed{\Delta N_{\text{eff}} = \frac{\rho_{\text{extra}}}{\rho_{1\nu}}}. \quad (4.6)$$

The key idea of the above equation is that it is possible to reproduce the effect of an extra neutrino species by adding any other kind of radiation source.

It is important to notice that the ratio between one neutrino specie and cold dark matter energy density at the matter-radiation equality ( $t = t_{\text{eq}}$ ) is

$$\left. \frac{\rho_{1\nu}}{\rho_{CDM}} \right|_{t=t_{\text{eq}}} = \frac{\Omega_{\nu,0}\rho_c}{3a_{\text{eq}}^4} \times \left( \frac{\Omega_{CDM,0}\rho_c}{a_{\text{eq}}^3} \right)^{-1} = 0.16. \quad (4.7)$$

Where the factor 1/3 comes from the consideration that only one neutrino species contributes to the ratio,  $\Omega_{\nu,0} = 3.65 \times 10^{-5}$  [11],  $\Omega_{DM,0} = 0.265$  [13] and  $a_{\text{eq}} = 3 \times 10^{-4}$ .<sup>2,3</sup>

The above equation informs that the energy density of one neutrino specie is equal to 16% of the dark matter energy density at matter-radiation equality.

Let's suppose that a heavy particle  $\chi'$  decays into dark matter  $\chi$  and photons  $\gamma$  or SM neutrinos  $\nu$ , i.e.,  $\chi' \rightarrow \chi + \nu$  or  $\chi' \rightarrow \chi + \gamma$ . I am considering that this happened at a time between neutrino decoupling and matter-radiation equality, i.e., the decay happened in the radiation era.

In  $\chi'$  resting frame, the four-momentum of particles are:

$$p_{\chi'} = (m_{\chi'}, \mathbf{0}), \quad (4.8a)$$

$$p_{\chi} = (E(\mathbf{p}), \mathbf{p}), \quad (4.8b)$$

$$p_{\nu,\gamma} = (|\mathbf{p}|, -\mathbf{p}). \quad (4.8c)$$

Therefore, with these expressions and the 4-momentum conservation I find the energy of dark matter immediately after the decay,

$$\begin{aligned} p_{\chi'} = p_{\chi} + p_{\nu,\gamma} &\Rightarrow p_{\chi'} - p_{\chi} = p_{\nu,\gamma} \Rightarrow m_{\chi'}^2 - 2p_{\chi'} \cdot p_{\chi} + m_{\chi}^2 = 0 \Rightarrow 2m_{\chi'}E_{\chi} = m_{\chi'}^2 + m_{\chi}^2 \\ &\Rightarrow E_{\chi}(\tau) = m_{\chi} \left( \frac{m_{\chi'}}{2m_{\chi}} + \frac{m_{\chi}}{2m_{\chi'}} \right) \equiv m_{\chi}\gamma_{\chi}(\tau). \end{aligned} \quad (4.9)$$

Where  $\tau$  is the lifetime of the mother particle  $\chi'$  and  $\gamma(\tau)$  is the Lorentz factor at this moment. I highlight that I am adopting the instant decay approximation, i.e., that all mother particles decay in the same moment.<sup>4</sup>

<sup>2</sup> You may think that the neutrino density used here is in conflict with the value shown in Tab. 1, however, it is not. In the phase considered in this section, the neutrinos are ultrarelativistic, therefore the approximation of massless neutrinos is completely fine. In Tab. 1 the present-day neutrinos are cold particles.

<sup>3</sup> In the previous chapters I used  $\Omega_{c,0}$  to denote the present-day cold dark matter density. In this chapter, I change this notation because in my analyses I utilize dark matter in cold and hot stages.

<sup>4</sup> I intend to alleviate this instant decay approximation in future work.

The above equation indicates that dark matter generated from  $\chi'$  decay is ultrarelativistic. This is because the condition  $m_{\chi'} \gg m_\chi$  implies that  $E_\chi \gg m_\chi$ .

Using the above result and the fact that the momentum of a particle is inversely proportional to the scale factor (Eq. 2.63), I obtain

$$\begin{aligned} E_\chi^2 - m_\chi^2 &= \mathbf{p}_\chi^2 \propto \frac{1}{a^2} \\ \Rightarrow (E_\chi^2(t) - m_\chi^2) a^2(t) &= (E_\chi^2(\tau) - m_\chi^2) a^2(\tau) \\ \Rightarrow \frac{E_\chi(t)}{m_\chi} &= \left[ 1 + \left( \frac{a(\tau)}{a(t)} \right)^2 (\gamma_\chi^2(\tau) - 1) \right]^{1/2} \equiv \gamma_\chi(t). \end{aligned}$$

As I pointed out early, I am considering that the universe is in the radiation domination phase, where  $a(\tau)/a(t) = \sqrt{\tau/t}$  (see Eq. 2.146). In this way, the dark matter Lorentz factor is

$$\gamma_\chi(t) = \sqrt{\frac{(m_\chi^2 - m_{\chi'}^2)^2}{4m_\chi^2 m_{\chi'}^2} \left( \frac{\tau}{t} \right) + 1}. \quad (4.10)$$

In the non-relativistic regime, the mass of a particle is the dominant contribution to its energy. Thus, rewriting the dark matter energy as

$$E_\chi = m_\chi (\gamma_\chi - 1) + m_\chi \quad (4.11)$$

provides the interpretation that in the ultrarelativistic regime  $m_\chi (\gamma_\chi - 1)$  dominates. Consequently, the total energy of the dark matter particle can be written as

$$E_{\text{DM}} = N_{\text{HDM}} m_\chi (\gamma_\chi - 1) + N_{\text{CDM}} m_\chi.$$

Here,  $N_{\text{HDM}}$  is the total number of ultrarelativistic dark matter particles (hot particles), whereas  $N_{\text{CDM}}$  is the total number of nonrelativistic DM (cold particles). Obviously,  $N_{\text{HDM}} \ll N_{\text{CDM}}$  to be consistent with the cosmological data.<sup>5</sup>

The ratio between hot and cold dark matter energy density is

$$\frac{\rho_{\text{HDM}}}{\rho_{\text{CDM}}} = \frac{N_{\text{HDM}} m_\chi (\gamma_\chi - 1)}{N_{\text{CDM}} m_\chi} \equiv f (\gamma_\chi - 1). \quad (4.12)$$

Where  $f$  is the fraction of dark matter particles which are produced via this non-thermal process.

As aforementioned,  $f$  ought to be small. For calculation purposes, I consider  $f = 0.01$ , as a conservative benchmark. In Sect. 4.3, I clarify further this choice.

<sup>5</sup> The CMB power spectrum and structure formation observations support the idea that dark matter should be predominantly cold [27, 18, 13]. Therefore, I assume that the fraction of hot dark matter particles is much smaller than that of cold dark matter.



Considering that in Eq. 4.6 the extra source of radiation is the hot dark matter produced by the  $\chi'$  decay, and applying Eq. 4.12 and Eq. 4.7 to Eq. 4.6 provides that

$$\Delta N_{\text{eff}} = \frac{\rho_{\text{HDM}}}{\rho_{1\nu}} = \frac{\rho_{\text{HDM}}}{0.16 \times \rho_{\text{CDM}}(t_{\text{eq}})} = \lim_{t \rightarrow t_{\text{eq}}} \frac{f(\gamma_\chi - 1)}{0.16}. \quad (4.13)$$

In the regime  $m_{\chi'} \gg m_\chi$ , the Lorentz factor at matter-radiation equality becomes

$$\gamma_\chi(t_{\text{eq}}) - 1 \approx \gamma_\chi(t_{\text{eq}}) \approx \frac{m_{\chi'}}{2m_\chi} \sqrt{\frac{\tau}{t_{\text{eq}}}},$$

and Eq. 4.13 reduces to

$$\Delta N_{\text{eff}} \approx 2.5 \times 10^{-3} \sqrt{\frac{\tau}{10^6 \text{ s}}} \times f \frac{m_{\chi'}}{m_\chi}. \quad (4.14)$$

Where the approximation  $t_{\text{eq}} \approx 50000 \text{ years} \approx 1.6 \times 10^{12} \text{ s}$  was used.

The  $\Delta N_{\text{eff}}$  is a function of four parameters: (i) the lifetime and (ii) the mass of  $\chi'$ ; (iii) the mass of  $\chi$ ; (iv) the fraction of hot dark matter particles ( $f$ ), that as I pointed before, I assume to be 0.01.

As aforementioned, analyses of the CMB spectrum provide that  $N_{\text{eff}}$  and  $H_0$  are positively correlated [2, 17, 33, 6]. Therefore, Eq. 4.14 can be used to connect  $H_0$  with  $f m_{\chi'}/m_\chi$  for a given lifetime.

Assuming that the Hubble constant measured locally should indeed be larger than  $70 \text{ km s}^{-1} \text{ Mpc}^{-1}$ , one can conclude that the  $\Lambda\text{CDM}$  model does not suffice [2]. In other words, if there are no methodological mistakes in late measurements of  $H_0$ , the Hubble tension is a sign that small deviations from the standard cosmological model are needed [2]. Here, I will consider the addition of phantom-like fluid in the Freedman equation [63], as the cosmological model extension. I do this because phantom-like cosmologies alone allow  $H_0$  values larger than  $70 \text{ km s}^{-1} \text{ Mpc}^{-1}$ , and consequently can solve the  $H_0$  trouble [2, 6].

In the first column of Fig. 4 is shown the regions of the parameter that correlate  $H_0$  and  $N_{\text{eff}}$  found in [2]. They do that via likelihood analyses of the CMB power spectrum, together with BAO<sup>6</sup> and type Ia supernovae data. In the figure, there are three cases: the standard  $\Lambda\text{CDM}$  model (Fig. 4(a)), a universe with a phantom-like fluid without curvature (Fig. 4(c)), and other phantom-like case but with small curvature (Fig. 4(e)).<sup>7,8</sup> Applying this correlation between  $H_0$  and  $N_{\text{eff}}$  into Eq. 4.14, I determine the allowed values of  $H_0$  for

<sup>6</sup> BAO is an abbreviation for baryonic acoustic oscillations.

<sup>7</sup> An important observation is that in Fig. 4 the non-flat  $\Lambda\text{CDM}$  case is not contemplated, because it does not ameliorate the Hubble tension [64].

<sup>8</sup> The phantom-like case with null curvature has the equation of state  $P = -1.004^{+0.038}_{-0.016} \times \rho$ , while the non-zero curvature scenario has  $-1.06\rho < P < -\rho$ . The likelihood analyses of these two setups have been carried out in [2], where they are labeled as  $P_7$  and  $P_{18}$ .

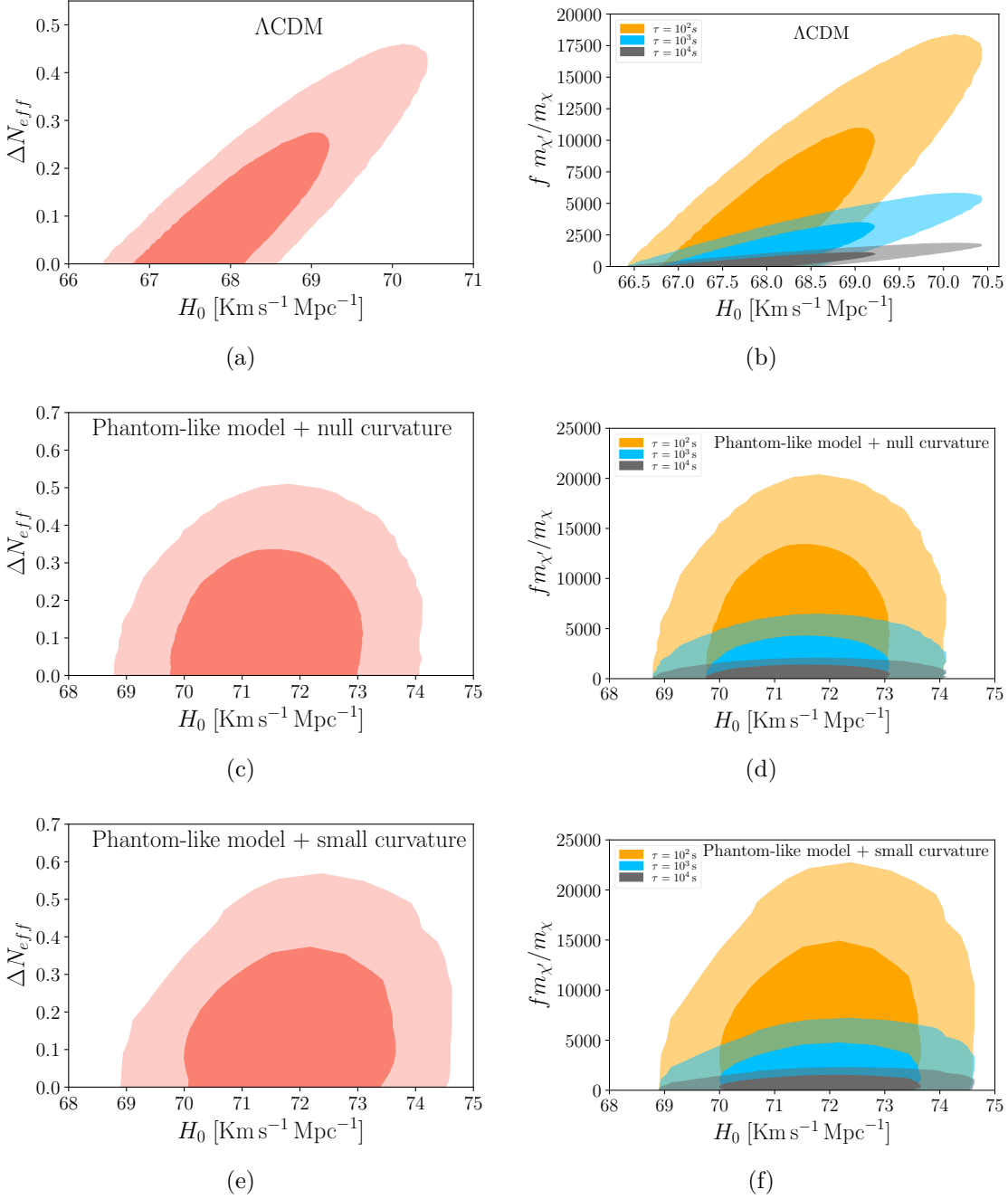


Figure 4 – Allowed regions of parameters that connect the non-thermal dark matter mechanism presented here and the value of Hubble constant in the  $\Lambda\text{CDM}$  and phantom-like cases [1]. The first row corresponds to the  $\Lambda\text{CDM}$  model, and in the second and third rows, a phantom-like quintessence is introduced, first in a spatially flat model, then with non-null spatial curvature. The data set that connects  $\Delta N_{\text{eff}}$  and  $H_0$  showed in (a), (c), and (e) is taken from [2]. In all figures, the lighter regions correspond to 99% of CL, while the darkest regions correspond to 68% of CL. In (b), (d), and (f) the orange, blue and gray regions correspond to the cases where  $\chi'$  lifetime is  $10^2 \text{s}$ ,  $10^3 \text{s}$  and  $10^4 \text{s}$  respectively. The bounds use Planck 2018 CMB data, BAO, and type Ia data from the Pantheon sample.

different choices of the product  $fm_{\chi'}/m_{\chi}$  at  $\tau = 10^2$  s,  $10^3$  s, and  $10^4$  s. That procedure generates the second column of Fig. 4.14.<sup>9</sup>

In Fig. 4, it is clear that Phantom-like cosmologies alone allow  $H_0$  values larger than  $70 \text{ km s}^{-1} \text{ Mpc}^{-1}$ , and consequently can solve the  $H_0$  trouble. This explains why in all cases  $fm_{\chi'}/m_{\chi}$  can go to zero.

The Fig. 4(a) and Fig. 4(b) imply that if local measurements pointing to  $H_0 \leq 70 \text{ km s}^{-1} \text{ Mpc}^{-1}$  is adopted, there would be no need for a Phantom-like cosmology. In this case, the mechanism described here can yield  $N_{\text{eff}} = 3.3$ , and consequently, provides  $H_0 = 70 \text{ km s}^{-1} \text{ Mpc}^{-1}$  [2]. Nevertheless, it is clear that it is not possible to obtain  $H_0 > 71 \text{ km s}^{-1} \text{ Mpc}^{-1}$  adopting the  $\Lambda\text{CDM}$  as a prior. It is needed to go beyond the  $\Lambda\text{CDM}$  model to find values of  $H_0$  consistent with local measurements.

In Fig. 4, phantom-like cases have a mild difference in the allowed parameter space. Thus, I can safely say that with or without curvature, the proposal used here can alleviate the  $H_0$  tension.

I stress that the advantage of this mechanism is a small introduction of new concepts to alleviate the Hubble tension. In other words, the dark matter particle hypothesis is an already well-established idea, therefore, to alleviate the cited cosmological tension, it was needed add only a phantom-like fluid, a new particle, the dark matter “mother”, and the  $\chi' \rightarrow \chi + \gamma$  and/or  $\chi' \rightarrow \chi + \nu$  decay channels. These considerations are not too extravagant. Furthermore, observing the central values of the parameters contained in [2], it is clear that the phantom-like cases considered here are small deviations from the standard cosmological model.

By observing the phantom-like cases depicted in Figure 4, it is evident that the inclusion of the phantom-like fluid alone can potentially provide a solution to the Hubble tension, as no additional  $\Delta N_{\text{eff}}$  is required. However, when  $\Delta N_{\text{eff}}$  is not null, the mechanism employed here can explain the presence of an additional radiation source.

Figures 4(a), 4(c), and 4(e) offer a means to establish an upper bound on the lifetime of  $\chi'$ . To illustrate, I set  $\tau$  to  $10^3$  s and  $10^4$  s, and  $f = 0.01$ , and generated Fig. 5. For  $m_{\chi'}/m_{\chi} = 10^3$  the upper limit is  $\tau \lesssim 5 \times 10^8$  s, while for  $m_{\chi'}/m_{\chi} = 10^4$  it is  $\tau \lesssim 5 \times 10^6$  s. I anticipate that these limits will be improved soon, in a more restrictive way. These chosen mass ratio values will be clear in the next subsection.

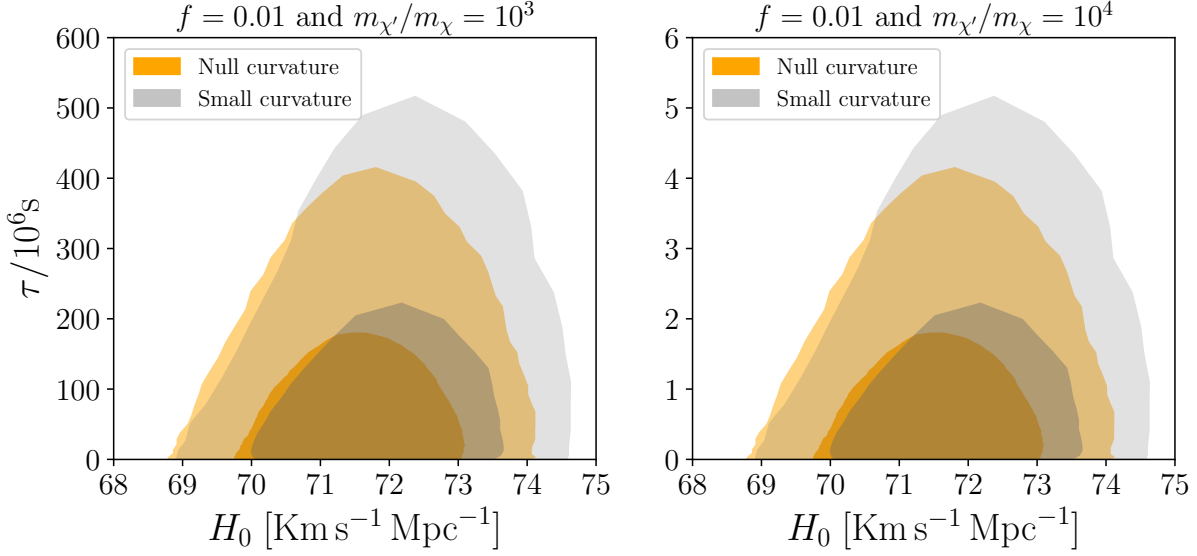


Figure 5 – Allowed parameter space for dark matter lifetime  $\tau$  and Hubble constant  $H_0$  for phantom-like cases. The data used to create this figure is the same as in Fig. 4. The lighter regions in both figures represent 99% of the confidence level, while the darkest regions represent 68% of the confidence level. The orange region represents the null curvature case, while the gray region represents the curved case. In both cases, it is assumed that only 1% of the present-day dark matter abundance is generated by the  $\chi'$  decay, i.e.,  $f = 0.01$ . The left figure considers a mass ratio of  $m_{\chi'}/m_{\chi} = 10^3$ , while the right figure represents the case where  $m_{\chi'}/m_{\chi} = 10^4$ .

#### 4.1.1 Energy evolution of dark matter

Here, the fraction of dark matter particles are created in a hot stage. At matter-radiation equality, the kinetic energy of these particles is lost as the universe expands and they become cold. It is important for this event to occur before matter-radiation equality ( $t_{\text{eq}}$ ). I use Eq. 4.11 to assess whether dark matter particles produced in this way are non-relativistic at  $t_{\text{eq}}$ .

Taking  $\tau \sim 10^2 \text{ s} - 10^4 \text{ s}$  and  $m_{\chi'}/m_{\chi} \sim 10^4 - 10^6$ , which is within the region of interest to solve the  $H_0$  problem, I show in Figs. 6(a) and 6(b) that the dark matter particles are non-relativistic at matter-radiation equality for  $m_{\chi'}/m_{\chi} = 10^3$  and  $m_{\chi'}/m_{\chi} = 10^4$ . In Figs. 6(c) and 6(d), it is shown that for  $m_{\chi'}/m_{\chi} = 10^5$  and  $m_{\chi'}/m_{\chi} = 10^6$ , dark matter particles are still relativistic at matter-radiation equality.

Fig. 6 informs  $m_{\chi'}/m_{\chi} \sim 10^4$  is an upper limit. This holds independent of  $f$ . Despite the energy of dark matter being independent of  $f$ , I assume  $f$  to be small, for reasons that I will explain deeply soon. Anyway, the mechanism used here may have a cold and

<sup>9</sup> The two phantom-like cases considered here do not appreciably alter the matter-radiation equality. Thus, Eq. 4.7 is still valid as well as the Eq. 4.14. For more details of the cosmological central value parameters see [2].

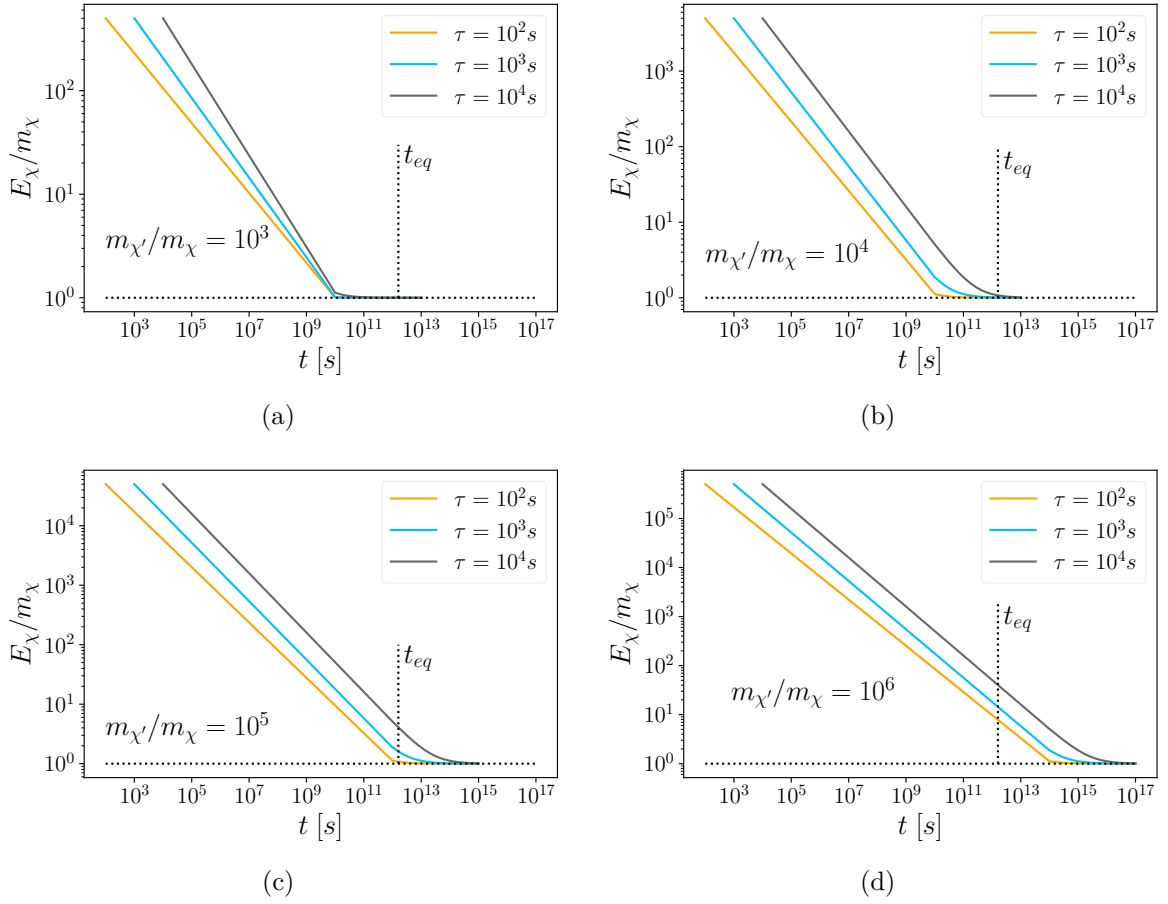


Figure 6 – Time evolution of dark matter energy [1]. Dark matter mother lifetime is  $\tau = \{10^2 \text{ s}, 10^3 \text{ s}, 10^4 \text{ s}\}$  and the ratio between dark matter mother and dark matter mass is  $m_{\chi'}/m_\chi = \{10^3, 10^4, 10^5, 10^6\}$ . In all situations of (a) and (b), dark matter is cold at matter-radiation equality ( $t_{eq}$ ), while in (c) and (d) dark matter is hot in all lifetime scenarios.

hot dark matter contribution (see Figs. 6(c) and 6(d)), i.e., it is a mixed scenario, which may solve some small-scale problems appearing in purely cold dark matter simulations [13, 65, 66, 67, 68].

I am also considering that  $\chi'$  decay occurs after the dark matter freeze-out, which implies that the dark matter particles added to the fundamental plasma are not able to be annihilated in standard model particles in an efficient way, i.e., the process  $\chi + \bar{\chi} \rightarrow SM + SM$  is basically irrelevant in the stages of the Universe that I am considering.

My next step is to calculate the dark matter present-day density parameter due to the considered mechanism. I denote  $\tilde{\rho}_\chi$  as the dark matter energy density generated the  $\chi'$  decay, to distinguish the dark matter energy density from any other mechanism  $\rho_\chi$ . The ratio between these two values is

$$\frac{\tilde{\rho}_\chi}{\rho_\chi} = \frac{\tilde{n}_\chi m_\chi \gamma_\chi}{n_\chi m_\chi} \Rightarrow \frac{\tilde{\Omega}_\chi}{\Omega_\chi} = f \gamma_\chi. \quad (4.15)$$

Where I use the density parameter definition:  $\Omega = \rho/\rho_{\text{crit}}$ .

Today  $\gamma_\chi = 1$ . Then, I can write

$$\frac{\tilde{\Omega}_{\chi,0}}{\Omega_{\chi,0}} = f. \quad (4.16)$$

Thus, the parameter density for cold dark matter at present-day is

$$\Omega_{CDM,0} = \tilde{\Omega}_{\chi,0} + \Omega_{\chi,0} = (1 + f)\Omega_{\chi,0}. \quad (4.17)$$

Which allows me to write

$$\tilde{\Omega}_{\chi,0}h^2 = \frac{f}{1+f}\Omega_{CDM,0}h^2 \approx 0.0012. \quad (4.18)$$

Where I used  $f \approx 0.01$  and  $\Omega_{CDM,0}h^2 \approx 0.12$  [13].

The above equation is the contribution of this mechanism for the currently cold dark matter density parameter.

## 4.2 BBN constraints

The Big Bang Nucleosynthesis is well-supported by the observational data, being one of the cosmology cornerstones. Any energy injection episode that happens around this period of time may alter the BBN predictions, therefore, BBN can be used as a bound.

The decay  $\chi' \rightarrow \chi + \gamma$  adds new photons to the cosmological fluid, increases its electromagnetic energy, and may lead to significant perturbations in the abundance of light elements such as Helium, Deuterium, and Lithium. The decay  $\chi' \rightarrow \chi + \nu$  also can generate a photon cascade as pointed in [69, 60]. The goal of this section is to avoid these perturbations in the BBN results and generates a parameter space that agrees with BBN bounds.

Before  $\chi'$  decay, the universe has a background of photons. Therefore, the energy of photons detected in the CMB is the addition of the energy of this photon background and the energy of new photons generated from the mechanism presented here. For that reason, I write the mean energy of CMB photons as

$$E_\gamma^{CMB} = E_\gamma^{BG} \left( \frac{n_\gamma^{BG}}{n_\gamma^{CMB}} \right) + E_\gamma \left( \frac{\tilde{n}_\gamma}{n_\gamma^{CMB}} \right), \quad (4.19)$$

where  $E_\gamma^{BG}$  is the mean energy of background photons,  $E_\gamma$  the mean energy of photons due to the  $\chi'$  decay,  $n_\gamma^{BG}$  the number density of background photons,  $n_\gamma^{CMB}$  the number density of CMB photons, and  $\tilde{n}_\gamma$  the number density of photons generated by the  $\chi'$  decay mechanism.

The above equation motivates the definition of the electromagnetic energy released by  $\chi'$  decay as

$$\zeta_{EM} \equiv E_\gamma Y_\gamma. \quad (4.20)$$

Where  $Y_\gamma = \tilde{n}_\gamma/n_\gamma^{CMB}$ . The kinematics of  $\chi'$  decay provides  $E_\gamma$ , and cosmology gives  $Y_\gamma$  factor.

Taking the definition of  $Y_\gamma$  as inspiration, I define the ratio between the dark matter number density and the CMB photons as

$$\begin{aligned} Y_{DM} &\equiv \frac{n_{DM}}{n_\gamma^{CMB}} \\ &= \frac{n_{CDM} + n_{HDM}}{n_\gamma^{CMB}} \\ &= \frac{n_{CDM}}{n_\gamma^{CMB}} (1 + f). \end{aligned}$$

Which provides a natural way to define

$$Y_\chi \equiv \frac{n_{CDM}}{n_\gamma^{CMB}} \times f. \quad (4.21)$$

Applying the definition of critical density ( $\rho_{\text{crit}} \equiv 3H/(8\pi G)$ ), the definition of density parameter ( $\Omega \equiv \rho/\rho_{\text{crit}}$ ), the cold particle energy density expression ( $\rho = nm$ ), and the time evolution of number density of CMB photons ( $n_\gamma^{CMB} = n_{\gamma,0}^{CMB}/a^3$ ) to  $Y_\chi$  gives

$$Y_\chi \equiv \frac{n_{CDM}}{n_\gamma^{CMB}} \times f = \frac{f}{m_\chi n_{\gamma,0}^{CMB}} \times \Omega_{CDM} a^3 \rho_{\text{crit}}. \quad (4.22)$$

To calculate  $\Omega_{CDM} a^3 \rho_{\text{crit}}$ , I use the dark matter density parameter definition,  $\Omega_{DM} = \rho_{DM}/\rho_{\text{crit}}$ , together with the dark matter energy density evolution,  $\rho_{DM} = \rho_{DM,0}/a^3$ :

$$\Omega_{CDM} a^3 \rho_{\text{crit}} = \frac{\rho_{DM}}{\rho_{\text{crit}}} \times a^3 \rho_{\text{crit}} = \frac{\rho_{DM,0}}{a^3} \times a^3 = \Omega_{CDM,0} \rho_{\text{crit},0}. \quad (4.23)$$

Consequently, the expression for  $Y_\chi$  depends only on some of the present-day cosmological parameters:

$$Y_\chi = \frac{f}{m_\chi n_{\gamma,0}^{CMB}} \times \Omega_{CDM,0} \rho_{\text{crit},0}. \quad (4.24)$$

Adopting  $\rho_{\text{crit},0} \approx 1.05 \times 10^{-5} h^2 \text{ GeV}/\text{cm}^3$  [13],  $n_{\gamma,0}^{CMB} = 412 \text{ cm}^{-3}$  (Eq. 2.127), and  $\Omega_{CDM,0} h^2 = 0.12$  [13], gives

$$Y_\chi = 3.01 \times 10^{-9} \left( \frac{\text{GeV}}{m_\chi} \right) \times f. \quad (4.25)$$

The decay  $\chi' \rightarrow \chi + \gamma$  implies that  $n_{\chi'} = n_\chi = \tilde{n}_\gamma$ . This provides the relation  $Y_\chi = Y_\gamma$ . Therefore, to calculate  $\zeta_{EM}$  for this decay channel, it is only necessary to calculate  $E_\gamma$ . To do that, I use four-momentum conservation:  $p_{\chi'} - p_\gamma = p_\chi$ , where each of these four-momenta is defined in Eq. 4.8, under the limit where  $m_{\chi'} \gg m_\chi$ .

$$p_{\chi'} - p_\gamma = p_\chi \Rightarrow m_{\chi'}^2 - 2p_{\chi'} \cdot p_\gamma = m_\chi^2 \Rightarrow 2m_{\chi'} E_\gamma = m_{\chi'}^2 - m_\chi^2$$

$$\Rightarrow E_\gamma = \frac{m_{\chi'}}{2} \left[ 1 - \left( \frac{m_\chi}{m_{\chi'}} \right)^2 \right] \approx \frac{m_{\chi'}}{2}. \quad (4.26)$$

Thus, the electromagnetic energy released by  $\chi' \rightarrow \chi + \gamma$  is

$$\zeta_{EM} = E_\gamma Y_\gamma = E_\gamma Y_\chi \Rightarrow \boxed{\zeta_{EM} = 1.5 \times 10^{-9} \text{GeV} \times \left( f \frac{m_{\chi'}}{m_\chi} \right)}. \quad (4.27)$$

By calculating the ratio of Eq. 4.27 to Eq. 4.14, the relation between  $\zeta_{EM}$  and  $\Delta N_{\text{eff}}$  is obtained, which is given by:

$$\zeta_{EM} = 6 \times 10^{-7} \text{GeV} \sqrt{\frac{10^6 \text{s}}{\tau}} \Delta N_{\text{eff}}. \quad (4.28)$$

Now, I will calculate  $\zeta_{EM}$  for the decay  $\chi' \rightarrow \chi + \nu$ . In this case, the number density relation is  $n_{\chi'} = n_\chi = \tilde{n}_\nu$ , where  $\tilde{n}_\nu$  is not the total neutrinos number density, it is the number density of neutrinos included in the universe due to the  $\chi'$  decay. The  $\chi'$  decay generates neutrinos that can interact with particles in the background resulting in high-energy photons which induce nuclear reactions and consequently alter the BBN predictions. I will adopt the illustrative example where all the neutrino energy is converted into electromagnetic energy, i.e.,  $E_\nu \approx E_\gamma$  and  $\tilde{n}_\nu \approx \tilde{n}_\gamma$ , which implies  $Y_\nu \approx Y_\gamma \approx Y_\chi$ . Because  $Y_\nu$  is being considered equivalent to Eq. 4.25, calculating  $\zeta_{EM}$  only requires determining the neutrino energy after the  $\chi'$  decay. To do that, I again use the four-momenta conservation ( $p_{\chi'} - p_\nu = p_\chi$ ), where each of these four-momenta is defined in Eq. 4.8, under the limits:  $m_{\chi'} \gg m_\chi$  and  $m_{\chi'} \gg m_\nu$ .

$$p_{\chi'} - p_\nu = p_\chi \Rightarrow m_{\chi'}^2 - 2p_{\chi'} \cdot p_\nu + m_\nu^2 = m_\chi^2 \Rightarrow 2m_{\chi'} E_\nu = m_{\chi'}^2 + m_\nu^2 - m_\chi^2 \quad (4.29)$$

$$\Rightarrow E_\nu = \frac{m_{\chi'}}{2} \left[ 1 + \left( \frac{m_\nu}{m_{\chi'}} \right)^2 - \left( \frac{m_\chi}{m_{\chi'}} \right)^2 \right] \Rightarrow E_\nu \approx m_{\chi'}/2 \quad (4.30)$$

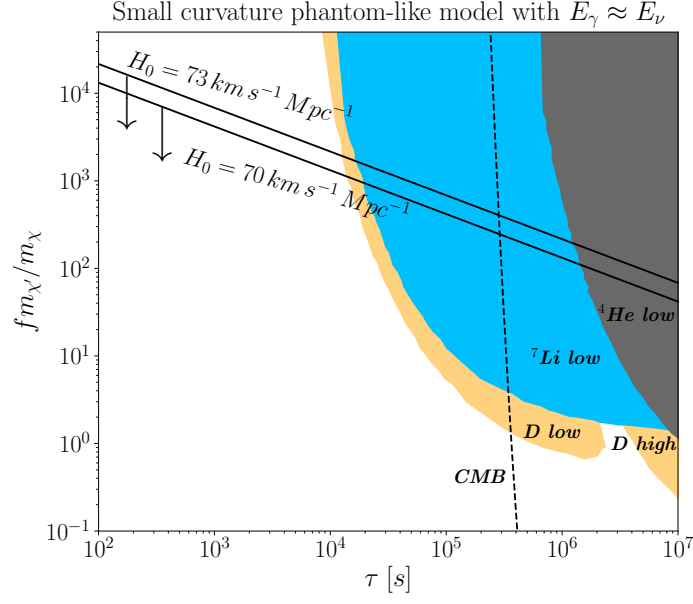
Thus, the electromagnetic energy released by the decay  $\chi' \rightarrow \chi + \nu$  is

$$\zeta_{EM} = E_\gamma Y_\gamma = E_\nu Y_\chi = 1.5 \times 10^{-9} \text{GeV} \times \left( f \frac{m_{\chi'}}{m_\chi} \right), \quad (4.31)$$

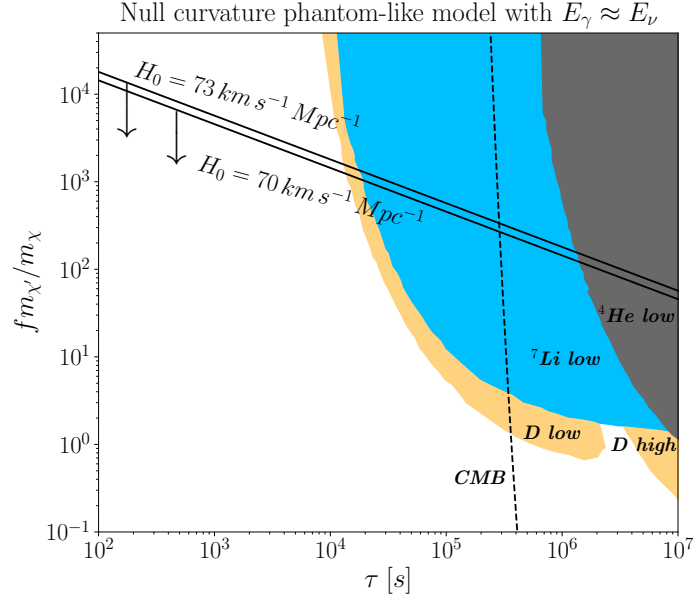
which is equivalent to the case  $\chi' \rightarrow \chi + \gamma$ .

The electromagnetic energy released by the decay of  $\chi'$  particles can have a significant impact on the abundance of light elements in the early universe. There are two primary ways in which this can occur. Firstly, the additional photons generated by the decay can be highly energetic and, in turn, destroy light elements such as Deuterium, Helium, and Lithium. Secondly, the injected neutrinos can induce the conversion of neutrons into protons and electrons, which can also generate an electromagnetic cascade and affect the abundance of light elements.





(a)



(b)

Figure 7 – BBN bounds based on light element abundances [3]. The shaded regions are excluded because they represent a situation where the electromagnetic energy released by  $\chi'$  decay alters the well-understood light element abundance. The nearly vertical dotted line is the constraint stemming from the spectral distortion of the CMB is also present. All region to its left is excluded. The diagonal lines are the superior limit for theoretical prediction for  $H_0$  using the non-thermal dark matter production mechanism. In Fig.7(a) I display the results for  $E_\gamma = E_\nu$  and  $k \neq 0$ , where  $E_\gamma$  is the energy of the gamma-rays produced after the  $\chi' \rightarrow \chi + \nu$  or  $\chi' \rightarrow \chi + \gamma$  decay. In Fig.7(b) I show the results for  $E_\gamma = E_\nu$ , but with  $k = 0$ . The detail of these geometrical considerations is in the text.

The numerical results from [70] provide constraints on  $\tau \times \zeta_{EM}$  parameter space, that could potentially lead to the destruction of light element abundances predicted by BBN. These bounds, along with Eq. 4.27, are used to construct Fig. 7, where the shaded regions represent the excluded  $\tau \times fm_{\chi'}/m_{\chi}$  parameter space that would either destroy Helium-4, Lithium-7, and Deuterium or induce a nuclear reaction that saturates the production of Deuterium. These shaded regions are in disagreement with astronomical observations [71, 72, 73, 74, 75, 76, 77].

Figure 7 also shows the excluded region of the parameter space that would alter the CMB power spectrum. This constraint is represented by the entire region to the left of the nearly vertical dotted line. In this figure, there are two diagonal lines that represent the allowed regions for  $H_0 = 73 \text{ km s}^{-1} \text{ Mpc}^{-1}$  and  $H_0 = 70 \text{ km s}^{-1} \text{ Mpc}^{-1}$ , respectively. All the regions below these lines permit the respective Hubble constant. The figure also shows that to satisfy both CMB and BBN constraints, it is necessary to have  $\tau \lesssim 10^4 \text{ s}$ . I reiterate that this means that there is a region in the relevant parameter space that allows the formalism presented here not to destroy the light element abundances and not deform the CMB power spectrum.

### 4.3 Entropy injection bounds

Equation 2.119 informs us that the entropy ratio between two moments  $t_i$  and  $t_f$  is given by

$$\frac{S_f}{S_i} = \frac{g_{*s}^f T_f^3 a_f^3}{g_{*s}^i T_i^3 a_i^3}. \quad (4.32)$$

In a radiation-dominated phase, the relations  $H = 1/(2t)$  and  $H^2 = 8\pi\rho_r/3$  can be used to write

$$\rho_r = \frac{3}{32\pi t^2}. \quad (4.33)$$

Comparing this result with  $\rho_r = \pi^2 g_* T^4/30$ , given by Eq. 2.100, I get

$$T = \left( \frac{45}{16\pi^3 g_* t^2} \right)^{1/4}, \quad (4.34)$$

which consequently gives

$$\frac{T_i}{T} = \left( \frac{g_*}{g_*^i} \right)^{1/4} \sqrt{\frac{t}{t_i}}. \quad (4.35)$$

During the radiation era, the following result holds :

$$\frac{a_f}{a_i} = \left( \frac{t_f}{t_i} \right)^{1/2}. \quad (4.36)$$

Applying the temperature ratio and the scale factor ratio to the entropy ratio provides

$$\frac{S_f}{S_i} = \frac{g_{*s}^f}{g_{*s}^i} \left( \frac{g_*^i}{g_*^f} \right)^{3/4}. \quad (4.37)$$

The immediate consequence of this result is that in the standard cosmology, between BBN and CMB,  $g_{*s}^i = g_{*s}^f$  and  $g_*^i = g_*^f$ , which implies that between these two events, there is no relevant addition to the entropy radiation, i.e.,  $S_f = S_i$  [78, 79, 59, 80].

The  $\chi'$  decay adds an effective number of neutrinos, which increases fundamental plasma entropy. Equation 4.37 informs that relative entropy variation is

$$\frac{S_f - S_i}{S_i} = \frac{\Delta S}{S_i} = \frac{g_{*s}^f}{g_{*s}^i} \left( \frac{g_*^i}{g_*^f} \right)^{3/4} - 1, \quad (4.38)$$

whose  $g$ 's factors are defined by

$$g_*^i = g_\gamma + \frac{7}{8} N_\nu \times 2 \times g_\nu \left( \frac{T_\nu}{T_\gamma} \right)^4 = 2 + \frac{21}{4} \left( \frac{4}{11} \right)^{4/3} = 3.36264, \quad (4.39a)$$

$$g_{*s}^i = g_\gamma + \frac{7}{8} \times N_\nu \times 2 \times g_\nu \left( \frac{T_\nu}{T_\gamma} \right)^3 = 2 + \frac{21}{4} \left( \frac{4}{11} \right) = 3.90909, \quad (4.39b)$$

$$g_*^f = g_\gamma + \frac{7}{8} (3 + \Delta N_{\text{eff}}) \times 2 \times g_\nu \left( \frac{T_\nu}{T_\gamma} \right)^4 = 2 + \frac{7}{4} (3 + \Delta N_{\text{eff}}) \left( \frac{4}{11} \right)^{4/3}, \quad (4.39c)$$

$$g_{*s}^f = g_\gamma + \frac{7}{8} \times (3 + \Delta N_{\text{eff}}) \times 2 \times g_\nu \left( \frac{T_\nu}{T_\gamma} \right)^3 = 2 + \frac{7}{4} \times (3 + \Delta N_{\text{eff}}) \left( \frac{4}{11} \right). \quad (4.39d)$$

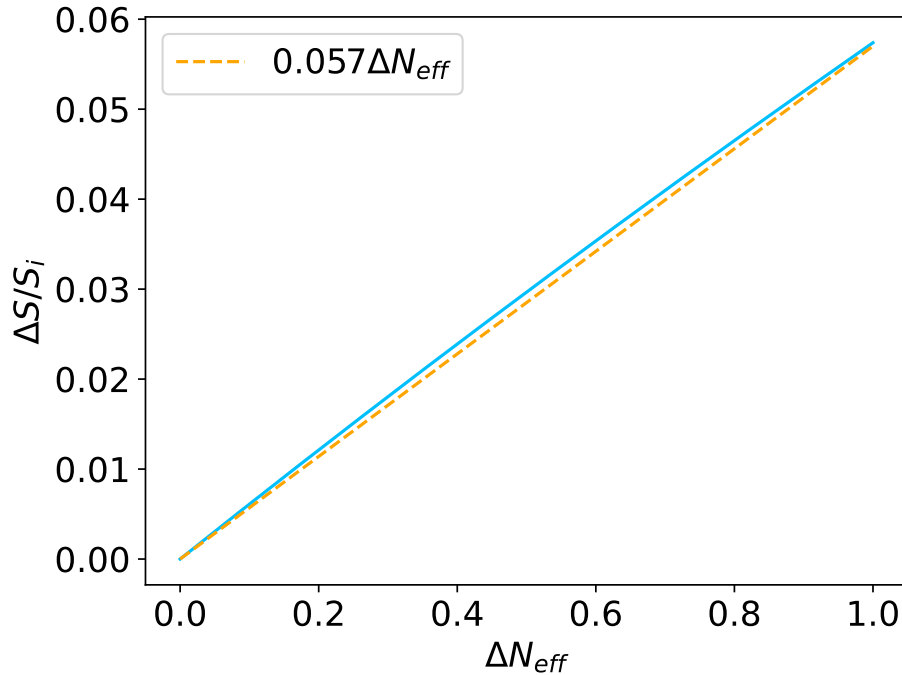


Figure 8 – Relative entropy variation as a function of  $\Delta N_{\text{eff}}$ . The blue solid line is obtained by Eq. 4.38, while the orange dotted line is a linear approximation.

In Fig. 8, I show how the relative entropy variation changes with  $\Delta N_{\text{eff}}$ . It is important to note that in the range  $0 \leq \Delta N_{\text{eff}} \leq 1$  the approximation

$$\boxed{\frac{\Delta S}{S_i} = 0.057 \Delta N_{\text{eff}}} \quad (4.40)$$

is quite accurate. Also, observe that for the superior limit,  $\Delta N_{\text{eff}} = 1$ , the relative entropy variation is less than 6%. This is an excellent sign that the formalism used here is not in strong disagreement with BBN and CMB data.

Figure 4 shows that  $\Delta N_{\text{eff}} \lesssim 0.6$ . Applying this inequality to Eq. 4.40, the limit  $\Delta S/S_i \lesssim 0.0342$  is obtained. This means that the formalism used here can increase the entropy by at most about 4%, avoiding problems with BBN and indicating that the mechanism is not excluded.

## 4.4 Effective theory for the case where decay yields dark matter and photons

Until this point, the procedure adopted here to alleviate the Hubble tension has been model-independent. The transition from a model-independent to a model-dependent description is accomplished by introducing specific Lagrangians that describe the decay of  $\chi'$  [81].

Up to the present day, the dark matter particle was not detected, and its spinorial nature remains unknown. If dark matter is a spin-0 particle, akin to the Higgs boson, it must be described by a scalar field  $\phi_\chi$ . If it possesses a spin of 1/2, like leptons and quarks, it should be described by a spinorial field  $\psi_\chi$ . Another possibility is that the dark matter particle has a spin of 1, similar to the photon,  $W^\pm$  boson,  $Z^0$  boson, and gluons, which would require a vector field  $\chi_\mu$  for its description [81].<sup>10 11</sup>

I will consider three effective operators of dimension five that encompass spin-0, spin-1, and spin-1/2 dark matter particles for the decay process  $\chi' \rightarrow \chi + \gamma$ . The corresponding Feynmann diagrams are shown in Fig. 9.

The decay rate  $\Gamma$  for the two-body decay process  $\chi' \rightarrow \chi + \gamma$  can be analytically calculated and is given by [82]:

$$\Gamma(\chi' \rightarrow \chi + \gamma) = \frac{|\mathbf{p}_\chi(\tau)|}{8\pi m_{\chi'}^2} |\mathcal{M}|^2. \quad (4.41)$$

<sup>10</sup> A higher spin case for the dark matter particle is theoretically possible. However, for the purpose of this analysis, I will not consider such exotic cases.

<sup>11</sup> This field notation also applies to the  $\chi'$  particle. If  $\chi'$  is a spin-0 particle, it is described by a scalar field  $\phi_{\chi'}$ . If  $\chi'$  is a spin-1/2 particle, it is described by a spinor field  $\psi_{\chi'}$ . If  $\chi'$  is a spin-1 particle, it is described by a vector field  $\chi'_\mu$ .

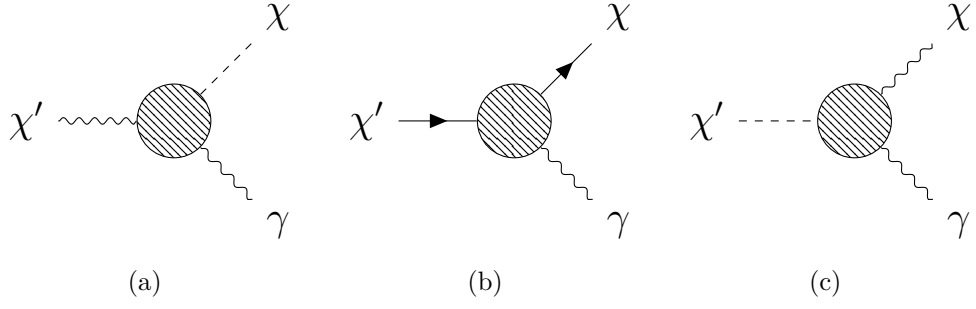


Figure 9 – Diagrammatic representation of a heavy particle ( $\chi'$ ) that decay in hot dark matter ( $\chi$ ) and photon ( $\gamma$ ). Three cases are considered: **(a)**  $\chi'$  is spin-1 and  $\chi$  is a spin-0 particle; **(b)**  $\chi'$  and  $\chi$  are spin-1/2 particles; **(c)**  $\chi'$  is spin-0 and  $\chi$  is a spin-1 particle.

Here,  $\mathcal{M}$  is the Feynman amplitude, which is determined from the specific Lagrangian that describes the decay process.

The kinematics of the decay allows us to determine the momentum of the  $\chi$  particle at  $t = \tau$ . In the rest frame of  $\chi'$ , the four-momentum of particles involved in the  $\chi'$  decay are given by Eq. 4.8. By imposing four-momentum conservation, I find that the magnitude of  $\mathbf{p}_\chi(\tau)$  is equal to

$$|\mathbf{p}_\chi(\tau)| = |\mathbf{p}| = m_{\chi'} - E_\chi(\tau) = m_{\chi'} - m_\chi \left( \frac{m_{\chi'}}{2m_\chi} + \frac{m_\chi}{2m_{\chi'}} \right) = \frac{1}{2}m_{\chi'} \left[ 1 - \left( \frac{m_\chi}{m_{\chi'}} \right)^2 \right]. \quad (4.42)$$

Where I have used the expression for  $E_\chi(\tau)$  given by Eq. 4.9.

After substituting the expression of the magnitude of the momentum, given by Eq. 4.42, into the decay rate formula, I obtain:

$$\Gamma = \frac{1}{16\pi m_{\chi'}} \left[ 1 - \left( \frac{m_\chi}{m_{\chi'}} \right)^2 \right] |\mathcal{M}|^2. \quad (4.43)$$

I will use this interaction rate expression to calculate the lifetime  $\tau = 1/\Gamma$  for three distinct effective operators presented below.

#### 4.4.1 Decay in spin-0 dark matter and photon

The first case to be considered is when the decay  $\chi' \rightarrow \chi + \gamma$  involves a spin-1  $\chi'$  particle and a spin-0  $\chi$  particle. The corresponding Feynman diagram is shown in Figure 9(a). The effective Lagrangian used to describe this decay is given by

$$\mathcal{L}_{\text{eff}} = \frac{1}{\Lambda} \phi_\chi \chi'_{\mu\nu} F^{\mu\nu}, \quad (4.44)$$

where the energy scale  $\Lambda$  is introduced to ensure that the Lagrangian has the correct energy dimension. The specific value of  $\Lambda$  needs to be determined through experiments

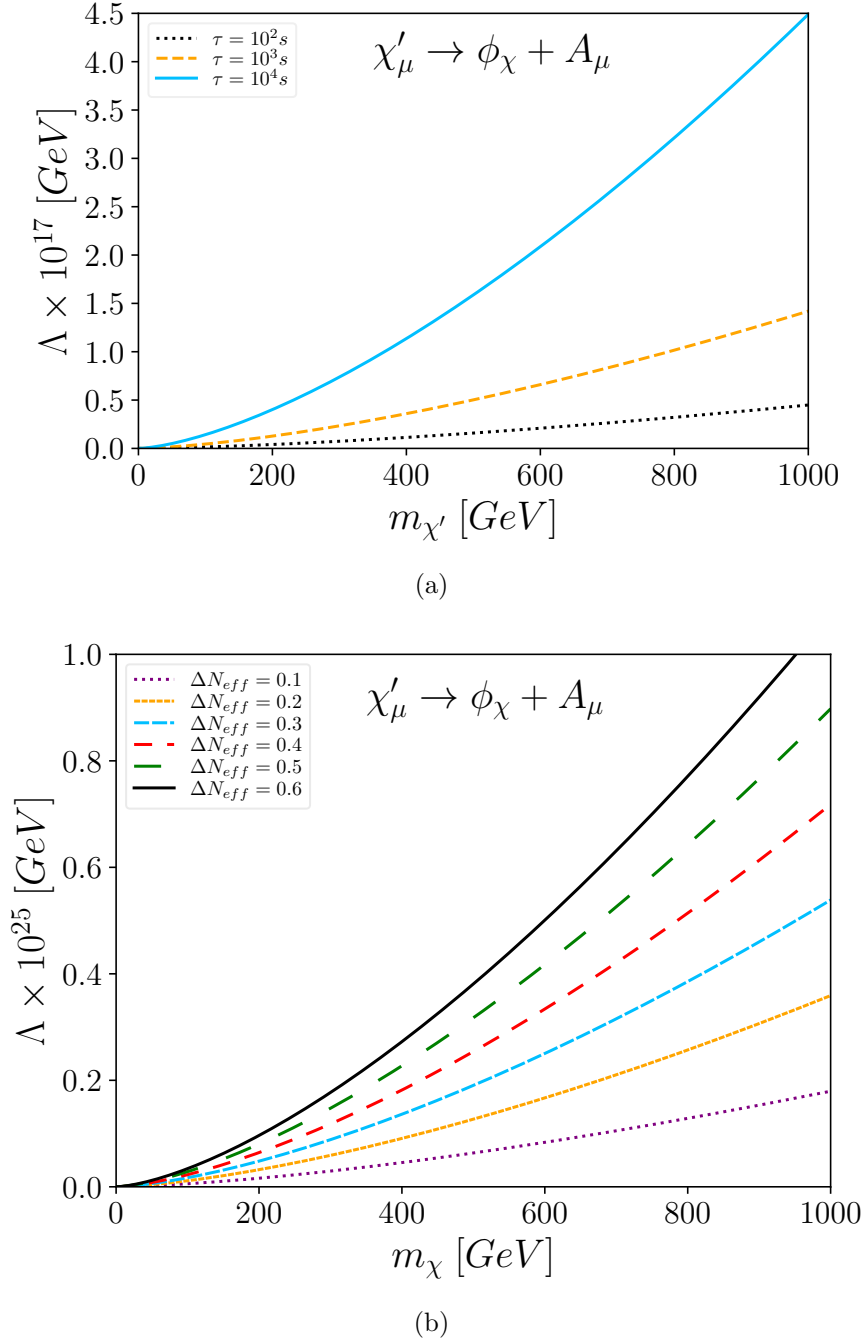


Figure 10 – The figure presents the plots of  $\Lambda$  as a function of  $m_{\chi'}$  and  $m_\chi$  for the scenario where  $\chi'$  is a spin-1 particle and  $\chi$  is a spin-0 particle [1]. In panel (a), the curves for  $m_{\chi'} \times \Lambda$  are shown, calculated using Eq. (4.46) for different lifetimes  $\tau = 10^2, 10^3$  and  $10^4 \text{ s}$ . In panel (b), the curves for  $m_\chi \times \Lambda$  are displayed, obtained from Eqs. (4.14) and (4.46). The parameter space is explored for cases where  $\Delta N_{\text{eff}} = 0.1 - 0.6$ , with a fixed ratio  $f = 0.01$  and  $m_{\chi'}/m_\chi = 10^4$ .

and observations.<sup>12</sup> In this equation, the notation  $\chi'_{\mu\nu} \equiv \partial_\mu \chi'_\nu - \partial_\nu \chi'_\mu$  is being used. The

<sup>12</sup> In the previous context, where  $\Lambda$  represented the cosmological constant, it referred to a specific physical quantity associated with the expansion of the universe. In the current context, where  $\Lambda$  represents the energy scale in the Lagrangian, it is used as a notation to ensure the correct energy dimension of the Lagrangian term. The difference in contexts and the clear distinction between the two uses of  $\Lambda$  should

object  $F^{\mu\nu}$  is the well know electromagnetic tensor, which is defined as  $F_{\mu\nu} = \partial_\mu A_\nu - \partial_\nu A_\mu$ , where  $A^\mu$  being the four-potential [81].

The Feynman amplitude for the present case is given by<sup>13</sup>

$$|\mathcal{M}|^2 = \frac{2m_{\chi'}^4}{3\Lambda^2} \left[ 1 - \left( \frac{m_\chi}{m_{\chi'}} \right)^2 \right]^2. \quad (4.45)$$

By substituting this expression into the general decay rate formula, Eq. 4.43, I obtain the specific decay rate for this case:

$$\Gamma = \frac{m_{\chi'}^3}{24\pi\Lambda^2} \left[ 1 - \left( \frac{m_\chi}{m_{\chi'}} \right)^2 \right]^3 \Rightarrow \boxed{\Gamma \approx \frac{m_{\chi'}^3}{24\pi\Lambda^2}}. \quad (4.46)$$

Therefore, the lifetime is determined by  $\Lambda$  and  $m_{\chi'}$ . I present this relation in Figure 10(a) for  $\tau = 10^2$  s,  $10^3$  s, and  $10^4$  s. It is worth noting that in this figure, the energy scale of  $\Lambda$  appears to be very large. However, this is not a problem since it simply reflects the fact that  $\chi'$  is very long-lived.

Equation 4.14 establishes a connection between  $\Delta N_{\text{eff}}$  and  $\tau$ , while Equation 4.46 relates  $\tau$  to  $m_{\chi'}$  and  $\Lambda$ . As a result,  $\Delta N_{\text{eff}}$  also depends on  $\Lambda$ . By considering these relationships, it becomes possible to identify the parameter space region that addresses the  $H_0$  problem. Figure 10(b) illustrates this region for  $m_\chi/m_{\chi'} = 10^4$ , displaying the values of  $\Lambda$  that result in  $\Delta N_{\text{eff}} = 0.1 - 0.6$ , corresponding to  $H_0 \sim 70 - 72 \text{ km s}^{-1} \text{ Mpc}^{-1}$  as shown in Figure 4(b). It is important to reiterate that if local measurements converge to  $H_0 \sim 70 \text{ km s}^{-1} \text{ Mpc}^{-1}$ , the proposed mechanism alone is sufficient to resolve the discrepancy in  $H_0$ , as demonstrated in Figure 4(a).

#### 4.4.2 Decay in spin-1/2 dark matter and photon

In the second scenario, I consider the decay  $\chi' \rightarrow \chi + \gamma$ , where both  $\chi'$  and  $\chi$  are spin-1/2 fermions. The corresponding Feynman diagram is depicted in Fig. 9(b). To

---

prevent any confusion between the two concepts.

<sup>13</sup> To obtain the Feynman rules for the specific vertices and the Feynman amplitude used in this analysis, I followed the following steps:

1. I implemented the effective Lagrangian into the LanHEP program [83] to generate the Feynman rules file. LanHEP allows for the automated derivation of Feynman rules from the Lagrangian.
2. The generated Feynman rules file was then incorporated into the CalcHEP program [84], which enables the computation of the Feynman amplitude ( $|\mathcal{M}|^2$ ) associated with the given Feynman rules.
3. Using CalcHEP, I obtained the Feynman amplitude ( $|\mathcal{M}|^2$ ) for the specific decay process.
4. Additionally, I utilized CalcHEP to generate a Wolfram Mathematica file containing the calculation of the decay rate ( $\Lambda$ ) based on the obtained Feynman amplitude.

By following this procedure, I was able to determine the Feynman rules, compute the Feynman amplitude, and perform the decay rate calculation for the all decay process under investigation.

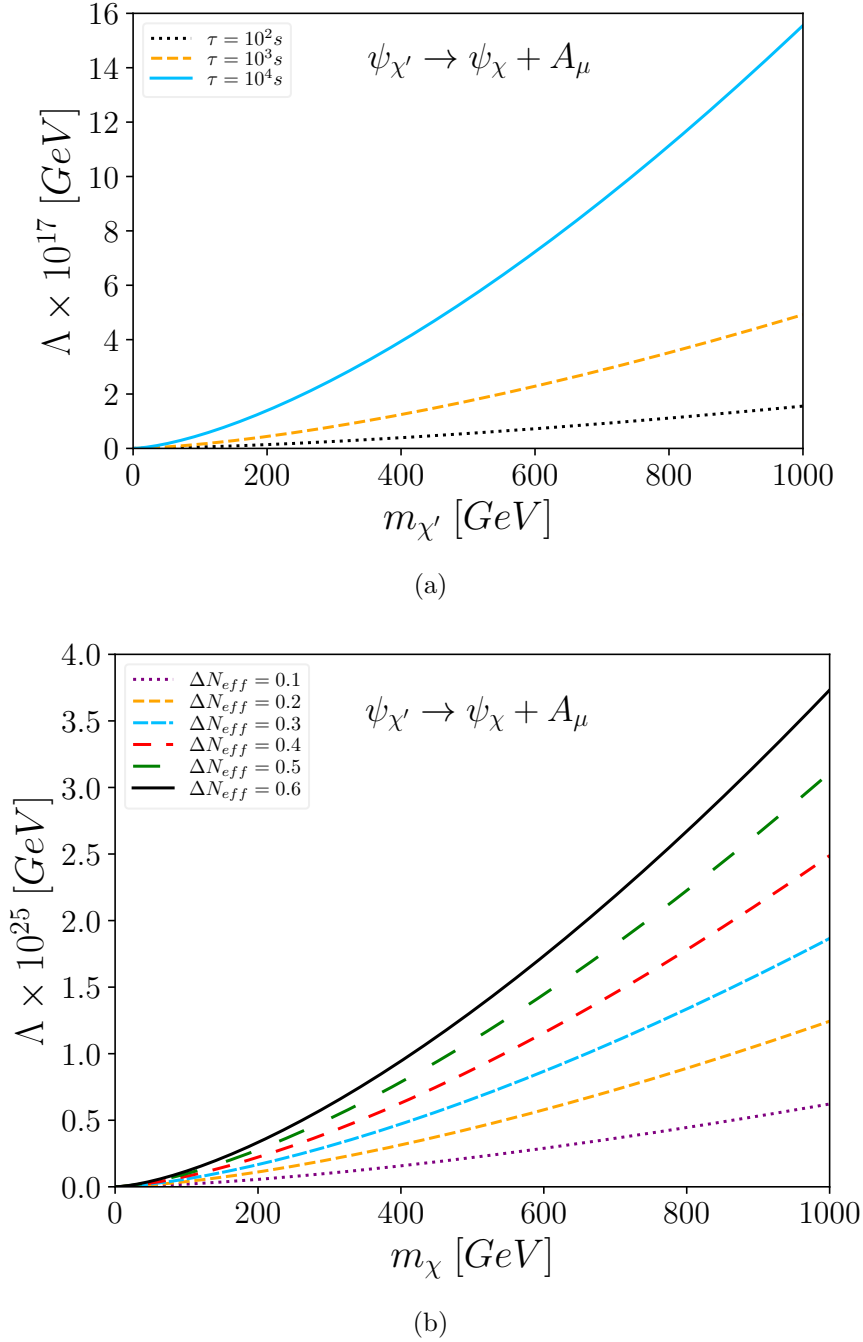


Figure 11 – Plot of  $\Lambda$  as a function of the masses of  $\chi$  and  $\chi'$  for the case where  $\chi'$  and  $\chi$  are spin-1/2 particles [1]. In panel (a), the curves of  $m_{\chi'} \times \Lambda$  are generated using Eq. 4.49 with  $\tau = 10^2, 10^3$ , and,  $10^4$  s. Panel (b) displays the curves of  $m_{\chi} \times \Lambda$  constructed from Eqs. 4.14 and 4.49. The cases where  $\Delta N_{\text{eff}} = 0.1 - 0.6$  are considered, with  $f = 0.01$  and  $m_{\chi'}/m_{\chi} = 10^4$ .

describe this decay, I utilize the effective theory given by the Lagrangian:

$$\mathcal{L}_{\text{eff}} = \frac{1}{\Lambda} \bar{\psi}_{\chi} \sigma^{\mu\nu} \psi_{\chi'} F_{\mu\nu} + h.c., \quad (4.47)$$



where  $\sigma^{\mu\nu} = \frac{i}{2}[\gamma^\mu, \gamma^\nu]$ . The Hermitian conjugate (*h.c.*) is added to ensure the Lagrangian's Hermiticity. The corresponding Feynman amplitude is

$$|\mathcal{M}|^2 = \frac{8m_{\chi'}^4}{\Lambda^2} \left[ 1 - \left( \frac{m_\chi}{m_{\chi'}} \right)^2 \right]^2. \quad (4.48)$$

Applying the obtained Feynman amplitude to the decay rate formula given by Eq. 4.43, I arrive at the following result:

$$\Gamma = \frac{m_{\chi'}^3}{2\pi\Lambda^2} \left[ 1 - \left( \frac{m_\chi}{m_{\chi'}} \right)^2 \right]^3 \approx \frac{m_{\chi'}^3}{2\pi\Lambda^2}. \quad (4.49)$$

In a similar manner to the previous case, I utilize Eq. (4.49) to generate a plot illustrating the relationship between  $\Lambda$  and  $m_{\chi'}$  for different values of  $\tau$  in Fig. 11(a). Additionally, I determine the energy scale  $\Lambda$  that corresponds to  $\Delta N_{\text{eff}} = 0.1 - 0.6$  and can potentially address the  $H_0$  discrepancy in Fig. 11(b). This analysis assumes  $m_{\chi'}/m_\chi = 10^4$  and  $f = 0.01$ .

#### 4.4.3 Decay in spin-1 dark matter and photon

The last case considered for the decay  $\chi' \rightarrow \chi + \gamma$  involves  $\chi'$  as a spin-0 particle and  $\chi$  as a spin-1/2 fermion. The corresponding Feynman diagram is shown in Fig. 9(c). The effective Lagrangian for this case is given by

$$\mathcal{L}_{\text{eff}} = \frac{1}{\Lambda} \phi_{\chi'} \chi_{\mu\nu} F^{\mu\nu}, \quad (4.50)$$

where  $\chi_{\mu\nu} \equiv \partial_\mu \chi_\nu - \partial_\nu \chi_\mu$ . The Feynman amplitude is then obtained as

$$|\mathcal{M}|^2 = \frac{2m_{\chi'}^4}{\Lambda^2} \left[ 1 - \left( \frac{m_\chi}{m_{\chi'}} \right)^2 \right]^2, \quad (4.51)$$

which leads to the decay rate

$$\Gamma = \frac{m_{\chi'}^3}{8\pi\Lambda^2} \left[ 1 - \left( \frac{m_\chi}{m_{\chi'}} \right)^2 \right]^3 \approx \frac{m_{\chi'}^3}{8\pi\Lambda^2}. \quad (4.52)$$

Figure 12(a) illustrates the relationship between  $\Lambda$  and  $m_{\chi'}$  for  $\tau = 10^2, 10^3, 10^4$  s. On the other hand, Fig. 12(a) presents the variation of  $\Lambda$  with  $m_\chi$  for different values of  $\Delta N_{\text{eff}}$ , which could potentially provide a solution to the  $H_0$  problem. These plots are generated under the assumptions of  $m_{\chi'}/m_\chi = 10^4$  and  $f = 0.01$ .

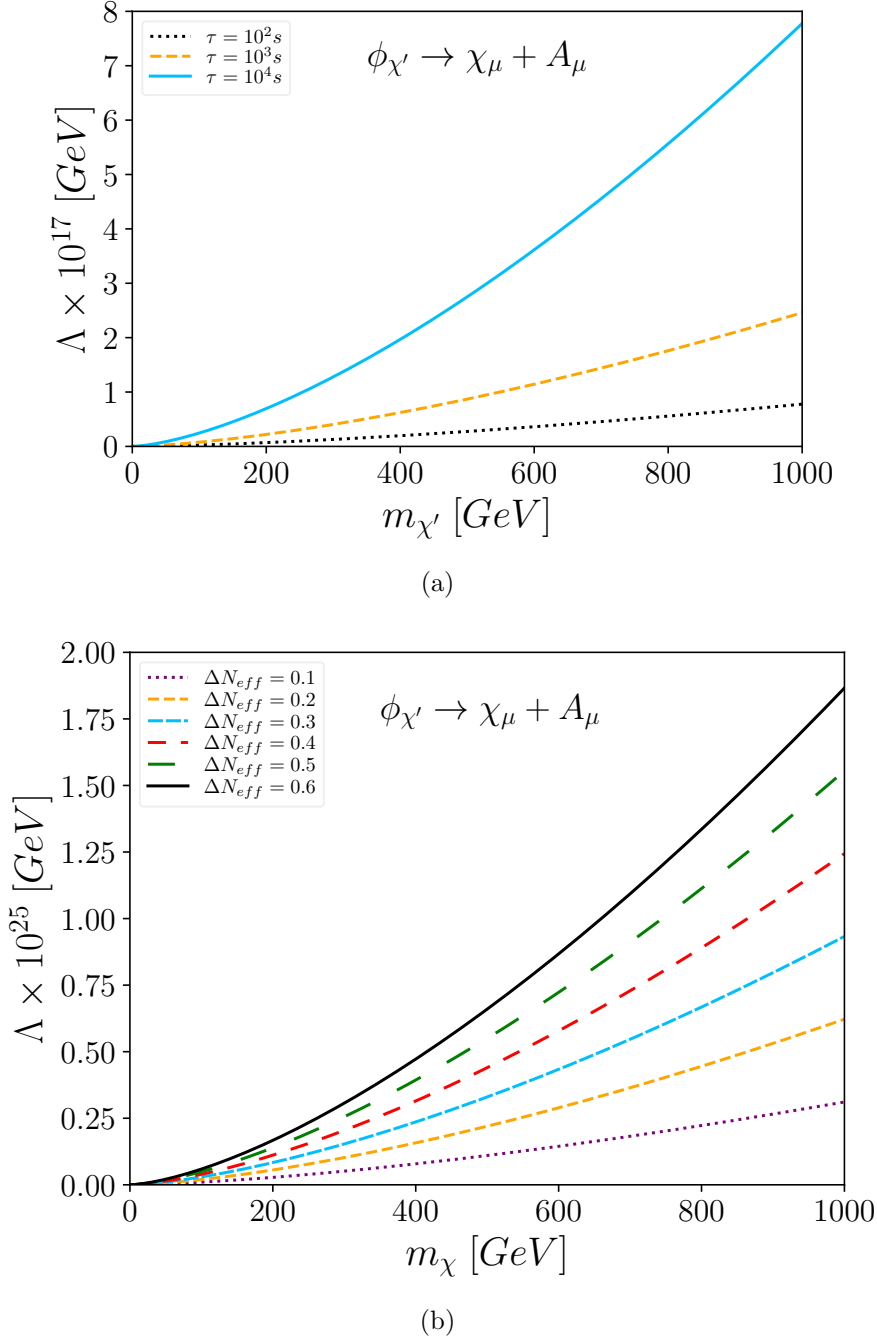


Figure 12 – Plot of  $\Lambda$  as a function of the  $\chi$  and  $\chi'$  masses for the case where  $\chi'$  is a spin-0 particle and  $\chi$  is a spin-1 particle [1]. **(a)** Curves of  $m_{\chi'} \times \Lambda$  are constructed using Eq. 4.52 with  $\tau = 10^2, 10^3$ , and  $10^4$  s. **(b)** Curves of  $m_\chi \times \Lambda$  are constructed using Eqs. 4.14 and 4.52 for different values of  $\Delta N_{\text{eff}}$  ranging from 0.1 to 0.6. The parameters  $f = 0.01$  and  $m_{\chi'}/m_\chi = 10^4$  are considered.

#### 4.4.4 Considerations about lifetime, energy scale and truncation of effective Lagrangians

In all the considered effective theories, the relation  $\tau \propto \Lambda^2/m_{\chi'}^3$  holds. Consequently, as the mass of the parent particle increases, its lifetime decreases. This observation is

not new and has been explored in previous studies searching for gamma-rays and x-rays emitted by long-lived particles [85]. These searches have provided lower mass limits for such particles. To achieve a long-lived  $\chi'$ , a large value of  $\Lambda$  is required. This correlation between the lifetime and the energy scale is evident in Figs. 10, 11, and 12. The connection between long-lived particles and suppression mechanisms, either in the coupling constant or the energy scale, is well-established. In the present work, the latter mechanism is employed [86].

Equation 4.46 provides the lifetime  $\tau_{\chi'_\mu} \approx 75.4 m_{\chi'}^3 / \Lambda^2$ . Similarly, Eq. 4.49 yields the lifetime  $\tau_{\psi_{\chi'}} \approx 6.28 m_{\chi'}^3 / \Lambda^2$ . Lastly, Eq. 4.52 gives the lifetime  $\tau_{\phi_{\chi'}} \approx 25.1 m_{\chi'}^3 / \Lambda^2$ . Based on these equations I can draw the following conclusions: the longest lifetime for  $\chi'$  is observed when it is a vector particle, while the intermediate case corresponds to its scalar nature, and the shortest lifetime is observed when  $\chi'$  is a spin-1/2 fermion.

It is worth noting that the effective Lagrangians used in this analysis have been truncated, specifically by considering only effective field blocks with dimension five. While incorporating additional effective terms could potentially lead to more precise results, it would require the inclusion of higher-order field combinations and additional energy scale constants to ensure the correct energy dimensions of the Lagrangian. However, it is important to acknowledge that there are limitations to the inclusion of more and more higher-order field blocks, as these additional terms would contribute increasingly minor corrections.

In the end, if the decay  $\chi' \rightarrow \chi + \gamma$  is a genuine physical phenomenon, it is expected that there exists a renormalizable theory capable of incorporating this new particle  $\chi'$  alongside the dark matter particle. Such a theory should provide an explanation for the generation of only a small fraction of dark matter through the decay of  $\chi'$ . It is important to note that the results presented here are based on an approximation within a certain energy scale, and there may exist a more complete theory that provides a better understanding of this phenomenon.

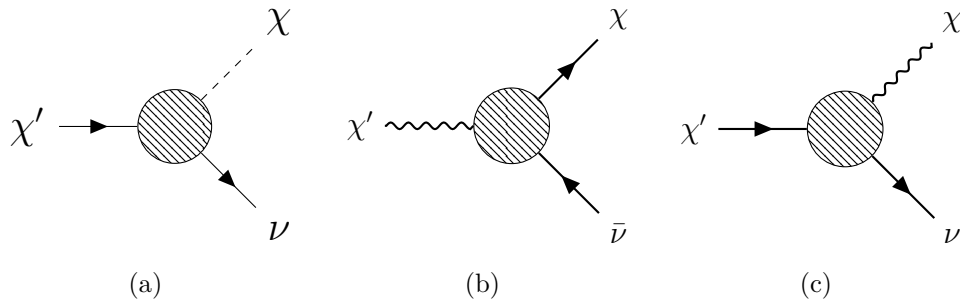


Figure 13 – Diagrammatic representation of a heavy particle ( $\chi'$ ) that decay in hot dark matter ( $\chi$ ) and neutrino ( $\nu$ ). Three cases are considered: **(a)**  $\chi'$  is spin-1/2 and  $\chi$  is a spin-0 particle; **(b)**  $\chi'$  has spin-1 and  $\chi$  has spin-1/2 particles; **(c)**  $\chi'$  is spin-1/2 and  $\chi$  is a spin-1 particle.

## 4.5 Effective theory for the case where decay yields dark matter and standard model neutrinos

In this section, I investigate the model-dependent scenario for the decay  $\chi' \rightarrow \chi + \nu$ . Similar to the previous section, I examine three cases: (a) when  $\chi'$  is a spin-1/2 particle and  $\chi$  is a spin-0 particle; (b) when  $\chi'$  is a spin-1 particle and  $\chi$  is a spin-1/2 particle; (c) when  $\chi'$  is a spin-1/2 fermion and  $\chi$  is a spin-1 boson. Diagrams illustrating these cases are shown in Figure 13.

Similar to the previous section, I use effective theories to calculate the Feynman amplitude for each decay case. Using this information, I determine  $\Gamma$  by applying Eq. 4.43. With the obtained decay rates, I plot the curves of  $m_{\chi'} = m_{\chi'}(\Lambda)$  and  $m_\chi = m_\chi(\Lambda)$  for each model.

### 4.5.1 Decay in spin-0 dark matter and neutrino

Here, I analyze the decay process depicted in Fig. 13(a), where  $\chi'$  is a spin-1/2 particle and  $\chi$  is represented by a real scalar field. The effective Lagrangian describing the decay  $\chi' \rightarrow \chi + \nu$  is given by

$$\mathcal{L}_{\text{eff}} = \sum_{\nu=\nu_e, \nu_\mu, \nu_\tau} \left[ \frac{1}{\Lambda_1} \bar{\psi}_\nu \frac{1}{2} (I + \gamma^5) \gamma^\mu (\partial_\mu \psi_{\chi'}) \phi_\chi + \frac{1}{\Lambda_2} \bar{\psi}_\nu \frac{1}{2} (I + \gamma^5) \gamma^\mu \psi_{\chi'} \partial_\mu \phi_\chi \right] + h.c., \quad (4.53)$$

where  $\Lambda_1$  and  $\Lambda_2$  are constants with mass dimensions. The chirality projection operators  $P_R = (I + \gamma^5)/2$  and  $P_L = (I - \gamma^5)/2$  are introduced to ensure that the neutrinos in the final states are left-handed.<sup>14</sup> Thus, the Feynman amplitude has three contributions, one for each neutrino, and its expression is:

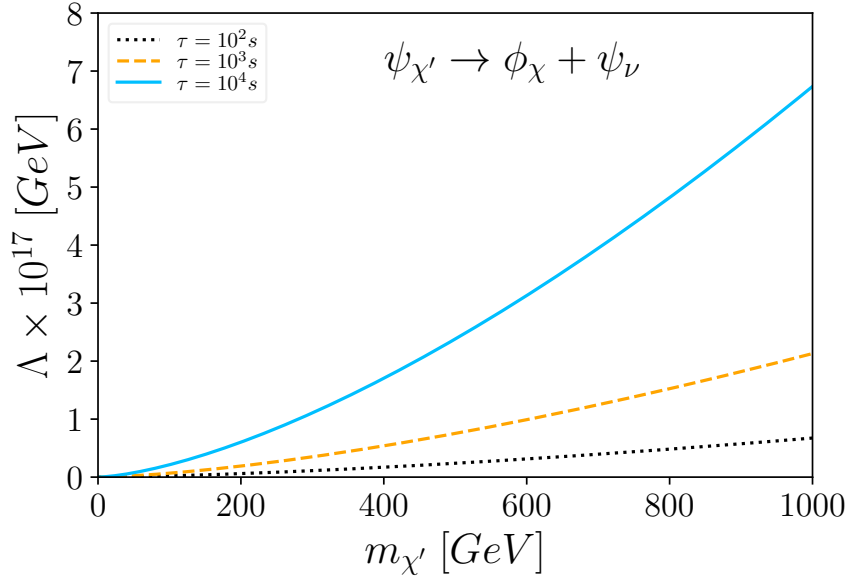
$$\sum_{\nu=\nu_e, \nu_\mu, \nu_\tau} |\mathcal{M}|^2 = \frac{3m_{\chi'}^4}{2} \left( \frac{1}{\Lambda_1} - \frac{1}{\Lambda_2} \right)^2 \left[ 1 - \left( \frac{m_\chi}{m_{\chi'}} \right)^2 \right]. \quad (4.54)$$

Applying this result to Eq. (4.43), I find that

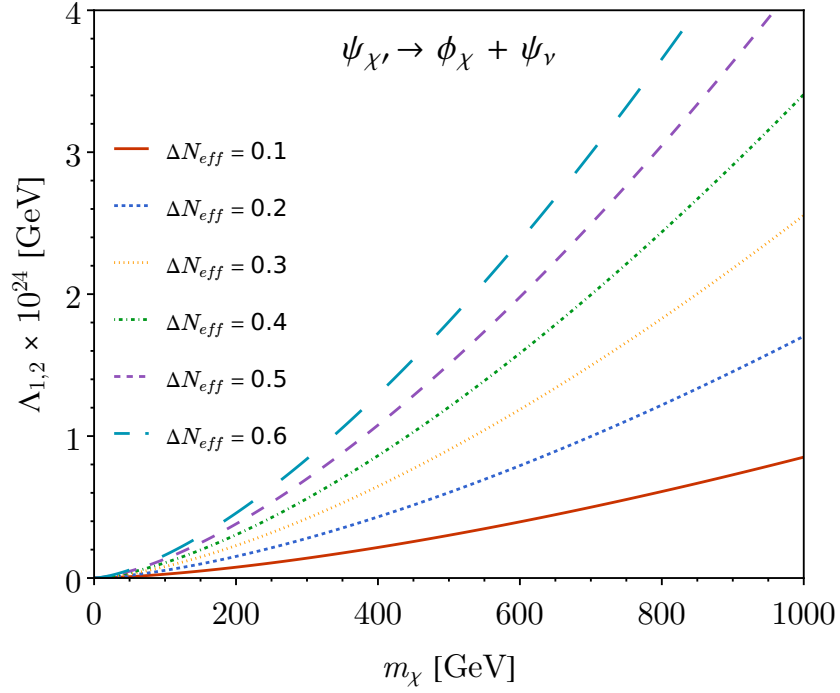
$$\begin{aligned} \Gamma &= \frac{3m_{\chi'}^3}{32\pi} \left( \frac{1}{\Lambda_1} - \frac{1}{\Lambda_2} \right)^2 \left[ 1 - \left( \frac{m_\chi}{m_{\chi'}} \right)^2 \right]^2 \\ \Rightarrow \Gamma &\approx \frac{3m_{\chi'}^3}{32\pi} \left( \frac{1}{\Lambda_1} - \frac{1}{\Lambda_2} \right)^2. \end{aligned} \quad (4.55)$$

There are two energy scales  $\Lambda_1$  and  $\Lambda_2$ . If both have the same value, the  $\chi'$  decay does not occur. If one is much larger than the other, I can ignore it and only the remaining scale energy is necessary. In this case, it is important to note that the surviving scale is

<sup>14</sup> Until now, only left-handed neutrinos have been detected, and thus the correct spinorial terms for neutrinos should be  $(I - \gamma^5)\psi_\nu/2$  and  $\bar{\psi}_\nu(I + \gamma^5)/2$  [81, 28, 13].



(a)

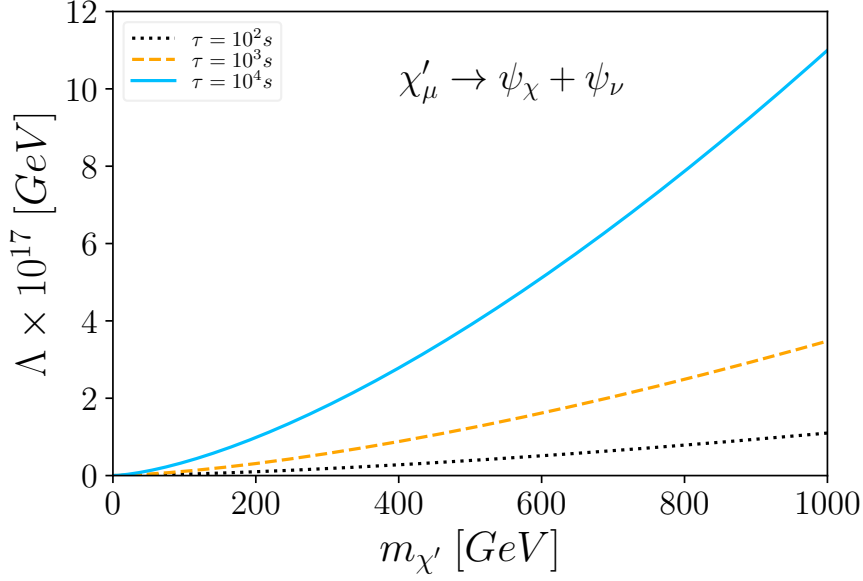


(b)

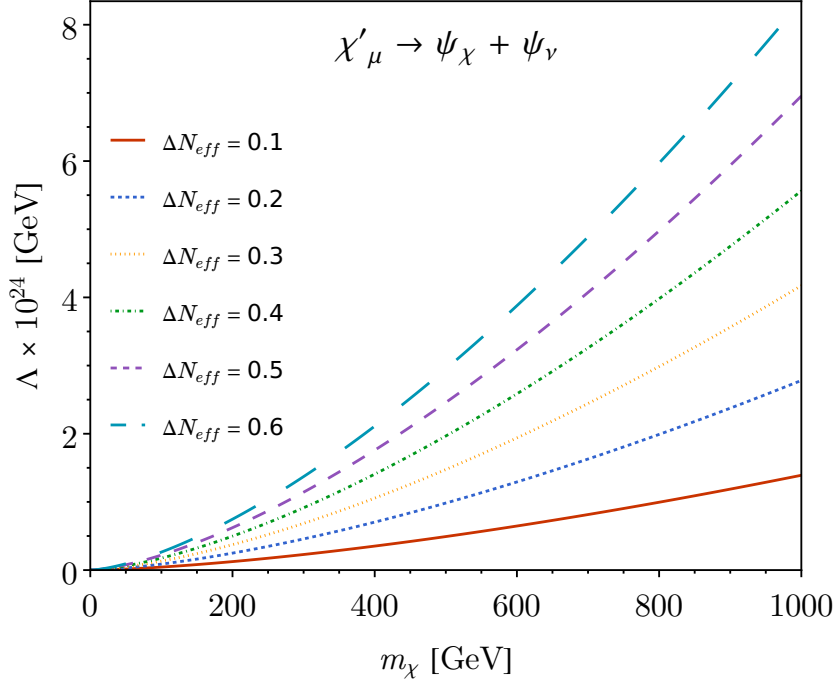
Figure 14 – Plot of  $\Lambda$  as a function of the  $\chi$  and  $\chi'$  masses for the case where  $\chi'$  is a spin-1/2 particle and  $\chi$  is a spin-0 particle. **(a)**  $m_{\chi'} \times \Lambda$  curves built from Eq. 4.55, using  $\tau = 10^2, 10^3$ , and,  $10^4$  s and  $\Lambda_1 = \Lambda_2 = \Lambda$ . **(b)**  $m_{\chi} \times \Lambda$  curves constructed from Eqs. 4.14 and 4.55. I consider the cases where  $\Delta N_{\text{eff}} = 0.1 - 0.6$ , with  $f = 0.01$  and  $m_{\chi'}/m_{\chi} = 10^3$ .

the lowest energy case, as the decay rate depends inversely on the energy scale, i.e., if  $\Lambda_1 \ll \Lambda_2$ , the relevant scale is  $\Lambda_1$ , while if  $\Lambda_2 \ll \Lambda_1$ , the relevant scale is  $\Lambda_2$ . Figure 14 illustrates the dependence of  $m_{\chi'}$  and  $m_{\chi}$  on the relevant scale energy,  $\Lambda$ .

### 4.5.2 Decay in spin-1/2 dark matter and neutrino



(a)



(b)

Figure 15 – Plot of  $\Lambda$  as a function of the masses  $m_{\chi'}$  and  $m_\chi$  for the case where  $\chi'$  is a spin-1/2 particle and  $\chi$  is a spin-0 particle. **(a)** Curves of  $m_{\chi'}$  as a function of  $\Lambda$  built from Eq. 4.58, using  $\tau = 10^2, 10^3$ , and  $10^4$  s. **(b)** Curves of  $\Lambda$  as a function of  $m_\chi$  constructed from Eqs. 4.14 and 4.58. I consider the cases where  $\Delta N_{\text{eff}} = 0.1 - 0.6$ , with  $f = 0.01$  and  $m_{\chi'}/m_\chi = 10^3$ .

In this subsection, I consider the decay  $\chi' \rightarrow \chi + \bar{\nu}$ , where  $\chi'$  is a spin-1 particle and  $\chi$  is a spin-1/2 particle. The Feynman diagram for this case is displayed in Fig. 13(b).

To describe this decay, I adopt the following effective Lagrangian:

$$\mathcal{L}_{\text{eff}} = \sum_{\nu=\nu_e, \nu_\mu, \nu_\tau} \frac{1}{\Lambda} \bar{\psi}_\chi \sigma^{\mu\nu} \chi'_{\mu\nu} \frac{1}{2} (I - \gamma^5) \psi_\nu + h.c., \quad (4.56)$$

where  $\Lambda$  is a constant with dimension of energy,  $\chi'_{\mu\nu} \equiv \partial_\mu \chi'_\nu - \partial_\nu \chi'_\mu$ , and  $\chi'_\mu$  is the vector field that describes  $\chi'$ . The Feynman amplitude for this model is

$$\sum_{\nu=\nu_e, \nu_\mu, \nu_\tau} |\mathcal{M}|^2 = \frac{4m_{\chi'}^4}{\Lambda^2} \left[ 1 + \left( \frac{m_\chi}{m_{\chi'}} \right)^2 - 2 \left( \frac{m_\chi}{m_{\chi'}} \right)^4 \right], \quad (4.57)$$

and the interaction rate is given by

$$\Gamma = \frac{m_{\chi'}^3}{4\pi\Lambda^2} \left[ 1 - \left( \frac{m_\chi}{m_{\chi'}} \right)^2 \right] \left[ 1 + \left( \frac{m_\chi}{m_{\chi'}} \right)^2 - 2 \left( \frac{m_\chi}{m_{\chi'}} \right)^4 \right].$$

This results in the  $m_{\chi'} \gg m_\chi$  limit becomes:

$$\Gamma \approx \frac{m_{\chi'}^3}{4\pi\Lambda^2}. \quad (4.58)$$

Once more, I present the plots illustrating the relationship between  $m_{\chi'}$  and  $\Lambda$  (Fig. 15(a)), as well as between  $m_\chi$  and  $\Lambda$  (Fig. 15(b)). Fig. 15(a) presents the results obtained using lifetimes that do not significantly impact the important outcomes of Big Bang Nucleosynthesis (BBN). In Fig. 15(b), the parameter choices of  $m_{\chi'}/m_\chi = 10^4$ ,  $f = 0.01$ , and  $\Delta N_{\text{eff}} = 0.1 - 0.6$  correspond to a useful parameter region for mitigating the Hubble tension.

### 4.5.3 Decay in spin-1 dark matter and neutrino

In the last case, I consider the decay  $\chi' \rightarrow \chi + \nu$ , where  $\chi'$  is a spin-1/2 particle and  $\chi$  is a spin-1 particle. The Feynman diagram representing this process is shown in Fig. 13(c). I adopt the following effective Lagrangian to describe this decay:

$$\mathcal{L}_{\text{eff}} = \sum_{\nu=\nu_e, \nu_\mu, \nu_\tau} \frac{1}{\Lambda} \bar{\psi}_\nu \frac{1}{2} (I + \gamma^5) \sigma^{\mu\nu} \psi_{\chi'} \chi_{\mu\nu} + h.c., \quad (4.59)$$

where  $\Lambda$  is a constant with dimension of mass,  $\chi_{\mu\nu} = \partial_\mu \chi_\nu - \partial_\nu \chi_\mu$ , and  $\chi_\mu$  is the vector field that describe  $\chi$ . The respective Feynman amplitude is given by:

$$\sum_{\nu=\nu_e, \nu_\mu, \nu_\tau} |\mathcal{M}|^2 = \frac{6m_{\chi'}^4}{\Lambda^2} \left[ 2 - \left( \frac{m_\chi}{m_{\chi'}} \right)^2 - \left( \frac{m_\chi}{m_{\chi'}} \right)^4 \right]. \quad (4.60)$$

Hence, the interaction rate gives

$$\Gamma = \frac{3m_{\chi'}^3}{8\pi\Lambda^2} \left[ 1 - \left( \frac{m_\chi}{m_{\chi'}} \right)^2 \right] \left[ 2 - \left( \frac{m_\chi}{m_{\chi'}} \right)^2 - \left( \frac{m_\chi}{m_{\chi'}} \right)^4 \right],$$

Using one more time the  $m_{\chi'} \gg m_\chi$  limit,  $\Gamma$  becomes:

$$\Gamma \approx \frac{3m_{\chi'}^3}{4\pi\Lambda^2}. \quad (4.61)$$

The graphical results for this case are displayed in Figs. 16(a) and 15(b). These figures show the dependence of  $m_{\chi'}$  and  $m_\chi$  on  $\Lambda$ . The parameter choices for  $\tau$ ,  $f$ ,  $\Delta N_{\text{eff}}$ , and  $m_{\chi'}/m_\chi$  are selected to investigate the potential alleviation of the Hubble tension.

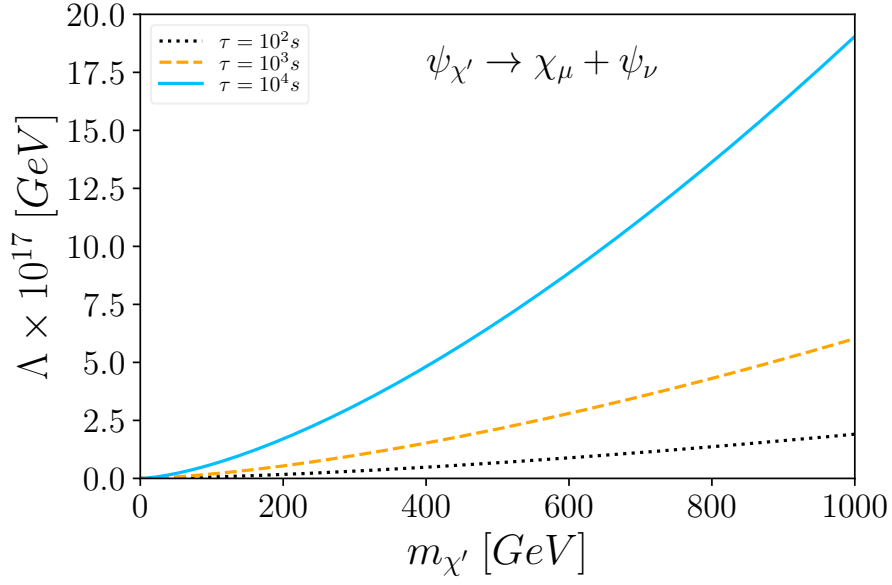
## 4.6 Considerations about the decay dynamics

The results for the  $\chi' \rightarrow \chi + \nu$  decay are very similar to those obtained for the  $\chi' \rightarrow \chi + \gamma$  decay, as can be observed by examining the decay rate case and the curves of  $\Lambda(m_{\chi'})$  and  $\Lambda(m_\chi)$ . In the neutrino case, the lifetime of  $\chi'$  is also proportional to  $\Lambda^2/m_{\chi'}^3$ , requiring a large energy scale  $\Lambda$  to address the Hubble tension.

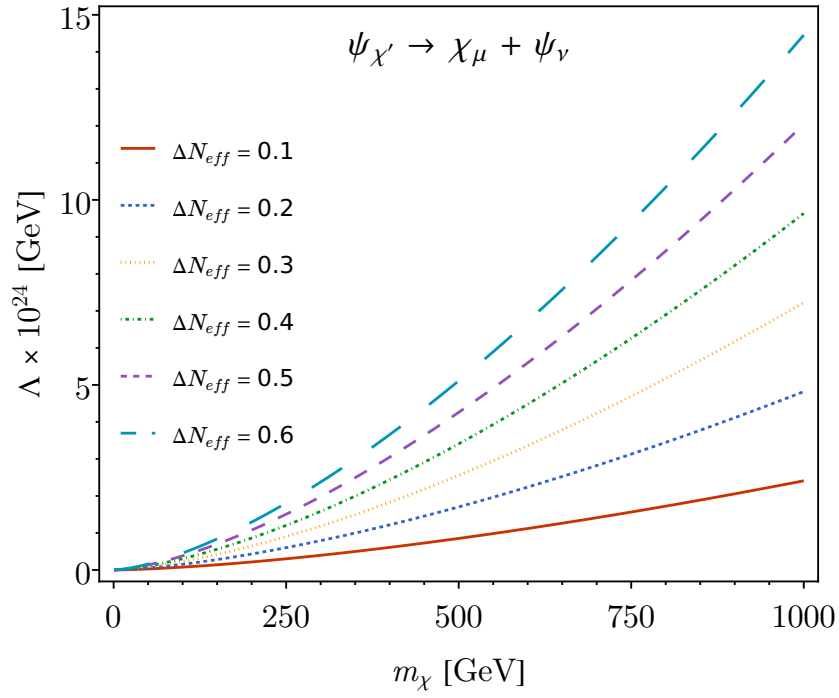
Equation 4.55 provides the lifetime  $\tau_{\phi_{\chi'}} = 33.5\Lambda^2/m_{\chi'}^3$ . On the other hand, Equation 4.58 yields  $\tau_{\chi'_\mu} = 12.6\Lambda^2/m_{\chi'}^3$ . Lastly, Equation 4.61 gives  $\tau_{\psi_{\chi'}} = 4.19\Lambda^2/m_{\chi'}^3$ . These equations demonstrate that for the same  $\Lambda^2/m_{\chi'}^3$  value, the longest-lived scenario occurs when  $\chi'$  is a spin-0 particle, followed by the case of spin-1, and the shortest-lived situation corresponds to the spin-1/2 nature of  $\chi'$ . This hierarchy of lifetimes is different from what was observed in the photonic case.

In the previous case, it seems unlikely that there exists a fundamental vertex connecting dark matter particles and neutrinos. The use of effective theory addresses this issue by providing an approximation of a more complex Feynman diagram that may involve loops and multiple vertex diagrams. Initially, dark matter and neutrinos can be treated within the same fundamental vertex, and the effective theory is employed because the nature of this fundamental interaction remains unknown. The significant advantage of using an effective theory lies in the flexibility to propose effective Lagrangians, which represent an energetically limited description of the fundamental theory [87, 81].





(a)



(b)

Figure 16 – Plot of  $\Lambda$  as a function of the  $\chi$  and  $\chi'$  masses for the case where  $\chi'$  is a spin-1/2 and  $\chi$  is a spin-0 particle. **(a)**  $m_{\chi'} \times \Lambda$  curves built from Eq. (4.61), using  $\tau = 10^2, 10^3$  and  $10^4$  s. **(b)**  $m_{\chi} \times \Lambda$  curves constructed from Eqs. (4.14) and (4.61). I consider the cases where  $\Delta N_{\text{eff}} = 0.1 - 0.6$ , with  $f = 0.01$  and  $m_{\chi'}/m_{\chi} = 10^3$ .



## 5 Conclusions

Considering that the Hubble tension is a genuine cosmological problem, not stemming from biases, statistical errors, or methodological issues, it becomes evident, through CMB analyses, that the  $\Lambda$ CDM model alone fails to reconcile the discrepancy between early and late measurements. This is clear upon direct inspection of Figure 4. Whether or not an effective number of neutrinos is considered, the  $\Lambda$ CDM model fails to alleviate the tension. However, Figure 4 also illustrates that the inclusion of phantom-like fluids can reduce the Hubble tension, and the degree of reduction is somewhat associated with  $N_{\text{eff}}$ . While the phantom-like scenario introduces changes to the cosmology, the set of parameters needed to fit the CMB data remains only a minor perturbation from the  $\Lambda$ CDM case. This is a good feature since the standard cosmological model is excellent in explaining many observed phenomena. It was considered a phantom-like scenario with null and non-null curvatures. The discrepancy between both cases is not substantial, suggesting that the scenario which effectively mitigates the Hubble tension and has flat geometry is favored. Of course, adopting Occam's razor philosophy, where the case with fewer parameters is better.

Given the requirement for an additional  $N_{\text{eff}}$ , the framework utilized in this study provides a compelling explanation for the presence of extra radiation in the early universe. The decay processes  $\chi' \rightarrow \chi + \gamma$  or  $\chi' \rightarrow \chi + \nu$  offer a viable solution as they are consistent with both CMB and BBN constraints. Moreover, these processes possess the advantage of requiring only one additional particle, the dark matter "mother". The existence of dark matter particles is widely accepted by the scientific community, so the only real new particle added here is  $\chi'$ . Nevertheless, this work considers multiple scenarios encompassing different natures of dark matter particles, because its precise properties, such as mass, spin, and Lagrangian description, remain unknown. The proposed formalism is applicable to all of them.

It is evident that the framework employed in this study is not the ideal solution for fully understanding the  $\chi'$  decay. The ideal case would be having access to the renormalizable Lagrangian that precisely describes  $\chi'$ ,  $\chi$ , and their interactions with standard model particles. Unfortunately, such knowledge remains hazy, and it may take time before the complete theory is confirmed. In the meantime, progress can be reached by utilizing effective theories that encompass various dark matter scenarios. This approach circumvents the challenges associated with determining the fundamental theory governing these particles. Importantly, even if a more comprehensive theory of  $\chi'$  decay is eventually discovered, the results obtained in this study will remain valuable. These effective cases serve as approximations that capture the essential behavior of the decay process within

the appropriate energy regime.

Furthermore, it is worth noting that all the effective cases considered in this study exhibit similar outcomes. Despite slight variations in proportional constants, the lifetimes of  $\chi'$  exhibit consistent behavior across all scenarios.

In summary, the adopted mechanism successfully explains the observed range of  $0 < \Delta N_{\text{eff}} \lesssim 0.5$  and provides a consistent estimate for the CMB-based value of  $H_0$  within the range of  $70 - 74 \text{ km s}^{-1} \text{ Mpc}^{-1}$ , i.e., it alleviates the Hubble tension. In order to ensure compatibility with Big Bang Nucleosynthesis (BBN) and other cosmological constraints, certain choices were made for the theory. Specifically, a decay lifetime  $\tau$  less than  $10^4$  seconds was selected to avoid conflicts with BBN. Additionally, a constraint of  $\Delta N_{\text{eff}} < 1$  was imposed to prevent excessive entropy addition, which could lead to incompatibility with BBN predictions. Furthermore, it was found that maintaining a ratio of  $m_{\chi'}/m_{\chi} \lesssim 10^4$  guarantees that  $\chi$  is in a cold state at matter-radiation equality.

This work has several possible deepening to be done in future investigations. Firstly, it is crucial to refine the approximations used throughout the study. The instantaneous decay approximation, the assumption of mean energy for the particles, and the instantaneous thermalization of the decay products from  $\chi'$  are all crude approximations that can be improved. A more rigorous analysis would involve considering a decay process that follows the traditional exponential reduction in the number of particles. Additionally, incorporating the Boltzmann equations that account for all relevant interactions would provide a more comprehensive understanding of the system. Furthermore, conducting an independent analysis of the CMB power spectrum is necessary since the inclusion of additional particle physics parameters can potentially alter the allowed parameter space. I also did not investigate how this no-standard cosmology can change local measurements of  $H_0$ . In future analyses, I intend to add this information. By addressing these aspects and refining the calculations, a more detailed and accurate description of the phenomenon can be achieved. This would contribute to a deeper understanding of the decay dynamics and its implications for the Hubble tension.

# Bibliography

- 1 JESUS, A. S. de; PINTO-NETO, N.; QUEIROZ, F. S.; SILK, J.; SILVA, D. R. da. The hubble rate trouble: an effective field theory of dark matter. *Eur. Phys. J. C*, v. 83, n. 3, p. 203, 2023. Available from Internet: <https://doi.org/10.1140/epjc/s10052-023-11366-5>. Cited 9 times on pages 13, 14, 15, 26, 80, 83, 92, 94, and 96.
- 2 ANCHORDOQUI, L. A.; VALENTINO, E. D.; PAN, S.; YANG, W. Dissecting the  $H_0$  and S8 tensions with Planck + BAO + supernova type Ia in multi-parameter cosmologies. *JHEAp*, v. 32, p. 28–64, 2021. Available from Internet: <https://doi.org/10.1016/j.jheap.2021.08.001>. Cited 9 times on pages 13, 69, 71, 73, 75, 79, 80, 81, and 82.
- 3 ALCANIZ, J. S.; NETO, J. P.; QUEIROZ, F. S.; SILVA, D. R. da; SILVA, R. The Hubble constant troubled by dark matter in non-standard cosmologies. *Sci. Rep.*, v. 12, n. 1, p. 20113, 2022. Available from Internet: <https://doi.org/10.1038/s41598-022-24608-5>. Cited 3 times on pages 14, 26, and 87.
- 4 AGHANIM, N. et al. Planck 2018 results. VI. Cosmological parameters. *Astron. Astrophys.*, v. 641, p. A6, 2020. [Erratum: *Astron. Astrophys.* 652, C4 (2021)]. Available from Internet: <https://doi.org/10.1051/0004-6361/201833910>. Cited 4 times on pages 25, 69, 71, and 73.
- 5 VALENTINO, E. D. et al. In the realm of the hubble tension - a review of solutions. *Classical and Quantum Gravity*, IOP Publishing, v. 38, n. 15, p. 153001, jul. 2021. Available from Internet: <https://doi.org/10.1088/1361-6382/ac086d>. Cited 4 times on pages 25, 71, 72, and 73.
- 6 VAGNOZZI, S. New physics in light of the  $H_0$  tension: An alternative view. *Phys. Rev. D*, American Physical Society, v. 102, p. 023518, Jul 2020. Available from Internet: <https://link.aps.org/doi/10.1103/PhysRevD.102.023518>. Cited 4 times on pages 25, 73, 75, and 79.
- 7 ANCHORDOQUI, L. A.; GOLDBERG, H. Neutrino cosmology after WMAP 7-Year data and LHC first Z' bounds. *Phys. Rev. Lett.*, v. 108, p. 081805, 2012. Available from Internet: <https://doi.org/10.1103/PhysRevLett.108.081805>. Cited 2 times on pages 25 and 73.
- 8 HOBSON, M. P.; EFSTATHIOU, G. P.; LASENBY, A. N. *General relativity: an introduction for physicists*. [S.l.]: Cambridge University Press, 2006. Cited 15 times on pages 29, 34, 35, 36, 39, 40, 51, 52, 61, 62, 63, 65, 66, 67, and 118.
- 9 TAYLOR, J. R.; TAYLOR, J. R. *Classical mechanics*. [S.l.]: Springer, 2005. v. 1. Cited 3 times on pages 29, 39, and 66.
- 10 WEINBERG, S. *Cosmology*. [S.l.]: OUP Oxford, 2008. Cited 7 times on pages 35, 36, 40, 53, 58, 69, and 76.
- 11 RYDEN, B. *Introduction to cosmology*. [S.l.]: Cambridge University Press, 2017. Cited 8 times on pages 35, 40, 59, 65, 66, 67, 68, and 77.

- 12 DODELSON, S.; SCHMIDT, F. *Modern cosmology*. [S.l.]: Academic press, 2020. Cited 12 times on pages 36, 40, 50, 53, 54, 57, 58, 59, 60, 62, 63, and 69.
- 13 WORKMAN, R. L. et al. Review of Particle Physics. *PTEP*, v. 2022, p. 083C01, 2022. Available from Internet: <<https://doi.org/10.1093/ptep/ptac097>>. Cited 17 times on pages 40, 53, 54, 56, 57, 59, 60, 71, 76, 77, 78, 83, 84, 85, 98, 117, and 118.
- 14 SHANKAR, R. *Principles of quantum mechanics*. [S.l.]: Springer Science & Business Media, 2012. Cited 2 times on pages 41 and 67.
- 15 PATHRIA, R. K. *Statistical mechanics*. [S.l.]: Elsevier, 2016. Cited 3 times on pages 43, 50, and 118.
- 16 PIATTELLA, O. *Lecture notes in cosmology*. [S.l.]: Springer, 2018. Cited 6 times on pages 46, 47, 48, 50, 54, and 57.
- 17 Planck Collaboration et al. Planck 2018 results - vi. cosmological parameters. *A&A*, v. 641, p. A6, 2020. Available from Internet: <<https://doi.org/10.1051/0004-6361/201833910>>. Cited 7 times on pages 49, 53, 54, 56, 59, 75, and 79.
- 18 BERTONE, G.; HOOPER, D. History of dark matter. *Rev. Mod. Phys.*, American Physical Society, v. 90, p. 045002, Oct 2018. Available from Internet: <<https://link.aps.org/doi/10.1103/RevModPhys.90.045002>>. Cited 4 times on pages 55, 56, 57, and 78.
- 19 ZWICKY, F. Republication of: The redshift of extragalactic nebulae. *General Relativity and Gravitation*, Springer, v. 41, n. 1, p. 207–224, 2009. Available from Internet: <<https://doi.org/10.1007/s10714-008-0707-4>>. Cited on page 55.
- 20 ZWICKY, F. On the masses of nebulae and of clusters of nebulae. *The Astrophysical Journal*, v. 86, p. 217, out. 1937. Available from Internet: <<https://ui.adsabs.harvard.edu/abs/1937ApJ....86..217Z>>. Cited on page 55.
- 21 WOOLF, N. J. On the stabilization of clusters of galaxies by ionized gas. *Astrophysical Journal*, vol. 148, p. 287, v. 148, p. 287, 1967. Available from Internet: <<https://adsabs.harvard.edu/full/record/seri/ApJ../0148/1967ApJ...148..287W.html>>. Cited on page 55.
- 22 TURNROSE, B. E.; ROOD, H. J. On the hypothesis that the coma cluster is stabilized by a massive, ionized intergalactic gas. *The Astrophysical Journal*, v. 159, p. 773, 1970. Available from Internet: <<https://adsabs.harvard.edu/full/1970ApJ...159..773T>>. Cited on page 55.
- 23 Rubin, V. C.; Ford W. KENT, J. Rotation of the Andromeda Nebula from a Spectroscopic Survey of Emission Regions. *The Astrophysical Journal*, v. 159, p. 379, fev. 1970. Available from Internet: <<https://ui.adsabs.harvard.edu/abs/1970ApJ...159..379R>>. Cited on page 55.
- 24 Rubin, V. C.; Ford W. K., J.; Thonnard, N. Extended rotation curves of high-luminosity spiral galaxies. IV. Systematic dynamical properties, Sa -> Sc. *The Astrophysical Journal*, v. 225, p. L107–L111, nov. 1978. Available from Internet: <<https://ui.adsabs.harvard.edu/abs/1978ApJ...225L.107R>>. Cited on page 55.

- 25 Tisserand, P. et al. Limits on the macho content of the galactic halo from the eros-2 survey of the magellanic clouds. *A&A*, v. 469, n. 2, p. 387–404, 2007. Available from Internet: <<https://doi.org/10.1051/0004-6361:20066017>>. Cited on page 56.
- 26 HINSHAW, G. et al. Nine-year wilkinson microwave anisotropy probe (wmap) observations: Cosmological parameter results. *The Astrophysical Journal Supplement Series*, The American Astronomical Society, v. 208, n. 2, p. 19, sep 2013. Available from Internet: <<https://dx.doi.org/10.1088/0067-0049/208/2/19>>. Cited on page 56.
- 27 BERTONE, G.; HOOPER, D.; SILK, J. Particle dark matter: evidence, candidates and constraints. *Physics Reports*, v. 405, n. 5, p. 279–390, 2005. ISSN 0370-1573. Available from Internet: <<https://www.sciencedirect.com/science/article/pii/S0370157304003515>>. Cited 2 times on pages 57 and 78.
- 28 THOMSON, M. *Modern particle physics*. [S.l.]: Cambridge University Press, 2013. Cited 2 times on pages 57 and 98.
- 29 FRIEMAN, J. A.; TURNER, M. S.; HUTERER, D. Dark energy and the accelerating universe. *Annu. Rev. Astron. Astrophys.*, Annual Reviews, v. 46, p. 385–432, 2008. Available from Internet: <<https://doi.org/10.1146/annurev.astro.46.060407.145243>>. Cited 2 times on pages 59 and 60.
- 30 TONG, D. Lectures on cosmology. *Cambridge University*, 2019. Cited 3 times on pages 67, 68, and 69.
- 31 RYDEN, B.; PETERSON, B. M. *Foundations of astrophysics*. [S.l.]: Cambridge University Press, 2020. Cited on page 68.
- 32 PITKIN, M.; REID, S.; ROWAN, S.; HOUGH, J. Gravitational Wave Detection by Interferometry (Ground and Space). *Living Rev. Rel.*, v. 14, p. 5, 2011. Available from Internet: <<https://doi.org/10.12942/lrr-2011-5>>. Cited on page 69.
- 33 BERNAL, J. L.; VERDE, L.; RIESS, A. G. The trouble with  $H_0$ . *JCAP*, v. 10, p. 019, 2016. Available from Internet: <<https://doi.org/10.1088/1475-7516/2016/10/019>>. Cited 4 times on pages 69, 70, 75, and 79.
- 34 Dawson, K. S. et al. The Baryon Oscillation Spectroscopic Survey of SDSS-III. *The Astronomical Journal*, v. 145, n. 1, p. 10, jan. 2013. Available from Internet: <<https://ui.adsabs.harvard.edu/abs/2013AJ...145...10D>>. Cited on page 70.
- 35 ABBOTT, T. M. C. et al. Dark energy survey year 3 results: Cosmological constraints from galaxy clustering and weak lensing. *Phys. Rev. D*, American Physical Society, v. 105, p. 023520, Jan 2022. Available from Internet: <<https://link.aps.org/doi/10.1103/PhysRevD.105.023520>>. Cited on page 70.
- 36 RIESS, A. G. et al. Cosmic Distances Calibrated to 1% Precision with Gaia EDR3 Parallaxes and Hubble Space Telescope Photometry of 75 Milky Way Cepheids Confirm Tension with  $\Lambda$ CDM. *Astrophys. J. Lett.*, v. 908, n. 1, p. L6, 2021. Available from Internet: <<https://doi.org/10.3847/2041-8213/abdbaf>>. Cited 2 times on pages 70 and 71.
- 37 FREEDMAN, W. L. Measurements of the Hubble Constant: Tensions in Perspective. *Astrophys. J.*, v. 919, n. 1, p. 16, 2021. Available from Internet: <<https://doi.org/10.3847/1538-4357/ac0e95>>. Cited 2 times on pages 70 and 72.



- 38 WONG, K. C. et al. H0LiCOW – XIII. A 2.4 per cent measurement of H0 from lensed quasars:  $5.3\sigma$  tension between early- and late-Universe probes. *Mon. Not. Roy. Astron. Soc.*, v. 498, n. 1, p. 1420–1439, 2020. Available from Internet: <https://doi.org/10.1093/mnras/stz3094>. Cited on page 70.
- 39 ABBOTT, B. P. et al. A gravitational-wave standard siren measurement of the Hubble constant. *Nature*, v. 551, n. 7678, p. 85–88, 2017. Available from Internet: <https://doi.org/10.1038/nature24471>. Cited on page 70.
- 40 PALMESE, A. et al. A statistical standard siren measurement of the Hubble constant from the LIGO/Virgo gravitational wave compact object merger GW190814 and Dark Energy Survey galaxies. *Astrophys. J. Lett.*, v. 900, n. 2, p. L33, 2020. Available from Internet: <https://doi.org/10.3847/2041-8213/abaeff>. Cited on page 70.
- 41 HINSHAW, G. et al. Nine-Year Wilkinson Microwave Anisotropy Probe (WMAP) Observations: Cosmological Parameter Results. *Astrophys. J. Suppl.*, v. 208, p. 19, 2013. Available from Internet: <https://doi.org/10.1088/0067-0049/208/2/19>. Cited on page 71.
- 42 DUTCHER, D. et al. Measurements of the E-mode polarization and temperature-E-mode correlation of the CMB from SPT-3G 2018 data. *Phys. Rev. D*, v. 104, n. 2, p. 022003, 2021. Available from Internet: <https://doi.org/10.1103/PhysRevD.104.022003>. Cited on page 71.
- 43 WANG, K.; HUANG, Q.-G. Implications for cosmology from Ground-based Cosmic Microwave Background observations. *JCAP*, v. 06, p. 045, 2020. Available from Internet: <https://doi.org/10.1088/1475-7516/2020/06/045>. Cited on page 71.
- 44 IVANOV, M. M.; SIMONOVIĆ, M.; ZALDARRIAGA, M. Cosmological Parameters from the BOSS Galaxy Power Spectrum. *JCAP*, v. 05, p. 042, 2020. Available from Internet: <https://doi.org/10.1088/1475-7516/2020/05/042>. Cited on page 71.
- 45 ALAM, S. et al. Completed SDSS-IV extended Baryon Oscillation Spectroscopic Survey: Cosmological implications from two decades of spectroscopic surveys at the Apache Point Observatory. *Phys. Rev. D*, v. 103, n. 8, p. 083533, 2021. Available from Internet: <https://doi.org/10.1103/PhysRevD.103.083533>. Cited on page 71.
- 46 CARDONA, W.; KUNZ, M.; PETTORINO, V. Determining  $H_0$  with Bayesian hyper-parameters. *JCAP*, v. 03, p. 056, 2017. Available from Internet: <https://doi.org/10.1088/1475-7516/2017/03/056>. Cited on page 71.
- 47 CAMARENA, D.; MARRA, V. Local determination of the Hubble constant and the deceleration parameter. *Phys. Rev. Res.*, v. 2, n. 1, p. 013028, 2020. Available from Internet: <https://doi.org/10.1103/PhysRevResearch.2.013028>. Cited on page 71.
- 48 BREUVAL, L. et al. The Milky Way Cepheid Leavitt law based on Gaia DR2 parallaxes of companion stars and host open cluster populations. *Astron. Astrophys.*, v. 643, p. A115, 2020. Available from Internet: <https://doi.org/10.1051/0004-6361/202038633>. Cited on page 71.
- 49 FREEDMAN, W. L. et al. The Carnegie-Chicago Hubble Program. VIII. An Independent Determination of the Hubble Constant Based on the Tip of the Red Giant



Branch. 7 2019. Available from Internet: <https://doi.org/10.3847/1538-4357/ab2f73>. Cited on page 71.

50 BOEHM, C.; DOLAN, M. J.; MCCABE, C. Increasing  $N_{\text{eff}}$  with particles in thermal equilibrium with neutrinos. *JCAP*, v. 12, p. 027, 2012. Available from Internet: <https://doi.org/10.1088/1475-7516/2012/12/027>. Cited on page 73.

51 BRUST, C.; KAPLAN, D. E.; WALTERS, M. T. New Light Species and the CMB. *JHEP*, v. 12, p. 058, 2013. Available from Internet: [https://doi.org/10.1007/JHEP12\(2013\)058](https://doi.org/10.1007/JHEP12(2013)058). Cited on page 73.

52 HOOPER, D.; QUEIROZ, F. S.; GNEDIN, N. Y. Non-Thermal Dark Matter Mimicking An Additional Neutrino Species In The Early Universe. *Phys. Rev. D*, v. 85, p. 063513, 2012. Available from Internet: <https://doi.org/10.1103/PhysRevD.85.063513>. Cited 2 times on pages 73 and 75.

53 CALDWELL, R. R. A Phantom menace? *Phys. Lett. B*, v. 545, p. 23–29, 2002. Available from Internet: [https://doi.org/10.1016/S0370-2693\(02\)02589-3](https://doi.org/10.1016/S0370-2693(02)02589-3). Cited on page 73.

54 CALDWELL, R. R.; KAMIONKOWSKI, M.; WEINBERG, N. N. Phantom energy and cosmic doomsday. *Phys. Rev. Lett.*, v. 91, p. 071301, 2003. Available from Internet: <https://doi.org/10.1103/PhysRevLett.91.071301>. Cited on page 73.

55 NOJIRI, S.; ODINTSOV, S. D.; TSUJIKAWA, S. Properties of singularities in (phantom) dark energy universe. *Phys. Rev. D*, v. 71, p. 063004, 2005. Available from Internet: <https://doi.org/10.1103/PhysRevD.71.063004>. Cited on page 73.

56 KELSO, C.; PROFUMO, S.; QUEIROZ, F. S. Non-thermal WIMPs as "Dark Radiation" in Light of ATACAMA, SPT, WMAP9 and Planck. *Phys. Rev. D*, v. 88, n. 2, p. 023511, 2013. Available from Internet: <https://doi.org/10.1103/PhysRevD.88.023511>. Cited on page 75.

57 ALLAHVERDI, R.; DUTTA, B.; QUEIROZ, F. S.; STRIGARI, L. E.; WANG, M.-Y. Dark Matter from Late Invisible Decays to/of Gravitinos. *Phys. Rev. D*, v. 91, n. 5, p. 055033, 2015. Available from Internet: <https://doi.org/10.1103/PhysRevD.91.055033>. Cited on page 75.

58 BRINGMANN, T.; KAHLHOEFER, F.; SCHMIDT-HOBERG, K.; WALIA, P. Converting nonrelativistic dark matter to radiation. *Phys. Rev. D*, v. 98, n. 2, p. 023543, 2018. Available from Internet: <https://doi.org/10.1103/PhysRevD.98.023543>. Cited on page 75.

59 FENG, J. L.; RAJARAMAN, A.; TAKAYAMA, F. SuperWIMP dark matter signals from the early universe. *Phys. Rev. D*, v. 68, p. 063504, 2003. Available from Internet: <https://doi.org/10.1103/PhysRevD.68.063504>. Cited 2 times on pages 75 and 89.

60 CYBURT, R. H.; ELLIS, J. R.; FIELDS, B. D.; OLIVE, K. A. Updated nucleosynthesis constraints on unstable relic particles. *Phys. Rev. D*, v. 67, p. 103521, 2003. Available from Internet: <https://doi.org/10.1103/PhysRevD.67.103521>. Cited 2 times on pages 75 and 84.

- 61 ABDALLA, E. et al. Cosmology intertwined: A review of the particle physics, astrophysics, and cosmology associated with the cosmological tensions and anomalies. *JHEAp*, v. 34, p. 49–211, 2022. Available from Internet: <https://doi.org/10.1016/j.jheap.2022.04.002>. Cited on page 75.
- 62 FROUSTEY, J.; PITROU, C.; VOLPE, M. C. Neutrino decoupling including flavour oscillations and primordial nucleosynthesis. *Journal of Cosmology and Astroparticle Physics*, v. 2020, n. 12, p. 015, dec 2020. Available from Internet: <https://dx.doi.org/10.1088/1475-7516/2020/12/015>. Cited on page 76.
- 63 YANG, W. et al. Tale of stable interacting dark energy, observational signatures, and the  $H_0$  tension. *JCAP*, v. 09, p. 019, 2018. Available from Internet: <https://doi.org/10.1088/1475-7516/2018/09/019>. Cited on page 79.
- 64 REZAEI, M.; NADERI, T.; MALEKJANI, M.; MEHRABI, A. A bayesian comparison between  $\lambda$ cdm and phenomenologically emergent dark energy models. *The European Physical Journal C*, Springer, v. 80, n. 5, p. 1–9, 2020. Available from Internet: <https://doi.org/10.1140/epjc/s10052-020-7942-6>. Cited on page 79.
- 65 KLYPIN, A.; HOLTZMAN, J.; PRIMACK, J.; REGOS, E. Structure formation with cold plus hot dark matter. *Astrophys. J.*, v. 416, p. 1–16, 1993. Available from Internet: <https://doi.org/10.1086/173210>. Cited on page 83.
- 66 BOSE, S. et al. ETHOS an Effective Theory of Structure Formation: detecting dark matter interactions through the Lyman- $\alpha$  forest. *Mon. Not. Roy. Astron. Soc.*, v. 487, n. 1, p. 522–536, 2019. Available from Internet: <https://doi.org/10.1093/mnras/stz1276>. Cited on page 83.
- 67 LOPEZ-CORREDOIRA, M.; MARMET, L. Alternative ideas in cosmology. *Int. J. Mod. Phys. D*, v. 31, n. 08, p. 2230014, 2022. Available from Internet: <https://doi.org/10.1142/S0218271822300142>. Cited on page 83.
- 68 LAHAV, O.; LIDDLE, A. R. The Cosmological Parameters (2021). 1 2022. Available from Internet: <https://doi.org/10.48550/arXiv.2201.08666>. Cited on page 83.
- 69 FENG, J. L.; RAJARAMAN, A.; TAKAYAMA, F. Superweakly interacting massive particle dark matter signals from the early universe. *Phys. Rev. D*, American Physical Society, v. 68, p. 063504, Sep 2003. Available from Internet: <https://link.aps.org/doi/10.1103/PhysRevD.68.063504>. Cited on page 84.
- 70 KAWASAKI, M.; KOHRI, K.; MOROI, T.; TAKAESU, Y. Revisiting Big-Bang Nucleosynthesis Constraints on Long-Lived Decaying Particles. *Phys. Rev. D*, v. 97, n. 2, p. 023502, 2018. Available from Internet: <https://doi.org/10.1103/PhysRevD.97.023502>. Cited on page 88.
- 71 HOLTSMANN, E.; KAWASAKI, M.; KOHRI, K.; MOROI, T. Radiative decay of a longlived particle and big bang nucleosynthesis. *Phys. Rev. D*, v. 60, p. 023506, 1999. Available from Internet: <https://doi.org/10.1103/PhysRevD.60.023506>. Cited on page 88.
- 72 KAWASAKI, M.; KOHRI, K.; MOROI, T. Hadronic decay of late - decaying particles and Big-Bang Nucleosynthesis. *Phys. Lett. B*, v. 625, p. 7–12, 2005. Available from Internet: <https://doi.org/10.1016/j.physletb.2005.08.045>. Cited on page 88.

- 73 KAWASAKI, M.; KOHRI, K.; MOROI, T. Big-Bang nucleosynthesis and hadronic decay of long-lived massive particles. *Phys. Rev. D*, v. 71, p. 083502, 2005. Available from Internet: <https://doi.org/10.1103/PhysRevD.71.083502>. Cited on page 88.
- 74 KOHRI, K.; TAKAYAMA, F. Big bang nucleosynthesis with long lived charged massive particles. *Phys. Rev. D*, v. 76, p. 063507, 2007. Available from Internet: <https://doi.org/10.1103/PhysRevD.76.063507>. Cited on page 88.
- 75 KAWASAKI, M.; KOHRI, K.; MOROI, T. Big-Bang Nucleosynthesis with Long-Lived Charged Slepton. *Phys. Lett. B*, v. 649, p. 436–439, 2007. Available from Internet: <https://doi.org/10.1016/j.physletb.2007.03.063>. Cited on page 88.
- 76 KAWASAKI, M.; KOHRI, K.; MOROI, T.; YOTSUYANAGI, A. Big-Bang Nucleosynthesis and Gravitino. *Phys. Rev. D*, v. 78, p. 065011, 2008. Available from Internet: <https://doi.org/10.1103/PhysRevD.78.065011>. Cited on page 88.
- 77 JITTOH, T. et al. Big-bang nucleosynthesis with a long-lived charged massive particle including  $^4\text{He}$  spallation processes. *Phys. Rev. D*, v. 84, p. 035008, 2011. Available from Internet: <https://doi.org/10.1103/PhysRevD.84.035008>. Cited on page 88.
- 78 KAPLINGHAT, M.; TURNER, M. S. Precision cosmology and the density of baryons in the universe. *Phys. Rev. Lett.*, American Physical Society, v. 86, p. 385–388, Jan 2001. Available from Internet: <https://link.aps.org/doi/10.1103/PhysRevLett.86.385>. Cited on page 89.
- 79 ALCANIZ, J.; BERNAL, N.; MASIERO, A.; QUEIROZ, F. S. Light dark matter: A common solution to the lithium and  $H_0$  problems. *Phys. Lett. B*, v. 812, p. 136008, 2021. Available from Internet: <https://doi.org/10.1016/j.physletb.2020.136008>. Cited on page 89.
- 80 KOLB, E. *The Early Universe*. [S.l.]: CRC Press, 2018. Cited on page 89.
- 81 SCHWARTZ, M. D. *Quantum field theory and the standard model*. [S.l.]: Cambridge university press, 2014. Cited 4 times on pages 90, 93, 98, and 102.
- 82 GRIFFITHS, D. *Introduction to elementary particles*. [S.l.]: John Wiley & Sons, 2020. Cited on page 90.
- 83 SEMENOV, A. V. *LanHEP - a package for automatic generation of Feynman rules in gauge models*. 1996. Available from Internet: <https://doi.org/10.48550/arXiv.hep-ph/9608488>. Cited on page 93.
- 84 BELYAEV, A.; CHRISTENSEN, N. D.; PUKHOV, A. Calchep 3.4 for collider physics within and beyond the standard model. *Computer Physics Communications*, v. 184, n. 7, p. 1729–1769, 2013. ISSN 0010-4655. Available from Internet: <https://www.sciencedirect.com/science/article/pii/S0010465513000313>. Cited on page 93.
- 85 BARING, M. G.; GHOSH, T.; QUEIROZ, F. S.; SINHA, K. New Limits on the Dark Matter Lifetime from Dwarf Spheroidal Galaxies using Fermi-LAT. *Phys. Rev. D*, v. 93, n. 10, p. 103009, 2016. Available from Internet: <https://doi.org/10.1103/PhysRevD.93.103009>. Cited on page 97.

- 86 MAMBRINI, Y.; PROFUMO, S.; QUEIROZ, F. S. Dark Matter and Global Symmetries. *Phys. Lett. B*, v. 760, p. 807–815, 2016. Available from Internet: <https://doi.org/10.1016/j.physletb.2016.07.076>. Cited on page 97.
- 87 BURGESS, C. An introduction to effective field theory. *Annual Review of Nuclear and Particle Science*, v. 57, n. 1, p. 329–362, 2007. Available from Internet: <https://doi.org/10.1146/annurev.nucl.56.080805.140508>. Cited on page 102.
- 88 TRANCANELLI, D. Grandezas físicas e análise dimensional: da mecânica à gravidade quântica. *Revista Brasileira de Ensino de Física*, SciELO Brasil, v. 38, 2016. Available from Internet: <https://doi.org/10.1590/1806-9126-RBEF-2015-0003>. Cited 2 times on pages 117 and 119.
- 89 TIESINGA, E.; MOHR, P. J.; NEWELL, D. B.; TAYLOR, B. N. Codata recommended values of the fundamental physical constants: 2018. *Rev. Mod. Phys.*, American Physical Society, v. 93, p. 025010, Jun 2021. Available from Internet: <https://link.aps.org/doi/10.1103/RevModPhys.93.025010>. Cited on page 118.

# Appendix



# APPENDIX A – Planck scale and natural units

Throughout this thesis, I use natural units (NU) and SI units. Therefore, in the appendix, I review the definition of NU, how to connect NU and SI, and the Planck units.

## A.1 Planck units

Each physical theory introduces a set of fundamental constants. Where I highlight four of them: the speed of light in the vacuum  $c$ , the Boltzmann constant  $k_B$ , the Planck constant  $\hbar$ , and the gravitational constant  $G$ . In SI units these constants have the following numerical values [13]:

$$c = 299792458 \text{ m s}^{-1}; \quad (\text{A.1a})$$

$$k_B = 1.380649 \times 10^{-23} \text{ J K}^{-1}; \quad (\text{A.1b})$$

$$\hbar = 1.054571817 \times 10^{-34} \text{ J s} = 6.582119569 \times 10^{-22} \text{ MeV s}; \quad (\text{A.1c})$$

$$G = 6.67430(15) \times 10^{-11} \text{ m}^3 \text{ Kg}^{-1} \text{ s}^{-2} = 6.70883(15) \times 10^{-39} \hbar c (\text{GeV}/c^2)^{-2}. \quad (\text{A.1d})$$

Using dimensional analyses, it is possible to construct four quantities: the Planck mass  $m_P$ , The Planck length  $l_P$ , the Planck time scale  $t_P$ , and the Planck temperature  $T_P$  [88]. The idea is to find the combination of  $\alpha, \beta, \gamma, \delta$  exponents in  $c^\alpha k_B^\beta \hbar^\gamma G^\delta$  that provides a number with the dimension of mass, length, time, and temperature. The solution to that is

$$m_P = \sqrt{\frac{\hbar c}{G}} \quad (\text{A.2a})$$

$$l_P = \sqrt{\frac{\hbar G}{c^3}} \quad (\text{A.2b})$$

$$t_P = \sqrt{\frac{\hbar G}{c^5}} \quad (\text{A.2c})$$

$$T_P = \sqrt{\frac{\hbar c^5}{G k_B^2}} \quad (\text{A.2d})$$

The numerical values of Planck units in SI are shown in Tab. 3.

Other Planck units can be obtained, for example, the Planck volume  $l_P^3$ , the Planck momentum  $m_P l_P / t_P$ , etc. One of these extra Planck units that I want to highlight is the Planck energy

$$E_P = m_P c^2 = \sqrt{\frac{\hbar c^5}{G}}. \quad (\text{A.3})$$

| Planck unit        | Symbol | Numerical value in SI [89]               |
|--------------------|--------|--|
| Planck mass        | $m_P$  | $2.176434(24) \times 10^{-8} \text{ Kg}$ |
| Planck length      | $l_P$  | $1.616255(18) \times 10^{-35} \text{ m}$ |
| Planck time        | $t_P$  | $5.391247(60) \times 10^{-44} \text{ s}$ |
| Planck temperature | $T_P$  | $1.416784(16) \times 10^{32} \text{ K}$  |

Table 3 – Numerical value of Planck units in SI.

## A.2 Natural units

Natural units (NU) are defined by setting  $c = k_B = \hbar = G = 1$ . This simplifies a lot of the mathematical expressions in quantum field theory and general relativity.

Usually, theoretical developments are made using natural units, and the experimental data are expressed in SI units or another convenient system of units.

For my proposal, it is useful to express 1 Kg, 1 m, 1 s, and 1 K in the GeV scale. To do that, I make use of the relation  $1 \text{ eV} = 1.602176634 \times 10^{-19} \text{ J}$  [13] and some energy relations that make easy this conversion.

Using the mass-energy relation  $E = mc^2$  [8], I can express the mass of a particle whose energy is 1 GeV:

$$m = \frac{1 \text{ GeV}}{c^2} = 1.78266 \times 10^{-27} \text{ Kg.} \quad (\text{A.4})$$

Using the wavelength-energy relation  $E = pc = 2\pi\hbar c/\lambda$  [8], I can find a wavelength of a particle whose energy is 1 GeV:

$$\lambda = \frac{2\pi\hbar c}{1 \text{ GeV}} = 1.23984 \times 10^{-15} \text{ m.} \quad (\text{A.5})$$

Using the period-energy relation  $E = 2\pi\hbar/t$  [8], I can express the period of a particle whose energy is 1 GeV:

$$t = \frac{2\pi\hbar}{1 \text{ GeV}} = 4.13567 \times 10^{-24} \text{ s.} \quad (\text{A.6})$$

Using the temperature-energy relation  $E = k_B T$  [15], I can provide the equivalent temperature of a system whose energy is 1 GeV:

$$T = \frac{1 \text{ GeV}}{k_B} = 1.16045 \times 10^{13} \text{ K.} \quad (\text{A.7})$$

With the four equations above, I built Tab. 4, where there are the desired conversion factors.

## A.3 Rewriting expressions in NU into SI

I have already shown how to connect numerical values from SI to NU. Now, I want to show how to recover all unit constants, hidden through the use of natural units. This



| Quantity    | SI   | Natural Units                             |
|-------------|------|---|
| Mass        | 1 Kg | $5.60959 \times 10^{26} \text{ GeV}$      |
| Length      | 1 m  | $5.06774 \times 10^{15} \text{ GeV}^{-1}$ |
| Time        | 1 s  | $1.51927 \times 10^{24} \text{ GeV}^{-1}$ |
| Temperature | 1 K  | $8.61735 \times 10^{-14} \text{ GeV}$     |
| Energy      | 1 J  | $6.24154 \times 10^9 \text{ GeV}$         |

Table 4 – Conversion factors from SI to natural units.

can be done using dimensional analyses and the Planck units [88]. As an example, in NU the energy of a massive particle is given by  $E^2 = p^2 + m^2$ . Looking at the dimension in SI units this equation is not right. The first thing to obtain this correspondent expression in SI is to write the  $p$  therm in the right SI dimension:

$$p \rightarrow \frac{p}{m_P \times (l_P/t_P)} \times E_P = pc. \quad (\text{A.8})$$

The next step is to do the same thing to the mass therm, i.e.,

$$m \rightarrow \frac{m}{m_P} \times E_P = mc^2. \quad (\text{A.9})$$

Finally, the dimensionally correct SI expression  $E^2 = p^2 c^2 + m^2 c^4$  is obtained.